Christian Wallner BSc.

Numerical analysis of “hard soil – soft rock” by utilizing the PLAXIS “Concrete Model”

Master’s Thesis

Submitted in fulfilment of the requirements for the degree of

Diplom-Ingenieur / Diplom-Ingenieurin

Master’s programme Civil Engineering, Geotechnics and Hydraulics

at

Graz University of Technology

Supervisor
Univ.-Prof. Dipl.-Ing. Dr.-Ing. Thomas Marcher
and
Dipl.Ing Stefan Stauder BSc.

Institute of Rock Mechanics and Tunnelling
Graz University of Technology

Graz, June 2020

EIDESSTATTLICHE ERKLÄRUNG

AFFIDAVIT

Ich erkläre an Eides statt, dass ich die vorliegende Arbeit selbstständig verfasst, andere als die angegebenen Quellen/Hilfsmittel nicht benutzt, und die den benutzten Quellen wörtlich und inhaltlich entnommenen Stellen als solche kenntlich gemacht habe. Das in TUGRAZonline hochgeladene Textdokument ist mit der vorliegenden Masterarbeit identisch.

I declare that I have authored this thesis independently, that I have not used other than the declared sources/resources, and that I have explicitly marked all material which has been quoted either literally or by content from the used sources. The text document uploaded to TUGRAZonline is identical to the present master‘s thesis.

Datum / Date

Unterschrift / Signature

Principle of equality

Due to reasons of legibility, this work does not include gender-specific formulations. However, the used male expressions stand for both genders.

Danksagung

An dieser Stelle möchte ich mich bei allen bedanken, die mich auf meinem Weg bis hierhin begleitet haben, und diesen Abschluss erst ermöglichten.

Zu aller erst möchte ich mich beim Institut für Felsmechanik und Tunnelbau und all seinen Mitgliedern bedanken, für die gute Betreuung während dieser Masterarbeit und den letzten drei Jahre am Institut als Studienassistent. Ganz besonders aber für die gute Freundschaft auch außerhalb der Arbeit.

Ohne den Geotechnik Zeichensaal wäre mein Studium nicht das gleiche gewesen. Mit den lebenslangen Freundschaften die sich hier bilden, dem Spaß am Lernen und dem „generationenübergreifenden“ studieren ist er wohl die wahrscheinlich wichtigste Institution dieser Universität.

Der wohl wichtigste Dank gebührt aber meiner Familie und meinen Freunden. In guten wie in schlechten Zeiten seid ihr immer für mich da. Ohne euch hätte ich das niemals geschafft.

Und Joe, danke für alles.

Abstract

The main target of this thesis is to approximate the main mechanical features hard soil and soft rock (HSSR) including non-linear hardening and strain-softening. This should be realised by utilizing the Concrete Model implemented in PLAXIS. In addition, a short overview of the mechanical behaviour and existing classification systems for this kind of material is summarised. Therefore, the first part of this thesis contains possible definitions for HSSR materials, the guiding mechanical behaviour, and the most important classification criteria according to strength, porosity, crumbling and several engineering classifications. To obtain the applicability of the Concrete Model for this challenge, it is explained in detail focusing on the behaviour in compression and the hardening and softening rules. This is including the assumptions that have been made for an application on modelling HSSR material. Especially a feasibility study using concrete parameters is done to obtain what stress/strain behaviour can be expected. To investigate the material behaviour, triaxial test simulations in 3D are used to reproduce real laboratory test results of marl, mudstone, and sandstone.

The herein introduced Standard G_c Variation contains of three different definitions for the material behaviour using varying failure strength approaches. Depending on their associated fracture energy this seems to cover the material characteristics from brittle to ductile in a sufficient way. The post peak behaviour and the softening regime of the numerical simulations develop successfully, but slightly overestimates the residual strength in the most cases. To check the model outcome a parameter study is conducted on the dilatancy angle ψ, the fitting parameter a, and the different strength parameter. Finally a case study is done to prove the applicability of the Concrete Model on a real boundary value problem. To crosscheck the plausibility of the results, the case study is additionally conducted with the Hardening Soil Model.

Kurzfassung

Das Hauptziel dieser Arbeit ist es das Entfestigungsverlhalten von überkonsolidierten Böden und Halbestgesteinen unter Verwendung des Concrete Models (PLAXIS) zu untersuchen und einen kurzen Überblick über das mögliche Materialverhalten und bestehende Klassifizierungssysteme zu geben. Diese Arbeit umfasst die möglichen Definitionen für HSSR-Materialien und untersucht das Mechanische Entfestigungsverhalten. Ebenfalls werden die wichtigsten Klassifizierungskriterien wie Festigkeit, Porosität, Veränderlichkeit unter Wassereinfluss und verschiedenen ingenieurmäßigen Klassifizierungssysteme erläutert. Um die Anwendbarkeit des Concrete Model in Bezug auf die mechanischen Eigenschaften zu überprüfen, wird es mit Schwerpunkt auf das Druckverhalten, sowie den ‟hardening‟ und ‟softening‟ Eigenschaften erläutert. Ferner wird erklärt welche Annahmen für eine Anwendung zur Modellierung von HSSR-Material getroffen wurden. Eine Machbarkeitsstudie mittels eines Einaxialen Druckversuches an Beton soll Einblick geben, welche Ergebnisse zu erwarten sind. Um das Materialverhalten mit diesem Modell zu untersuchen werden triaxiale Testsimulationen in 3D verwendet, um reale Labortestergebnisse von Mergel, Tonstein und Sandstein zu reproduzieren.

Die in dieser Arbeit präsentierte Standard G_c Variation verwendet drei unterschiedliche Definitionen für das Materialverhalten unter Verwendung unterschiedlicher Bruchfestigkeitsansätze. Die damit verbundene Bruchenergie scheint die Materialeigenschaften von spröde bis duktil in ausreichender Weise abzudecken. Das Post-Peak-Verhalten und der Residualbereich der numerischen Simulationen entwickelt sich erfolgreich, überschätzt jedoch die Restfestigkeit in den meisten Fällen noch geringfügig. Ebenfalls wird eine Parameterunterstudie von ψ, dem Parameter a und den Festigkeitsparametern f_{cfn} und f_{cun} durchgeführt, um ihren Einfluss im Zuge der numerischen Berechnungen zu klären. Abschließend soll eine Fallstudie die Anwendbarkeit des Concrete Model für geotechnische Randwertprobleme belegen. Die Ergebnisse werden mit den Resultaten von Berechnung mit dem PLAXIS Hardening Soil Model verglichen.

Table of contents

List of figures

List of tables

Symbols and Abbreviations

D	Diameter [m]
h	Height [m]
γ	Unit weight [kN/m^3]
σ_{cs}	Critical softening load [kPa]
K	Empiric softening factor [-]
φ	Friction angle [°]
A_{el}	Average element size
L_{eq}	Average element length
M_{stage}	Applied load [-]
ψ	Dilatancy angle
ε_{cp}^{p}	Plastic peak strain
m	Power law
c	Cohesion
ø	Diameter
’’	Inch
p_{ref}	Reference pressure [kPa]
E_{oed}	Oedometric modulus
E_{50}	Modulus for deviatoric loading
E_{ur}	Unloading reloading modulus
HSSR	Hard soil soft rock
UCS	Uniaxial compressive strength
G_c	Fracture energy
g_c	Fracture energy mesh dependent
q	Deviatoric stress
u_z	Vertical deformation

1 Introduction

The first chapter of this master thesis contains an explanation for the motivation of this thesis as well as a general overview related to the structure of this work.

1.1 Motivation

This thesis is dealing with the challenging material behaviour of hard soils and soft rocks which are a main part of geotechnical problems world-wide. The main feature of these materials group is the possibility of strain-softening which can cause progressive failures in tunnel excavations, slopes, and embankments. The goal is to find a proper way to model hard soil and soft rock behaviour including its main mechanical characteristics. These are considered as non-linear hardening as well as post peak strain-softening. Therefore, an already existing material model should be utilized to approximate the required mechanical characteristics of hard soil-soft rock. Concrete is considered as a material with similar mechanical properties showing non-linear hardening, strain-softening and a similar strength as weak rock. By reproducing real laboratory triaxial compression tests on soft rock samples, the applicability of the Concrete Model implemented in PLAXIS should be proved.

1.2 Thesis objectives and structure

Generally this master thesis is structured into Introduction, Used Material Models, Method, Results, and Discussion. In chapter 1 (Introduction) the main goal and the structure of this thesis is described. Therefore, the material hard soil soft rock is introduced (1.3) including several definitions. The main characteristics of the investigated material with respect to strain softening is explained in Mechanical properties (1.4). Finally the most common classification systems for hard soil and soft rock materials are shown (1.5). Chapter 2 (Used Material Models) is describing the Hardening Soil Model (2.1) and the Concrete Model (2.2) which are used for the numerical modelling of the triaxial tests and the case study. In chapter 3 (Method) the three investigated materials marl, mudstone, and sandstone are introduced. The following parameter determination (3.1) contains the method how the elasticity modulus (3.1.1), the linear elastic part (3.1.2), the specialised fitting parameter a (3.1.3), and the strength parameter (3.1.4) are derived. Especially the in this master thesis introduced Standard G_c Variation is explained in (3.1.6). Afterwards, the utilized numerical model is illustrated (3.2.1) and a first feasibility study (3.2.1) is done. Finally, the mesh dependency

of the model is checked (3.2.2) and the shear band development (3.2.3) is shown.
Chapter 4 (Results) is presenting the calculation results of the Parameter Study (4.1). There the Standard G_c Variation is applied on the three investigated materials and also a variation for the dilatancy angle ψ (4.1.4), the fitting parameter a (4.1.5), the failure strength f_{cfn} (4.1.6), and the residual strength (4.1.7) is done. This chapter includes, a Case Study which should prove the applicability of the Concrete Model on realistic boundary value problems (4.2). Chapter 5 (Discussion) is summarising this thesis including the Interpretation (5.1) and the Conclusion (5.2). Solved problems and open questions are discussed in (5.3). The Outlook (5.4) finishes this thesis.

1.3 Hard Soil – Soft Rock (HSSR)

The material HSSR is a critical geomaterial which can cause manifold problems in mining and tunnelling. It can show unfavourable behaviour like low strength, disaggregation, crumbling, high plasticity, slaking, and fast weathering. Mainly the characteristics of soft rocks are highly influenced by the current stress state and the existence of water. A typical property of this material is its intermediate strength between overconsolidated soils and hard rocks, which requires a specialized testing equipment, complicating the determination of material properties even further. (Kanji, 2014)

There is a wide spectrum of what is considered soft rock, depending on what classification system is used and which property is considered the leading parameter for the engineering case that should be obtained. The following table shows a general overview of some rock types which are usually classified as soft rock.

Table 1.1 Usual types of soft rocks (Kanji, 2014)

Basic types	Subclasses
Sedimentary rocks	Clastic: mudstones, shales, siltstones, sandstones, conglomerates, marl Evaporites: salt rock, carnallite Soluble: limestone, dolomite, gypsum, coal
Igneous rocks	Volcanic conglomerates, breccias, and lahar; Basaltic breccia; Pyroclastic deposits, volcanic ash, tuff and ignimbrite; and Weathering products of crystalline rocks
Metamorphic rocks	Slate, phyllite, schists, quartzite little cemented, Metavolcanic deposits

Soft rock is a term which covers a big variation of materials, properties, and characteristics which complicates finding a common denominator for a theoretical definition. Several definitions for soft rock material exist depending on which parameter they are focusing on. Namely, these are the descriptive, the quantitative and the engineering definition.
(Kanji, et al., 2020)

Descriptive Definition

The descriptive definition is specially focused on the geological characteristics of soft rock. The definition takes the lithology, structure, and the chemical properties into account. From this point of view, the classic soft rock shows a short diagenetic period, which causes its low strength, high degree of fracturing, large porosity, and a poor degree of cementation. It is also not atypical that soft rocks show a high degree of weathering and crumbling, especially when in contact with water. Swelling rocks can also be described as soft rocks, which includes the content of clay minerals as a soft rock indicator. (Kanji, et al., 2020)

Quantitative Definition

For the quantitative definition the main property of soft rock is the uniaxial strength. The most common approach is to define rocks with a uniaxial strength between 0.25 and 25 MPa as soft rocks which still provides a wide range by a factor of 100 for this definition. Another possible way is to take the in-situ stress state into account (Kanji, et al., 2020). There soft rock is defined as a ratio of the uniaxial strength and the in-situ stress state, which is given as:

$$UCS/(\gamma H) < 2 \tag{1.1}$$

Where γ is the unit weight and H is the overburden.

Engineering Definition

The definition of engineering soft rock is expressed as a relationship of the applied engineering stresses and the strength of the rock mass which causes large plastic deformations beyond the allowed design level in practice. If the resulting engineering force is higher than the rock mass strength and plastic or viscoplastic deformations occur, the rock is considered as soft rock. This definition allows the same material to appear as soft rock and also as hard rock, just depending on the current stress state. This definition is mainly used for tunnel excavations in china. Commonly the surrounding rock mass of an excavation is suggested as soft rock if the plastic radius is more than 1.5m (Kanji, et al., 2020). Generally, this definition could be written as:

$$\sigma \ \geq [\sigma] \tag{1.2}$$

Where σ is the engineering stress and $[\sigma]$ is the rock mass strength.

1.4 Mechanical properties

One of the main features of the mechanical behaviour of HSSR is strain-softening. Therefore, this section mainly considers the characteristics of friction and cohesion softening, as well as the guiding boundary conditions which are influencing the material behaviour.

1.4.1 Strain-softening behaviour

Generally, strain-softening describes how a material transits from a defined peak failure criterion to its residual state. As figure 1.1 below shows, typically a material starts its deformation in the elastic zone, where no plastic deformation would occur after stress release. Entering the plastic zone, the material behaves according to a non-linear stress/strain relation which generally is called hardening. Releasing the applied stresses between point A and D in the figure below leads to irreversible plastic strains. The mechanical background of the hardening in the plastic zone is commonly described as a mobilization of the friction angle φ from its initial state to its fully mobilized value when reaching the peak strength at point B. After the peak strength is reached a stress release can be observed with ongoing deformation. How significant the change in the stress/strain behaviour is, is mainly guided by the reduction of the strength parameters φ and c, but also on the occurring confining pressure state and the general geological conditions of the material. Finally, when the transition through the strain-softening zone is finished, the strength parameters have reached their residual value. This can be considered as the residual state, where perfectly plastic deformation occurs.

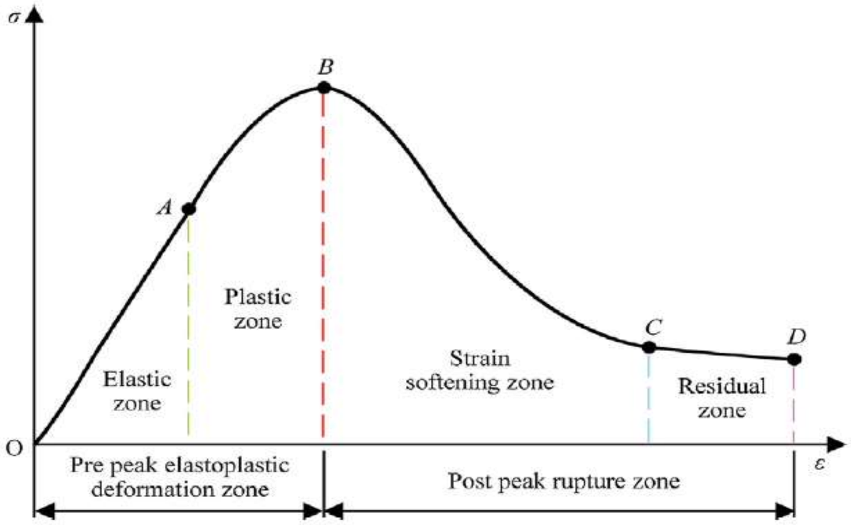

Figure 1.1 General stress-strain curve for softening (Wang Ruijie, 2018)

Especially for rock-like materials the initial part of the softening zone can show a brittle response, which is recognizable as a sudden stress release. This characteristic softening behaviour can be observed when the rock mass shows a high UCS, GSI, and low confinement.

In general, material which shows strain-softening behaviour can cause progressive failures by stress release with ongoing deformation. This occurs for example in embankments, slopes, and excavations. Failure can occur as late as up to 50 years after construction, caused by a redistribution of pore pressures. These delayed failures are well documented for London Clay by (Skempton, 1964)

1.4.2 Friction angle and cohesion softening

The softening behaviour is mainly guided by a reduction of either the cohesion or the friction angle and the cohesion. With ongoing deformation, the cohesion decreases. Generally, this leads to a parallel shift of the failure envelope until the residual level of the cohesion is reached. The softening of the friction angle can then be illustrated as a flattening of the failure envelope and a reduction of the friction angle to its residual state.

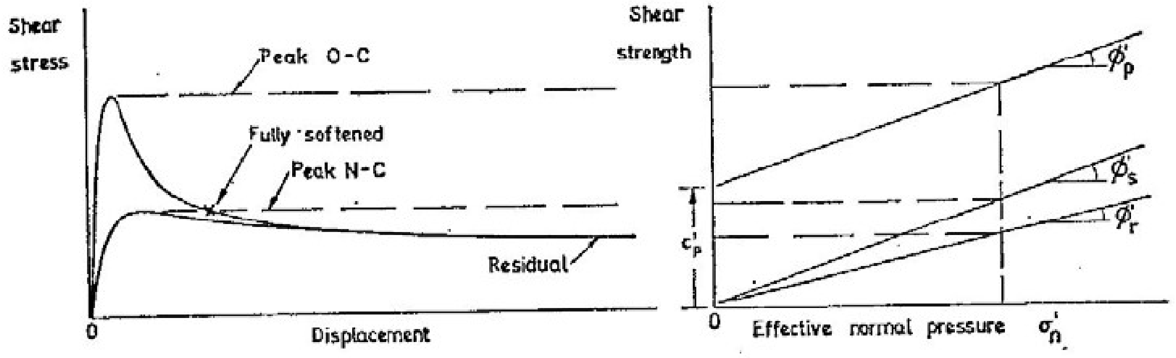

Figure 1.2 Comparison of peak, residual and fully softened shear strength (Stephen G. Wright, 2007)

The figure below illustrates a cohesion softening and friction angle hardening assumption. While the amount of plastic strains is low, the influence of friction is less significant than the cohesion. With ongoing deformation, the bonding between the particles and with this the cohesion is decreasing. Meanwhile, the displacement of particles leads to a mobilisation of the friction angle. This mechanism continues until the cohesion between the particles is at its residual value or zero and the friction angle is fully mobilised. (Majid Mirahmadi, 2018)

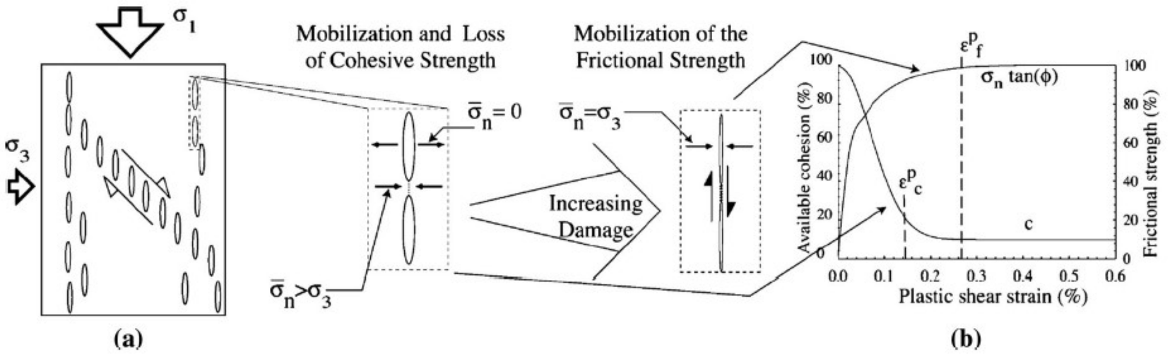

Figure 1.3 Cohesion softening and friction angle hardening (Majid Mirahmadi, 2018)

The combined softening behaviour illustrated in the following graph assumes that the friction angle and the cohesion decrease parallel from their mobilised peak value to their residual value.

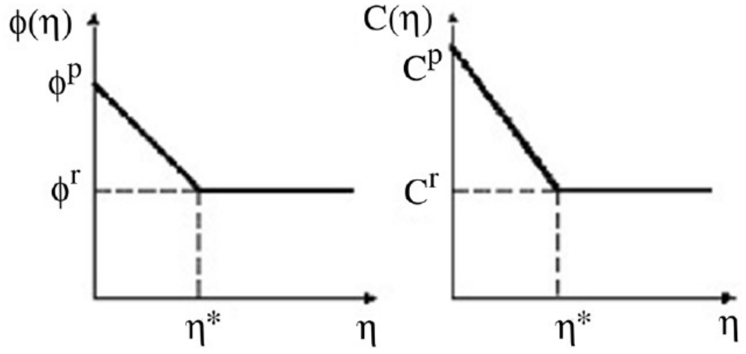

Figure 1.4 Cohesion and friction angle softening over the plastic parameter (η) (Majid Mirahmadi, 2018)

Two examples of friction and cohesion softening are the Buchberg sandstone and the Walton Wood clay. From a triaxial compression test of the sandstone a complete loss of the cohesion could be observed while the friction angle only pass through a hardening and is uninfected in the post peak area. A shear test on Walton Wood clay shows a complete loss of cohesion and a significantly lower friction angle. If the softening for both strength parameters in this case is acting at the same moment could not be observed. (Renani, et al., 2019)

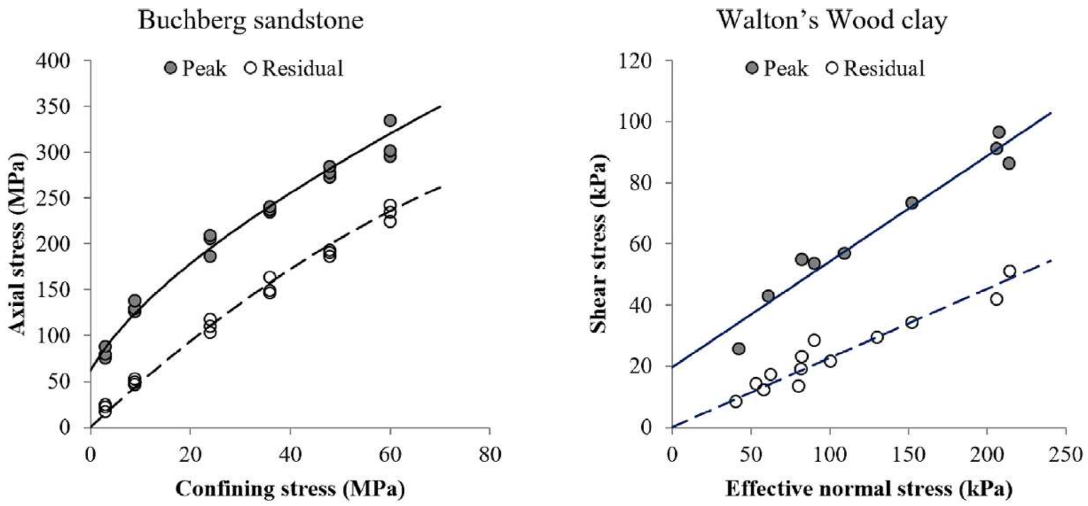

Figure 1.5 Peak and residual strength envelopes of Buchenberg sandstone and Walton Wood clay (Renani, et al., 2019)

The graph above shows the peak and residual envelopes for Buchberg sandstone and Walton Wood clay. These two graphs can clearly show that also the choice of the strength criterion is an important decision for the approximation of softening behaviour. The clay can be represented with the common Mohr-Coulomb failure criterion, using a linear function of effective stress. For more rock like material as the sandstone, non-linearity can be observed on both envelopes which requires a more improved failure criterion like Hoek and Brown. (Renani, et al., 2019)

1.4.3 Influence of confining pressure on softening

Strain-softening occurs in rock-like material as well as in overconsolidated clays and dense sands. It can be observed that for both material types the softening regime depends highly on the confining pressure. With increasing effective confining pressure the post peak regime tends to be approximating an ideal-plastic stress/strain state. The following graph shows the evolution of the softening behaviour for a rock-like material (Tennessee marble, drained triaxial test) and a soil-like material (Yellow clay, shear test) threw various confining pressure stages. For the marble a clear change of the post peak regime can be observed. The stress/strain behaviour changes from a highly brittle stress release in uniaxial conditions to a nearly perfectly plastic post peak state at high confining pressures. The shear test on Yellow clay shows that the stress/strain behaviour in the post peak regime of overconsolidated soils is less influenced by the confining pressure than for rock like material. (Renani, et al., 2019)

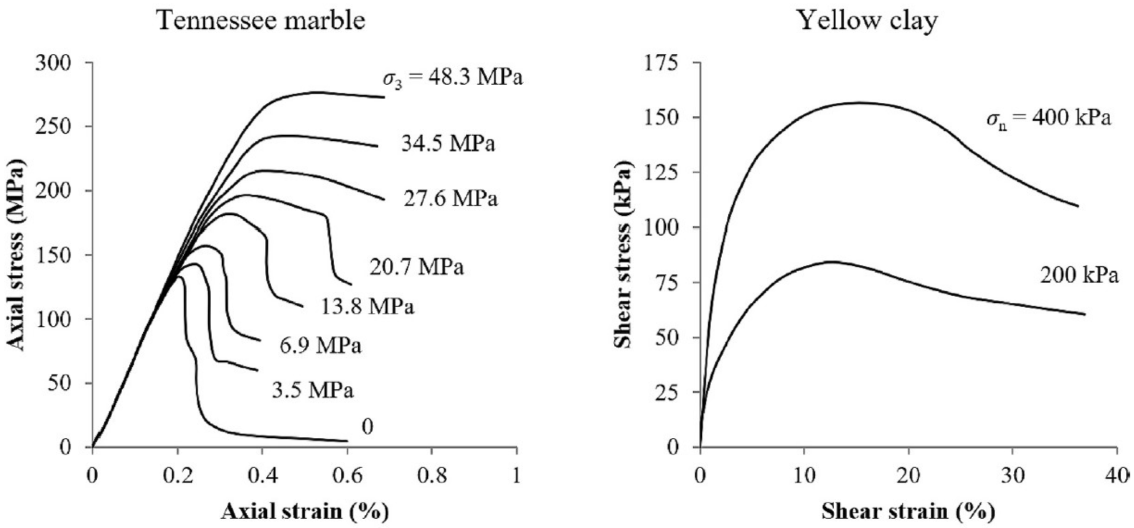

Figure 1.6 Softening behaviour at various confining pressure stages for rock-like material (Tennessee marble, drained triaxial test) and overconsolidated soil-like material (yellow clay, shear test) (Renani, et al., 2019)

For many geotechnical structures such as embankments, slopes, and excavations the confining pressure tends to be low. This can lead to progressive failures and should underline the importance of considering strain-softening behaviour for analysis and design. (Renani, et al., 2019)

1.4.4 Geological Strength Index and critical plastic strain

The post peak behaviour of rock mass and its transition to the residual state is also influenced by its density of jointing. For an average rock mass it can be assumed that the post peak behaviour is guided by a reduction of the GSI from its initial value to a lower residual one (E. Hoek, 1997). Based on this approach the post peak behaviour of rock masses can be classified into three categories which are illustrated in Figure 1.7.

- GSI > 75: The high GSI value indicates a good quality rock mass which mechanical behaviour is elastic-brittle, and the dilatation angle can be assumed as $\psi = \varphi/4$

- 25 < GSI < 75: For an average jointed rock mass softening can be considered and the dilatation angle is $\psi = \varphi/8$

- GSI < 25: Weak rock mass is assumed to act in a perfectly plastic behaviour and no dilatation should be assumed.

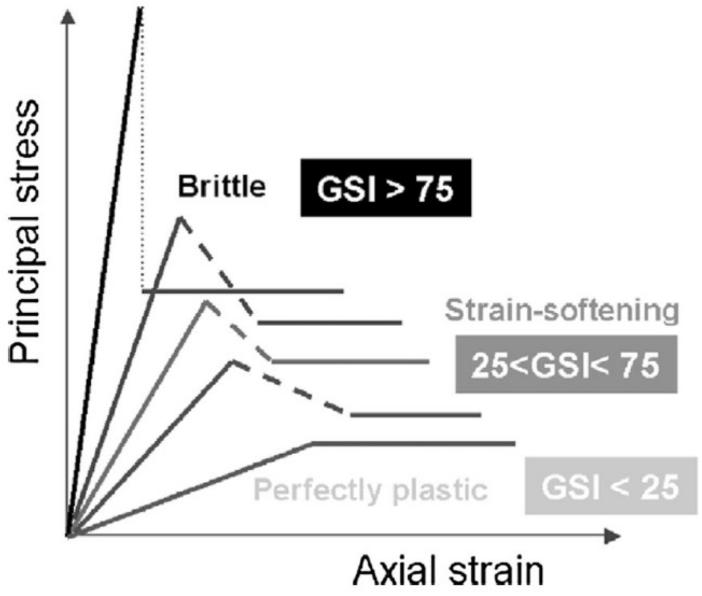

Figure 1.7 Rock masses with different post failure modes depending on geological strength index (Majid Mirahmadi, 2018)

The behaviour of a rock mass in its softening state can also be expressed with the term of critical plastic strain which is used in several numerical simulations. Currently, little is known about the critical plastic strain required for different rock masses. As an estimation of this critical plastic strain the following equation is used (Vakili, 2016):

$$Critical\ plastic\ strain = \frac{12.5 - 0.125\ GSI}{100\ d} \tag{1.3}$$

The GSI represents the geological strength index and d is the equivalent edge length of the mesh elements. With increasing GSI the critical plastic strain decreases and the stress/strain behaviour approximates a perfectly plastic state. (Vakili, 2016)

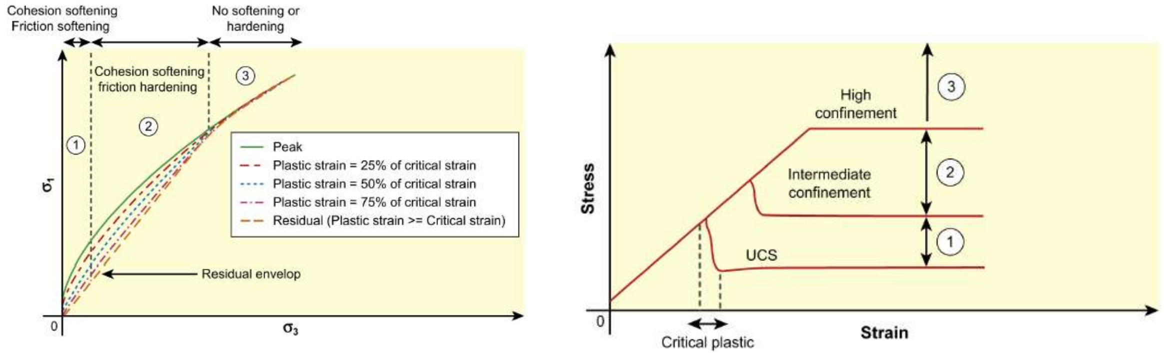

Figure 1.8 Conceptual representation of the post peak rock mass behaviour (Vakili, 2016)

1.5 Classification and Criteria

An overall classification system for soft rock does not exist at the moment. There are various classification methods depending on geological components, strength, weathering, or mechanical behaviour. The following section gives an overview of some classification systems in use and their various indicators.

1.5.1 Classification according to strength

The classical upper boundary using the strength characterisation for soft rock is considered with an uniaxial compressive strength of 25 MPa. The lower limit is more difficult to set and to differentiate from highly overconsolidated soil. A common limit is 0.25 to 0.4 MPa as lower boundary condition for the classification of soft rocks. But as the following chart will show, not all classification systems according to strength use these values. (Kanji, 2014)

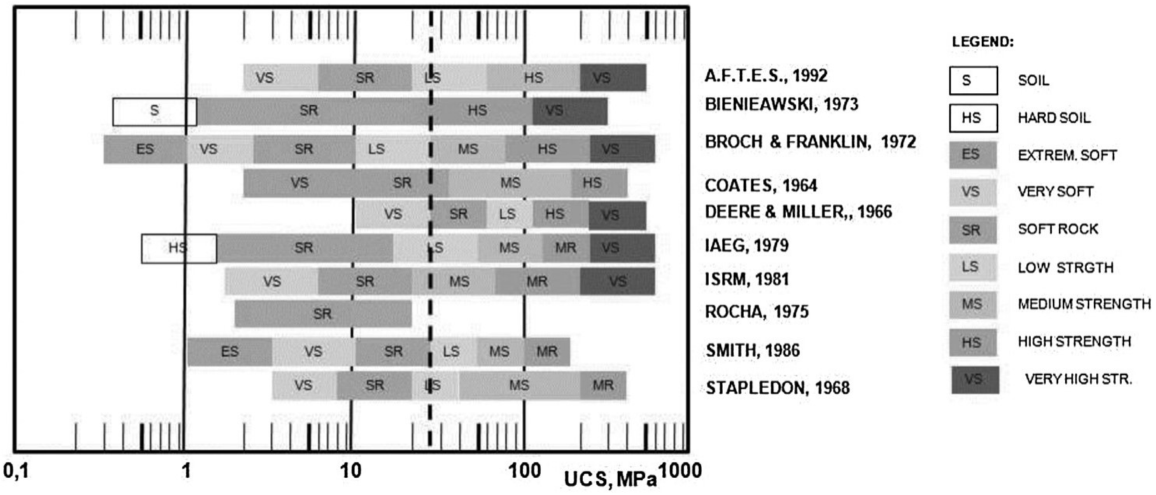

Figure 1.9 Classification according to the strength (Kanji, 2014)

1.5.2 Classification according to porosity

Using the theoretical relationship between dry density and porosity it is possible to show the transition from hard rock to soil and identify soft rock behaviour. The following figure shows that with decreasing dry density, the amount of porosity is increasing. The considered amount of porosity for hard soil or soft rock is between 4 and 20 percent.

The deviating results of specific rock samples like sandstone could be explained by the degree of cementation. Even it is the same lithological rock, a changing cementation degree could lead to very hard conditions or extreme soft soil behaviour.

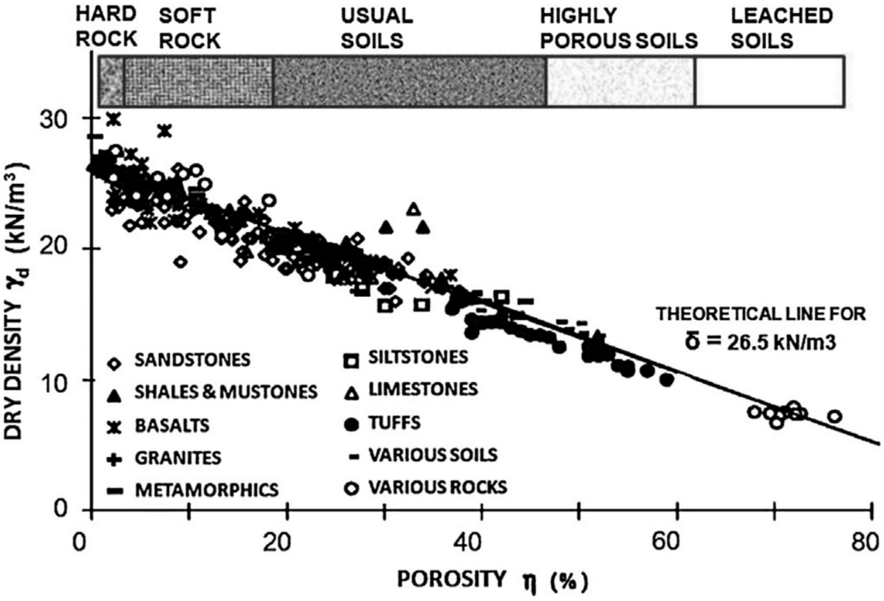

Figure 1.10 Classification according to porosity (Kanji, 2014)

1.5.3 Classification according to crumbling

Not all HSSR materials are highly affected by water, but the classification according to crumbling can be used as an additional support tool. Especially in Germany this classification for “veränderlich feste Gesteine” is used for hard soils or weak rocks. Beside the uniaxial strength, the main characteristic for this classification is the influence of water on the material. For the classification three characteristics have to be fulfilled:

- The material has the typical uniaxial strength between 3.6 to 25 MPa.
- The material disintegrates when in contact with water.
- This disintegration acts in a technical relevant time period.

The classification is depending on a storage water test were the rock sample lies 24 hours in a water bath. How the sample is changing and crumbling defines the state of slake durability. (Plinninger, et al., 2012). These states are described in the following table.

Table 1.2 States of slake durability (Plinninger, et al., 2012)

State	**Name**	**Description**
0	not changing	not changing
1	slight changing	just slight changing of the crystalline behaviour
2	slow changing	slow disintegration to pieces with max. 27.5 % mass of the sample which then stays intact
3	moderate changing	moderate fast disintegration to pieces smaller than 54 % of the initial sample
4	quick changing	quick disintegration to pieces smaller than 12.5 % of the initial sample
5	rapid changing	rapid disintegration to pieces smaller than 25 % of the initial sample

1.5.4 Classification according to critical softening load

This classification concept is only applicable for tunnel excavations and shows similarities to the concept of the plastic radius. Until the critical softening load is reached, the deformation shows a constant behaviour, but after passing the softening load the deformations start accelerating and the rock is getting unstable. Following this assumption it is possible for every material to reach this “soft rock state”. To figure out the empirical parameter K (1.4) the investigated material has to be categorised in one of three subcategories. These are swelling soft rock, high strength soft rock and jointed soft rock. Swelling soft rock typically contains a large amount of clay minerals and appears as a highly weathered rock mass with a uniaxial compressive strength lower than 25 MPa. High strength soft rock typically has a UCS higher than 25 MPa and shows high deformations if large stresses are applied. The major part of the deformation will occur when the critical softening depth is passed, or the critical softening load is reached. Before this state the normal engineering behaviour is like in hard rock. Typical jointed soft rock has little or no shale content but its rock mass shows significant joint sets. In a mining induced stress increase plastic deformations occur by shearing along the joint planes and dilatant behaviour occurs (Kanji, et al., 2020). As an assumption for the critical softening load the following empirical equation could be used:

$$\sigma_{cs} = K \times UCS \tag{1.4}$$

For K as an empiric value:

Swelling soft rocks	0.3 – 0.5
High strength soft rocks	0.5 – 0.7
Jointed soft rocks	0.4 – 0.8

2 Used Material Models

The goal of this master thesis is to find a proper way to model and represent hard soil and soft rock behaviour including its main mechanical characteristics. Therefore a suitable model must be able to take non-linear hardening as well as post peak strain-softening into account.

The idea is utilize an already existing material model, which is able to approximate the required mechanical characteristics of HSSR material in an adequate way. Concrete is considered as a material with similar mechanical properties showing non-linear hardening, strain-softening and a comparable strength. In Austria there are already several concrete models available from researchers of the Technical Universities of Innsbruck, Wien and Graz. The model from Aschaber (2017) is dealing mainly with the three-phase-mixture characteristics of concrete while Schneider (2010) develops his model for prediction of load bearing capacity of structures subjected to fire. Due to the fact that the model from Schütz (2010) and Schädlich (2016) is already implemented in PLAXIS as the Concrete Model and considers the required mechanical behaviour, this model is used throughout this thesis.

The following two subchapters summarise the material models which are used in this thesis. At first the Hardening Soil Model which is commonly used for modelling soil behaviour is introduced. This model should serve as a reference for the new introduced approaches. After that, the Concrete Model implemented in PLAXIS is described including the assumptions which have been made with respect to an application on HSSR material.

2.1 Hardening Soil Model

The yield surface of this hardening plasticity model is not fixed in principle stress space. In contrast to an elastic perfectly plastic model it is able to expand due to plastic straining.
In the Hardening Soil Model there are two types of hardening. On one side the shear hardening which is used to model irreversible strains due to primary deviatoric loading and on the other side compression hardening which is used to model irreverisble plastic strains due to primary compression in oedometer and isotropic loading. (PLAXIS, 2019)

Basic characteristics of the HS Model:

m	Stress dependent stiffness according to a power law	[-]
E_{50}^{ref}	Plastic staining due to primary deviatoric loading	[kN/m²]
E_{oed}^{ref}	Plastic straining due to primary compression	[kN/m²]
E_{ur}^{ref}	Elastic unloading/reloading	[kN/m²]
ν_{ur}	Poisons Ratio	[-]
c	Cohesion	[kN/m²]
φ	Friction angle	[°]
ψ	Dilatancy Angle	[°]

An important characteristic of the HS model is the stress dependency of soil stiffness. An implied relationship for oedometric conditions is for example:

$$E_{oed} = E_{oed}^{ref} \left(\frac{\sigma}{p_{ref}} \right)^{m} \tag{2.1}$$

2.2 The Concrete Model

The Concrete Model is an elastoplastic material model, which can take non-linear material behaviour into account. Especially the consideration of strain hardening and softening makes it a powerful tool beyond linear-elastic material behaviour. It is also possible to consider time dependency related to the stiffness and strength development as well as creep and shrinkage. In deviatoric loading, the Concrete Model shows two different behaviours. In the compression state, the stresses will increase non-linearly until the peak value is reached, and after that, it will soften to a residual value. For the tension case, it will be considered linear-elastic until reaching the peak and then softens to a residual state. The total strain consists of four independent components which are the elastic strain ε^{e}, the plastic strain ε^{p}, the creep strain ε^{cr}, and shrinkage strain ε^{shr} (PLAXIS, 2019).

$$\varepsilon = \varepsilon^{e} + \varepsilon^{p} + \varepsilon^{cr} + \varepsilon^{shr} \tag{2.2}$$

2.2.1 Parameters

The Concrete Model needs 25 independent input parameters for calculation. Generally, they are based on the special characteristics of concrete. Therefore several parameters have to be interpreted for HSSR material which will be described in chapter 3.1. The following list summarizes all needed parameters with an additional short description. (PLAXIS, 2019)

Elastic parameters

E_{28}	Young's modulus of cured concrete at t_{hydr}	[kN/m²]
$E_1\ /E_{28}$	Time-dependent ratio of elastic stiffness	[-]
ν	Poisson's ratio	[-]

Strength in compression

$f_{c,28}$	Uniaxial compressive strength of cured concrete at t_{hydr}	[kN/m²]
f_{c0n}	Normalised initially mobilised strength	[-]
f_{cfn}	Normalised failure strength	[-]
f_{cun}	Normalise residual strength	[-]
$G_{c,28}$	Compressive fracture energy of cured concrete at t_{hydr}	[kN/m]
φ_{max}	Maximum friction angle	[°]
ψ	Dilatancy angle	[°]

Time dependency of compressive strength

$f_{c,1}/f_{c,28}$	Time-dependency of compressive strength	[-]
t_{hydr}	Time for full hydration	[day]

Strength in tension

$f_{t,28}$	Uniaxial tensile strength of cured concrete at t_{hydr}	[kN/m²]
f_{tun}	Ratio of residual vs. peak tensile strength	[-]
$G_{t,28}$	Tensile fracture energy of cured concrete at t_{hydr}	[kN/m]

Ductility

$\varepsilon^{p}_{cp,1h}$	Uniaxial plastic failure strain at 1h (negative value)	[-]
$\varepsilon^{p}_{cp,8h}$	Uniaxial plastic failure strain at 8h (negative value)	[-]
$\varepsilon^{p}_{cp,24h}$	Uniaxial plastic failure strain at 24h (negative value)	[-]
a	Increase of ε_{cp} with increase of deviatoric mean stress	[-]

Creep

ϕ^{cr}	Ratio between creep and elastic strains	[-]
t^{cr}_{50}	Time for 50% of creep strains	[day]

Shrinkage

$\varepsilon_{\infty}^{shr}$	Final shrinkage strain (negative value)	[-]
t_{50}^{shr}	Time for 50% of shrinkage strains	[day]

Safety factors

γ_{fc}	Safety factor for compressive strength	[-]
γ_{ft}	Safety factor for tensile strength	[-]

2.2.2 Yield function in compression

In compression the Concrete Model uses a Mohr-Coulomb yield surface for deviatoric loading. In this definition the sign convention is strictly positive for tension and negative for compression. In equation (2.3), σ_1 is the major tensile stress and σ_3 the minor compressive principal stress. (PLAXIS, 2019)

$$F_c = \frac{\sigma_1 - \sigma_3}{2} + \frac{\sigma_1 + \sigma_3 - 2\sigma_{rot}}{2} \times \frac{f_{cy}}{2\sigma_{rot} + f_{cy}} \tag{2.3}$$

In the following equation σ_{rot} is defined as the intersection of the isotropic axis and the failure surface where φ_{max} gives the total inclination of the failure envelope.

$$\sigma_{rot} = \frac{f_c}{2}\left(\frac{1}{\sin\varphi_{max}} - 1\right) \tag{2.4}$$

In Figure 2.1 an illustration of the failure envelope and the yield surface in compression and tension is shown.

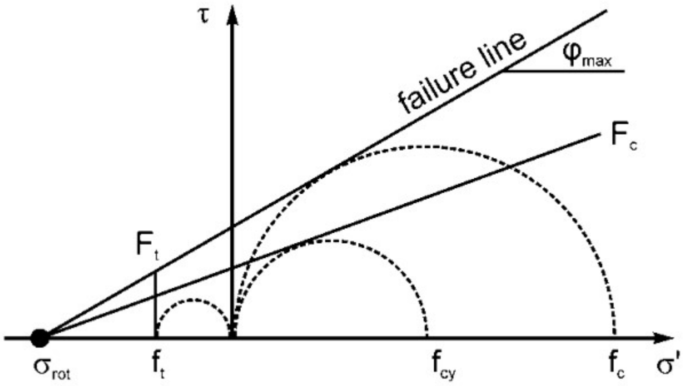

Figure 2.1 Mohr-Coulomb failure surface and yield surface for the Concrete Model (PLAXIS, 2019)

The Concrete Model provides no continuous failure function for the tension and the compression state. They are separated to prevent an interrelated influence on each other. Therefore, the focus of the parameter determination must be related to the expected stress state, which could be either tension or compression. (PLAXIS, 2019)

2.2.3 Strain hardening and softening

The calculation of the yield stress is divided into four different states or areas. These are from left to right (PLAXIS, 2019):

Zone 1: Quadratic strain hardening
Zone 2: Linear strain softening
Zone 3: Linear strain softening
Zone 4: Constant residual strength

These four areas are defined in a normalised uniaxial test, as can be seen in Figure 2.2. The grey marked area of zone 2 represents also the amount of the fracture energy g_c.

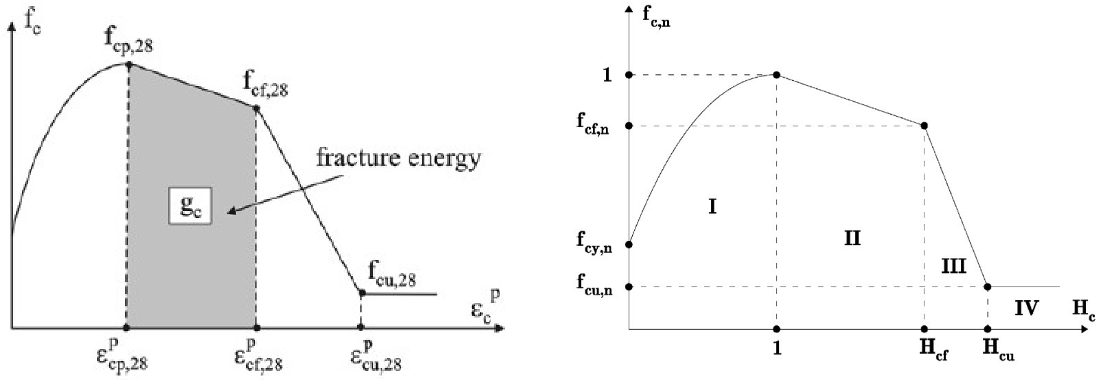

Figure 2.2 Uniaxial plastic strain curve (left) and normalised stress strain curve (right) (Schütz, et al., 2011)

Hardening and softening are depending on five dimensionless parameters which are based on the uniaxial compressive stress and the according strains (Schütz, et al., 2011). The values for f_{c0n}, f_{cfn} and f_{cun} can be derived form a normalised uniaxial compressive curve (Figure 2.2)

▪ f_{c0n}	Normalised initially mobilised strength
▪ f_{cfn}	Normalised failure strength

f_{cun}	Normalised residual strength
H_{cf}	State parameter for the softening regime
H_{cu}	State parameter for the residual state

Quadratic strain hardening: $0 \leq H_c \leq 1$

The elasto-plastic behaviour starts when the current linear elastic stress state intersects the yield surface. From that point on, the stress/strain curve describes a parabolic hardening until the peak strength is reached (Schütz, 2010). The following equation is adopted:

$$f_{cy,I} = f_c\left(f_{c0n} + (1 - f_{c0n})(2H_c - H_c^2)\right) \tag{2.5}$$

Linear strain softening: $1 \leq H_c \leq H_{cf}$

Is the deformation still ongoing after reaching the peak, the equation for a linear softening approach is applied until the defined stress state of the normalised compressive failure strength f_{cfn} is reached. For concrete this would mean that the material is crushed (Schütz, 2010). The equation for the adopted softening part is given as:

$$f_{cy,II} = f_c\left(1 + \left(f_{cfn} - 1\right)\left(\frac{H_c - 1}{H_{cf} - 1}\right)\right) \tag{2.6}$$

Linear strain softening: $H_{cf} \leq H_c \leq H_{cu}$

To prevent numerical issues, using the parameter f_{cun} will guide a linear reduction of stress until the residual value is reached (Schütz, 2010). The formula for this is:

$$f_{cy,III} = f_c\left(f_{cfn} + \left(f_{cun} - f_{cfn}\right)\left(\frac{H_c - H_{cf}}{H_{cf} - H_{cu}}\right)\right) \tag{2.7}$$

Linear strain softening: $H_c \geq H_{cu}$

From this stage on, perfect plasticity is acting and no changes in the stress state are occurring (Schütz, 2010). The residual part is guided by the following equation:

$$f_{cy,IV} = f_c\, f_{cun} \tag{2.8}$$

2.2.1 Assumptions

For an application of the Concrete Model on HSSR material several assumptions must be made depending on the characteristic properties of soil and rock opposed to concrete. This leads to a reduction of the independent input parameters from 25 to 11.

Time has a high influence on the behaviour of concrete, but for the calculation of the HSSR materials in this thesis time dependency is neglected. This includes the time dependency of stiffness and strength as well as creep and shrinkage. For the time dependent ratio of elastic stiffness $E_1\ /E_{28}$ and the ime-dependency of compressive strength $f_{c,1}/f_{c,28}$ the input value is set to one. The creep and shrinkage input parameters ϕ^{cr}, t_{50}^{cr}, $\varepsilon_{\infty}^{shr}$, t_{50}^{shr} as well as t_{hydr} are not implemented.

For the ductility parameters of the uniaxial plastic failure strain the assumption of $\varepsilon_{cp,1h}^{p} = \varepsilon_{cp,8h}^{p} = \varepsilon_{cp,24h}^{p} = \varepsilon_{cp}^{p}$ is made, neglecting the time dependency of the peak failure strain.

Several pre-studies show that the influence of an assumed tensile strength equal to the cohesion of the materials seems to have a neglectable influence on a triaxial compression test. Generally the Concrete Model typically recommends an input value of around 10 % of the strength in compression parameters for the strength in tension parameters $f_{t,28}$, f_{tun} and $G_{t,28}$. For the simulation of HSSR material in uniaxial and triaxial compression the tensile strength of the investigated materials is neglected and zero is recommended as input value. This assumption is made because no assured information of the tensile parameters for the investigated materials is available and the influence is not recognizable. Commonly the neglection of the tensile strength is assumed as a legit conservative assumption.

For the following calculations no safety factor is applied. Therefore the input parameters γ_{fc} and γ_{ft} are set to one.

3 Method

In this Master thesis three different materials are investigated using the Concrete Model. At first the equivalent parameters for the used material model will be determined and afterwards tested using a 3D drained triaxial test setup in PLAXIS. Additionally a case study will be done to test the applicability of the Concrete Model on a boundary value problem in 2D.

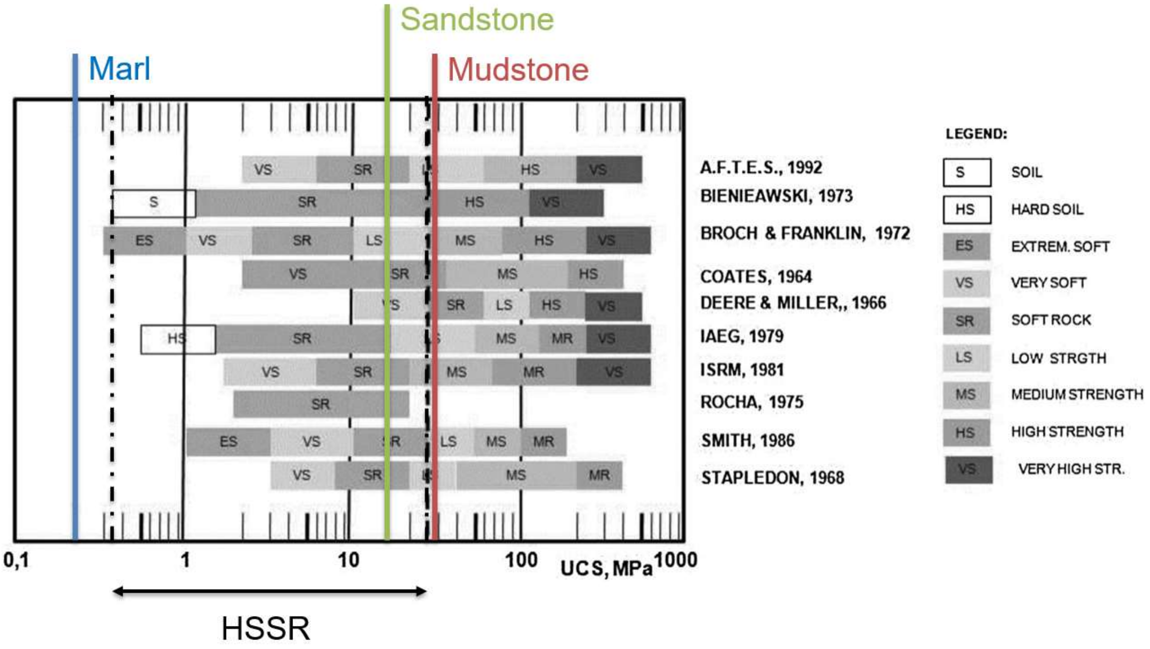

Figure 3.1 UCS of the investigated materials in correlation with several definitions of HSSR (Kanji, 2014)

All three materials are classified as HSSR materials as can be seen in Figure 3.1. The first material is a marl from Beaucaire which was investigated by Marcher (2003). With its UCS of 150 kPa this material lies on the lower end of the HSSR definition and should give information about the applicability of the model in a low stress regime. The sandstone laboratory results are provided by the Norwegian Geotechnical Institute and later on additionally published by Berre (2011). With a UCS of 17500 kPa this material will give some information of HSSR with medium strength. Finally, the Mudstone from Huang (2017) with an UCS of 26000 kPa represents the upper boundary of HSSR material. All three materials show a significant softening behaviour in the post peak regime.

3.1 Parameter determination

To apply the Concrete Model as a tool for hard soil-soft rock modelling the recommended parameters must be reinterpreted from concrete material behaviour to soil/rock behaviour. Therefore, several calculations and approaches are necessary which are explained in the following section. For these calculations the assumptions mentioned in 2.2.1 are valid. Other parameter determinations which are not mentioned here can be found in the Appendix.

3.1.1 Elasticity Modulus

The Concrete Model defines the elastic modulus E_{28} as a Young's modulus for fully cured concrete after 28 days. To find the equivalent modulus for HSSR a parameter study using the Soil Test Tool is done. Three different elastic moduli are applied in this stress point analysis to find the best fit. Therefore, the secant modulus at 50% of deviatoric loading (E_{50}), the oedometric loading modulus (E_{oed}) and the tangent modulus (E') are applied. The elastic modulus are derived from marl and applied in a uniaxial test (Figure 3.2).

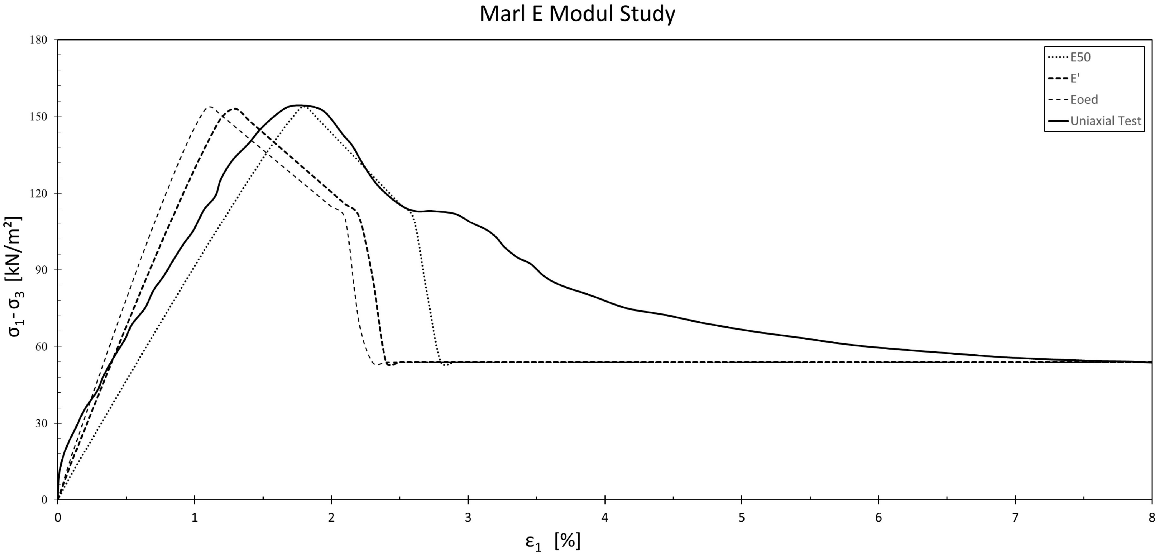

Figure 3.2 E Modul Study on marl (Soil Test Tool)

Figure 3.2 shows that the most suitable modulus as an equivalent for E_{28} in the Concrete Model is the secant modulus at 50% for deviatoric loading (E_{50}). The figure above shows, that E_{50} perfectly matches the peak strain and approximates the pre peak behaviour in a sufficient way. This study is searching for the most suitable elastic modulus for triaxial compression conditions, other loading situations will require further studies.

It must be considered that the Concrete Model has no stress dependent stiffness included, because generally the stiffness development for concrete is depending on time and not on the occurring stress state. Therefore, E_{50} is calculated for every applied confining pressure separately with respect to the original triaxial data. This should provide a proper modulus for every stress state.

The Poisson's ratio is assumed with 0.25 for all calculations in this thesis (CM and HS).

The following table shows the elasticity modulus for the investigated marl, sandstone and mudstone, with the corresponding reference pressure.

Table 3.1 E_{50} for Mudstone, Marl and Sandstone

Marl						
Reference Pressure [kPa]	0	50	100	200		
E_{50} [kPa]	10200	18000	31000	42000		

Mudstone						
Reference Pressure [MPa]	0	10	20	30	40	50
E_{50} [MPa]	5480	6000	6100	6100	6757	9695

Sandstone						
Reference Pressure [MPa]	0	2	5	10		
E_{50} [MPa]	2960	7795	9925	11840		

As shown in Table 3.1, the Young's Modulus is changed in every applied confining stage to guarantee a proper behaviour. Marl shows a high stress dependent stiffness while sandstone and mudstone are showing less increase with increasing confining pressure.

3.1.2 Linear Elastic Range

For the linear elastic behaviour, the Concrete Model uses the parameter f_{c0n}, which can be derived from a normalised uniaxial stress/strain curve. Figure 3.3 shows the influence of the parameter f_{c0n} pre-peak with various values using the PLAXIS soil test tool.

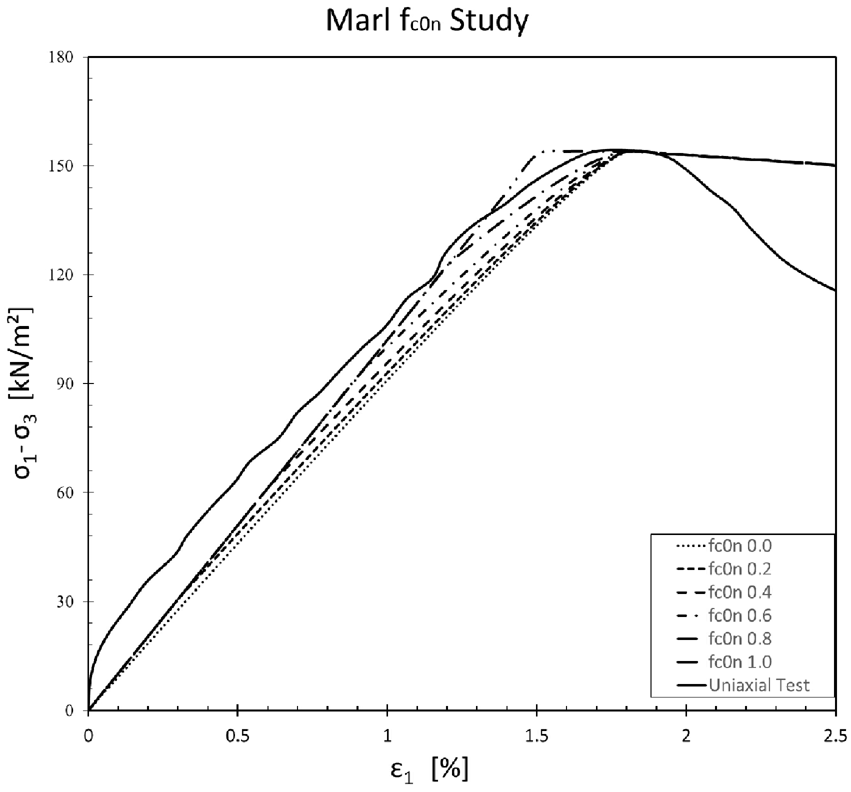

Figure 3.3 Linear elastic part of a uniaxial test on marl

In Figure 3.3 it can be seen that f_{c0n} has no influence on the post peak behaviour. In the pre peak area, the linear part increases with increasing f_{c0n}. The finally used values for f_{c0n} are:

Mudstone	0.1	[-]
Sandstone	0.05	[-]
Marl	0.05	[-]

3.1.3 Parameter a

With increasing confining pressure a more ductile behaviour and a shifting of the peak strain is possible. To take this into account, the parameter a gives a relation between the increase of ε_{cp} and the mean deviatoric stresses. This input parameter could be derived by the following equation using the uniaxial peak strain, the uniaxial strength and the applied confining pressure (PLAXIS, 2019):

$$\varepsilon_{cp} = \varepsilon_{cp,UC}\left(1 + a\frac{\sigma_3}{f_{c,28}}\right) \tag{3.1}$$

Using the equation above, the following table shows the back calculated values for the measured peak strains from the laboratory triaxial tests.

Table 3.2 Results of parameter a for mudstone, sandstone and marl

Marl				
σ3	εcp, TC	εcp, UC	$f_{c,28}$	a
[kPa]	[-]	[-]	[kPa]	[kPa]
0	0.01811	0.01811	154	-
50	0.01872	0.01811	154	0.1
100	0.02677	0.01811	154	0.7
200	0.02398	0.01811	154	0.2

Mudstone				
σ3	εcp, TC	εcp, UC	$f_{c,28}$	a
[kPa]	[-]	[-]	[kPa]	[kPa]
0	0.00637	0.00637	26 274	-
10000	0.01316	0.00637	26 274	2.8
20000	0.01521	0.00637	26 274	1.8
30000	0.01798	0.00637	26 274	1.6
40000	0.02187	0.00637	26 274	1.6
50000	0.01779	0.00637	26 274	0.9

Sandstone				
σ3	εcp, TC	εcp, UC	$f_{c,28}$	a
[kPa]	[-]	[-]	[kPa]	[kPa]
0	0.01253	0.01253	17 452	-
2000	0.00510	0.01253	17 452	-5.2
5000	0.00585	0.01253	17 452	-1.9
10000	0.00733	0.01253	17 452	-0.7

As it can be seen in Table 3.2 the range of parameter a for the used materials is between - 5.2 and 2.8, which is far less than the values of 16 to 20 which the PLAXIS material manual recommends for concrete. This indicates that the shifting of the peak for HSSR material is less than for concrete. Even though the parameter changes with the applied confining pressure, for every material only one representative value is used for all stages. The uniaxial test of sandstone shows a far more ductile behaviour than the triaxial tests, which leads to negative values for a. Therefore the resulting value for a is taken only from the triaxial results where the peak strain stays more or less constant.

Negative values for a are not possible as an input parameter in the Concrete Model. The finally used values for a are:

Mudstone	2 [-]
Sandstone	0 [-]
Marl	1 [-]

3.1.4 Friction and dilatancy angle

The friction angle for the investigated materials is derived from Mohr's circles by applying a tangent to provide an approximate fit for the friction angle φ. The following graphs from Figure 3.4 to Figure 3.6 show how the tangent is applied for the used materials.

The friction is overestimated for sandstone under high confining pressures.

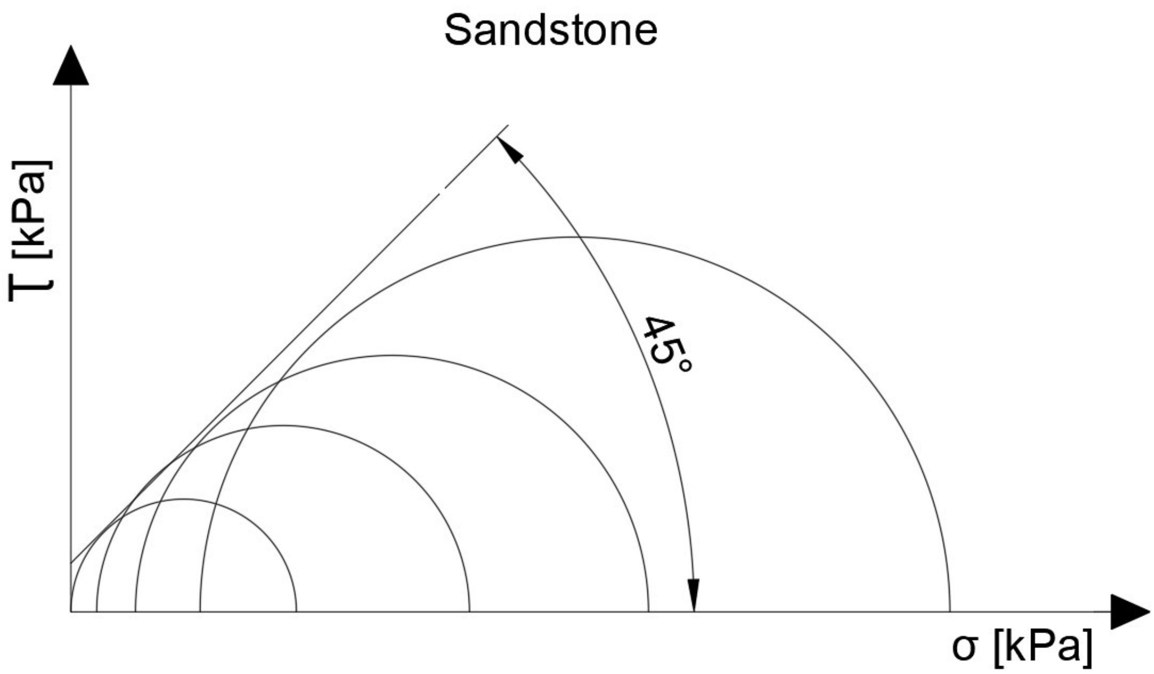

Figure 3.4 Mohr circles for sandstone

The friction angle for the applied confining pressure state of 100 kPa is underestimated, which is discussed later on in 5.1.

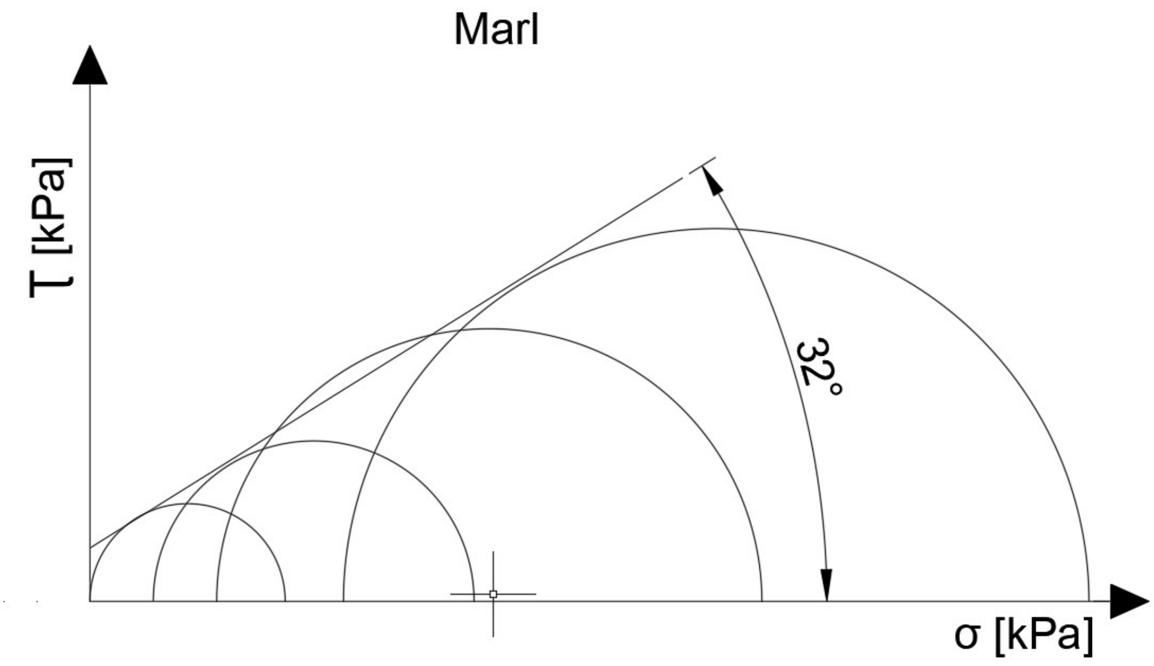

Figure 3.5 Mohr circles for marl

The second confining pressure state of 10.000 kPa must be neglected in order to provide an overall valid friction angle for the mudstone test series. This will lead to an underestimation of the peak strength in the following numerical simulation.

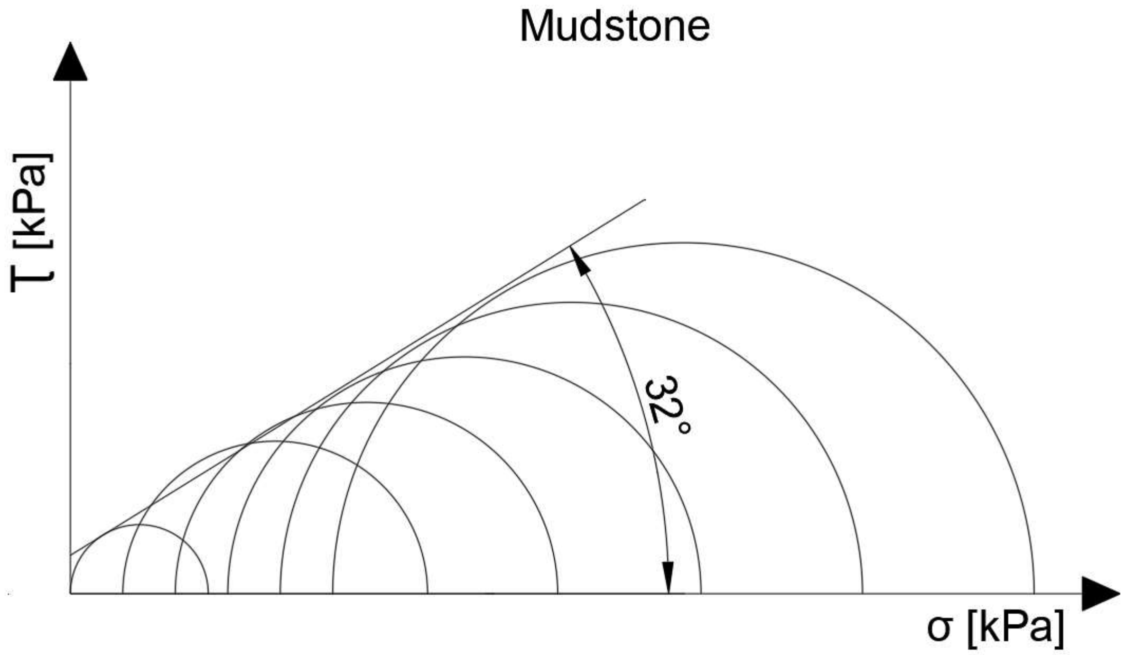

Figure 3.6 Mohr circles for mudstone

The friction angles used for the numerical analysis with the Concrete Model are:

Sandstone	45°
Marl	32°
Mudstone	32°

The dilatancy angle ψ was estimated for the mudstone and sandstone by using the following approximation:

$$\psi = \varphi - 30 \tag{3.2}$$

For the marl, the provided value from (Marcher, 2003) is used, were this parameter is investigated in more detail. The used values for the dilatancy angle in the numerical simulations are:

Sandstone	15°
Marl	10°
Mudstone	2°

3.1.5 Strength in compression

The fracture energy g_c is defined as the area under the first linear softening part (Figure 2.2) and can be derived from a normalised uniaxial test (PLAXIS, 2019) and (Schütz, 2010). The basic equation for deriving g_c is:

$$g_c = \frac{f_{c,28} * f_{cfn}}{2} \left(\varepsilon_{cp}^{p} - \varepsilon_{cf}^{p} \right) \tag{3.3}$$

For deriving the plastic peak and the plastic failure strain, the elastic strain component has to be subtracted from the total strain (Schütz, 2010). This is done using the following correlation:

$$\varepsilon_c^p = \varepsilon_c^{total} - \frac{f_c}{E} \tag{3.4}$$

The fracture energy is mesh dependent and has to be recalculated when the mesh geometry changes. To derive the right fracture energy the calculated g_c from the laboratory test must be multiplied with the equivalent length of the finite element L_{eq} (PLAXIS, 2019). The equivalent length could be derived from the average element size of the finite element A_{el} and the number of stress points per element n_{GP}.

$$L_{eq} = 2\sqrt{\frac{A_{el}}{n_{GP}\sqrt{3}}} \tag{3.5}$$

The original triaxial samples of the investigated materials (marl, mudstone, sandstone) have different sample sizes which is leading to different L_{eq} values depending on the used mesh. The stress point analysis using the soil test tool depends on the original sample height as characteristic element length. The original sample sizes are listed below:

▪ Marl (h = 0.1 m, ø = 0.1 m)	L_{eq} = 0.0574 m
▪ Mudstone (h = 0.1 m, ø = 0.05 m)	L_{eq} = 0.0477 m
▪ Sandstone (h = 0.075 m, ø = 0.038 m)	L_{eq} = 0.0395 m
▪ Soil test tool	L_{eq} = original sample height in meter

The final input parameter G_c can now be derived as:

$$G_c = g_c \times L_{eq} \tag{3.6}$$

3.1.6 Standard G_c Variation

The determination of the fracture energy G_c and the failure strength f_{cfn} has a crucial influence on the post peak behaviour of the investigated material. Both values are calculated from a normalised uniaxial stress/strain curve. Recommended values for the failure strength f_{cfn} and G_c are 0.1 – 0.2 and 30 – 70 kN/m respectively. These parameter range is generally valid for concrete. To estimate the fracture energy usually an iterative process within the proposed range is done using a best fit principle.

However, during this thesis it turned out that this values and procedure are representative for the material behaviour of hard soil soft rock. The definition of f_{cfn} as the point where the concrete structure is heavily destroyed is not suitable for HSSR simulations. Furthermore, the recommended fracture energy is overestimating the calculated G_c by a factor of 10 depending on the material. In addition, a decoupled variation of the fracture energy G_c and the failure strength f_{cfn} makes no sense because of their relation to each other forming Zone II in the stess/strain plot. To find a sufficient way to take the various conditions of the post peak state for HSSR materials into account a suitable method for determining f_{cfn} and G_c has to be introduced. Based on Hoek and Brown's classification of very good, average, and very poor quality rock mass with their assigned characteristics elastic-brittle, strain-softening, and elastic-plastic a corresponding way of determining the required strength parameters is introduced (Figure 3.7). Poor quality soft rock mass is generally considered with a GSI lower than 30, but according to the existing classification of Hoek and Brown for this method 25 is considered instead.

▪ High quality rock mass (GSI > 75)	Top Failure Strength
▪ Average quality rock mass (25 < GSI < 75)	Intermediate Failure Strength
▪ Very poor quality soft rock mass (GSI < 25)	Residual Failure Strength

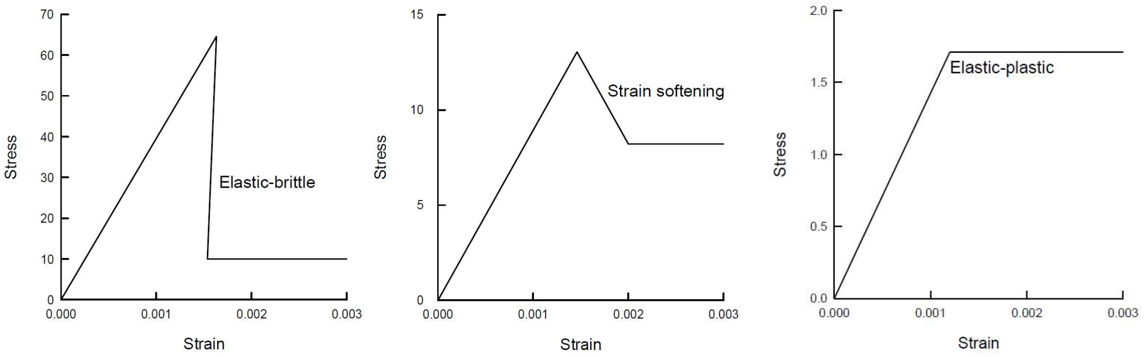

Figure 3.7 The post peak behaviour of different rock mass qualities (E. Hoek, 1997)

The idea is to couple the failure strength f_{cfn} and the fracture energy G_c with respect to the material behaviour to reproduce a proper post peak behaviour. The following three figures illustrate the principle of applying the Top, Intermediate, and Residual Failure Strength introduced in this thesis.

The Top Failure Strength definition assumes a f_{cfn} between 0.80 and 0.95 to represent brittle material behaviour. The coupled calculation of area II leads to a low amount of fracture energy which causes a drop down in the stress/strain curve. This is characteristic for HSSR materials with a high UCS.

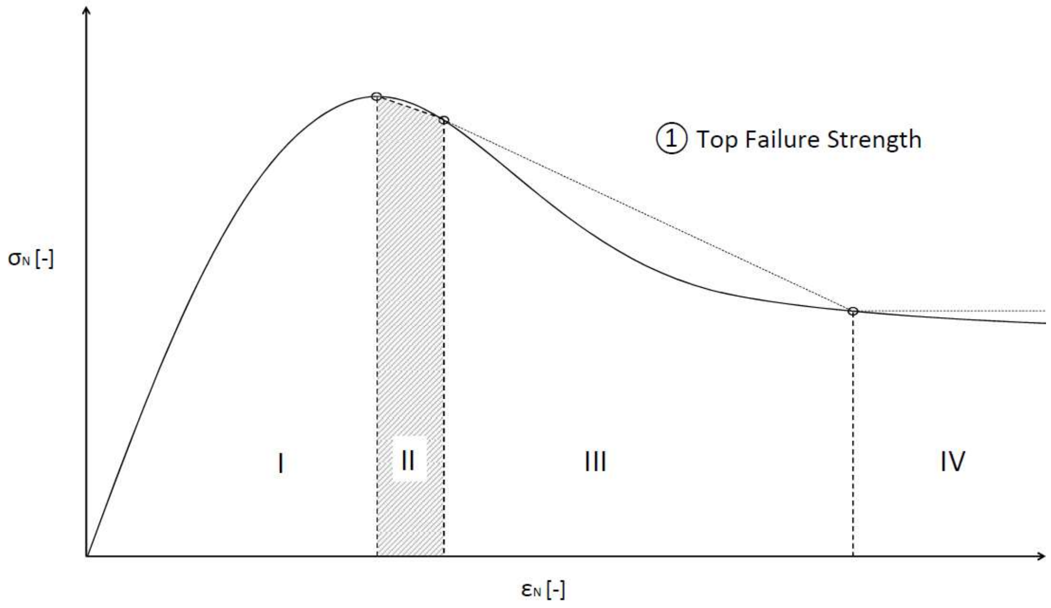

Figure 3.8 Top Failure Strength definition for brittle materials

If the material shows ductile behaviour combined with a high uniaxial strength an intermediate definition of the failure strength could serve as the best approximation for the material behaviour. Therefore, a failure strength in the range of 0.55 to 0.8 is suggested to deliver still a significant dropdown in the stress strain area. The lower value for f_{cfn} will also result in a higher fracture energy which should provide a more ductile behaviour in Zone II.

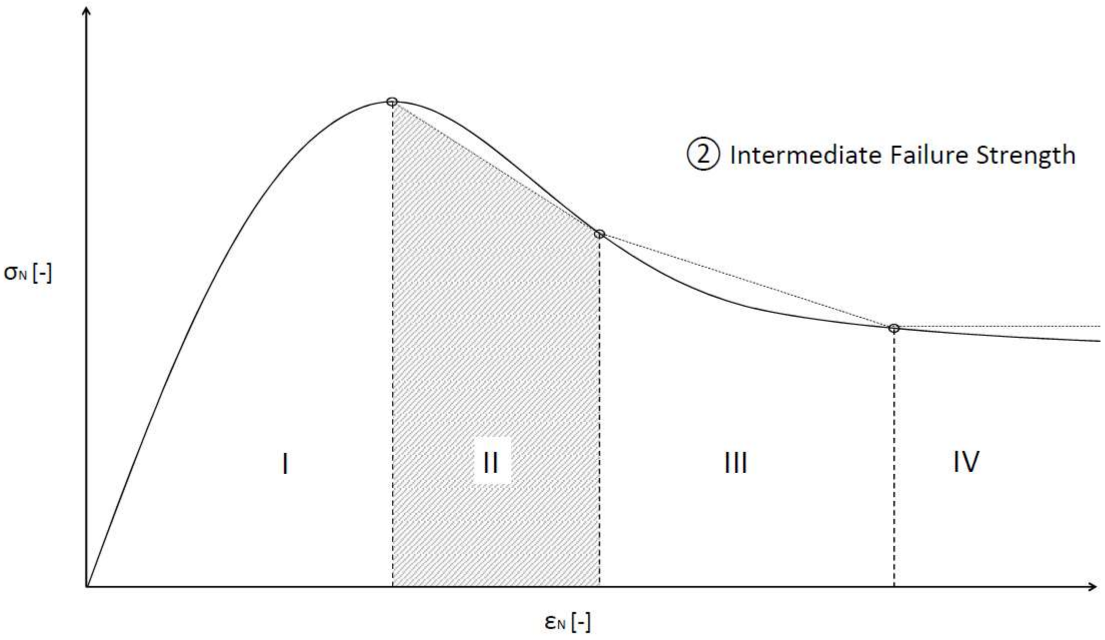

Figure 3.9 Intermediate Failure Strength

HSSR material with a low UCS show generally also a ductile post peak behaviour. To provide a smooth transition from peak to residual state the Residual Failure Strength definition should be applied. Therefore, f_{cfn} and f_{cun} can be set equal to create a combined softening area. This leads to the highest amount of fracture energy and should be applied for ductile material behaviour. To generate perfectly plastic conditions f_{cfn} and f_{cun} have a recommended value of 1 which will avoid any softening behaviour.

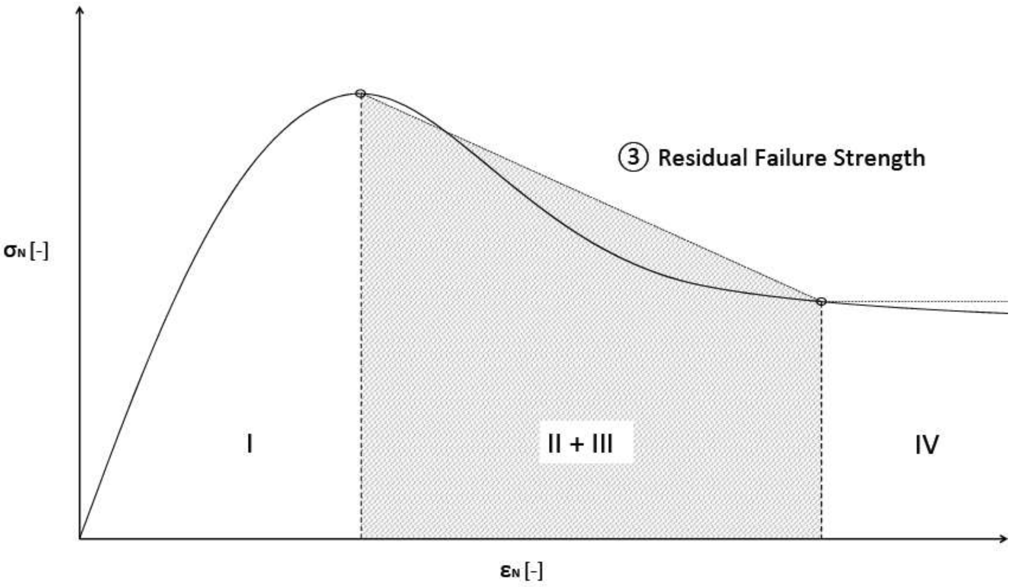

Figure 3.10 Residual Failure Strength

The here introduced values for the failure strength are valid for the investigated materials marl, mudstone, and sandstone. To obtain which Standard G_c Variation is approximating the individual mechanical behaviour the best, all three variations are applied on every material for all confining pressure stages.

3.1.7 Determination of strength parameters

In a first parameter study, all three methods for determining the strength parameters and the fracture energy are applied on the tested materials. How the parameters are determined is shown from Figure 3.11 to Figure 3.13. The position of the peak strength and the residual strength, which stay constant, are marked by a white dot, while the changing failure strength is noted by a black dot.

For the marl, the failure strength f_{cfn} is defined with 0.92, 0.7, and 0.35 percent of the peak strength f_c. The Residual Failure Strength definition generates a fracture energy nearly ten times bigger than the Top Failure Strength definition. The numerical simulations later on show what influence this will have on the post peak behaviour.

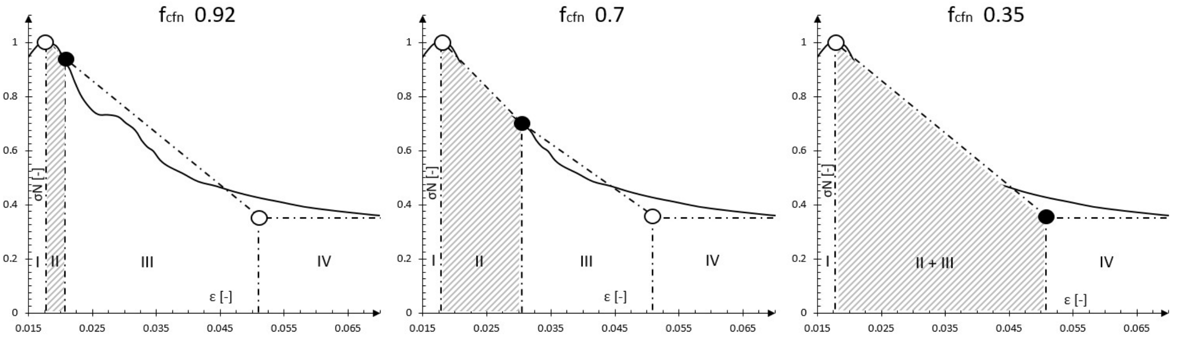

Figure 3.11 Standard G_c variation for marl

As it can be seen in Figure 3.11 the amount of fracture energy is increasing strongly with decreasing failure strength. In Table 2.3 the input parameters for the Standard G_c Variation are summarized.

Table 3.3 Parameters for the Standard G_c Variation of Marl

Marl							
	f_c [kPa]	ε_{cp} [-]	f_{cfn} [-]	ε_{cf} [-]	f_{cun} [-]	g_c [kN/m^2]	G_c [kN/m]
Top Failure strength	154	0.01811	0.95	0.021	0.35	0.434	0.0249
Intermediate Failure strength	154	0.01811	0.7	0.031	0.35	1.687	0.0968
Residual Failure strength	154	0.01811	0.35	0.051	0.35	3.292	0.1962

The mudstone shows a more brittle behaviour than the marl, including a high uniaxial strength. Because of the brittle failure, a clear definition of the residual strength is not possible. For this case, the residual strength is estimated with 0.55, just slightly before the test fails.

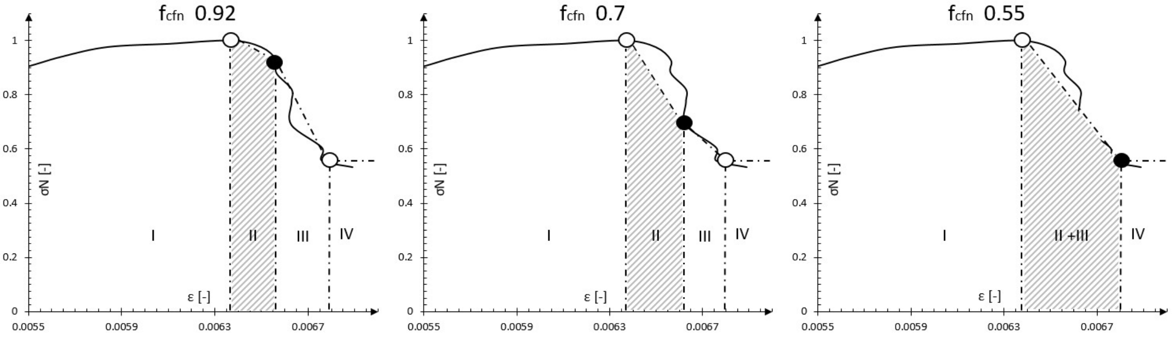

Figure 3.12 Standard Gc variation for mudstone

As shown in Figure 3.12 the amount of fracture energy is increasing with decreasing failure strength, but only by a factor of two as opposed to the behaviour of the marl. The following table shows the chosen input parameters for the numerical simulation of the mudstone.

Table 3.4 Parameters for the Standard G_c Variation of mudstone

Mudstone							
	f_c [kPa]	ε_{cp} [-]	f_{cfn} [-]	ε_{cf} [-]	f_{cun} [-]	g_c [kN/m^2]	G_c [kN/m]
Top Failure strength	26274	-0.00636	0.92	-0.00656	0.55	5.044	0.241
Intermediate Failure strength	26274	-0.00636	0.7	-0.00662	0.55	5.807	0.277
Residual Failure strength	26274	-0.00636	0.55	-0.00675	0.55	7.941	0.379

The sandstone shows the most brittle behaviour of all investigated materials. The uniaxial test fails slightly after the peak strength is reached. In this case the definitions for the Standard G_c Variation are done with respect to the triaxial test results. They show a constant softening regime at 35 % of their peak strength. Therefore, the residual strength f_{cun} is approximated on an imagined uniaxial residual state of 0.35. The Intermediate Failure Strength definition is interpolated between case one and three.

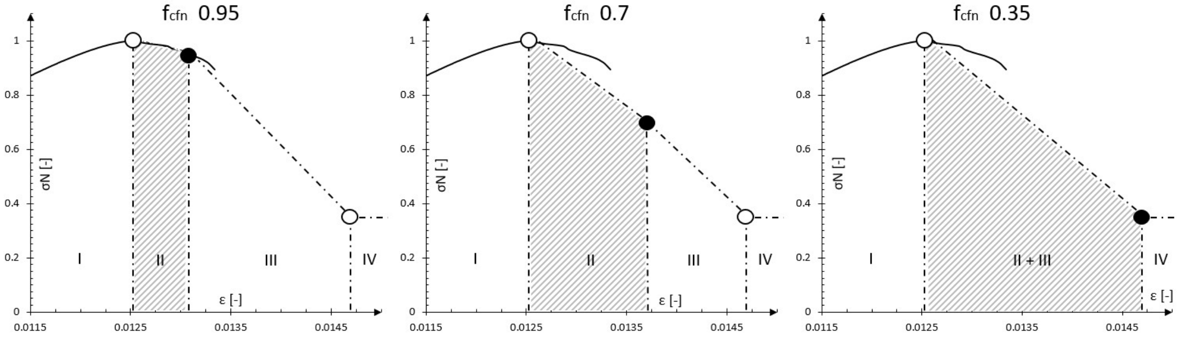

Figure 3.13 Standard G_c Variation for sandstone

The fracture energy increases from case one to three by a factor of three and provides with 1.023 kN/m the highest value for G_c of the three investigated materials.

Table 3.5 Parameters for the Standard G_c Variation of sandstone

Sandstone							
	f_c [kPa]	ε_{cp} [-]	f_{cfn} [-]	ε_{cf} [-]	f_{cun} [-]	g_c [kN/m²]	G_c [kN/m]
Top Failure strength	17452	-0.01253	0.95	-0.013	0.35	8.508	0.336
Intermediate Failure strength	17452	-0.01253	0.7	-0.0137	0.35	17.801	0.703
Residual Failure strength	17452	-0.01253	0.35	-0.0147	0.35	25.916	1.023

3.2 Modelling in 3D

To reproduce the triaxial and uniaxial test data a 3D model is generated on which the uniaxial and triaxial tests are simulated. The used software is Plaxis 3D.

3.2.1 3D Model

The model dimensions change slightly with respect to the original sample height and diameter. The sample parameters for the investigated materials are listed below:

- Marl (h = 0.1 m, ø = 0.1 m)
- Mudstone (h = 0.1 m, ø = 0.05 m)
- Sandstone (h = 0.075 m, ø = 0.038 m)

Generally the 3D model consists of a cylindrical volume which represents the HSSR sample. The upper and lower boundary conditions are surfaces with linear elastic properties and a high stiffness to represent the steel plates of the real test. Between the steel plates and the soil volume additional surfaces are introduced as interfaces to simulate the lubrification of the plates. The top interface has a friction angle of 2.5 degrees and the lower interface has a friction angle of five degrees.

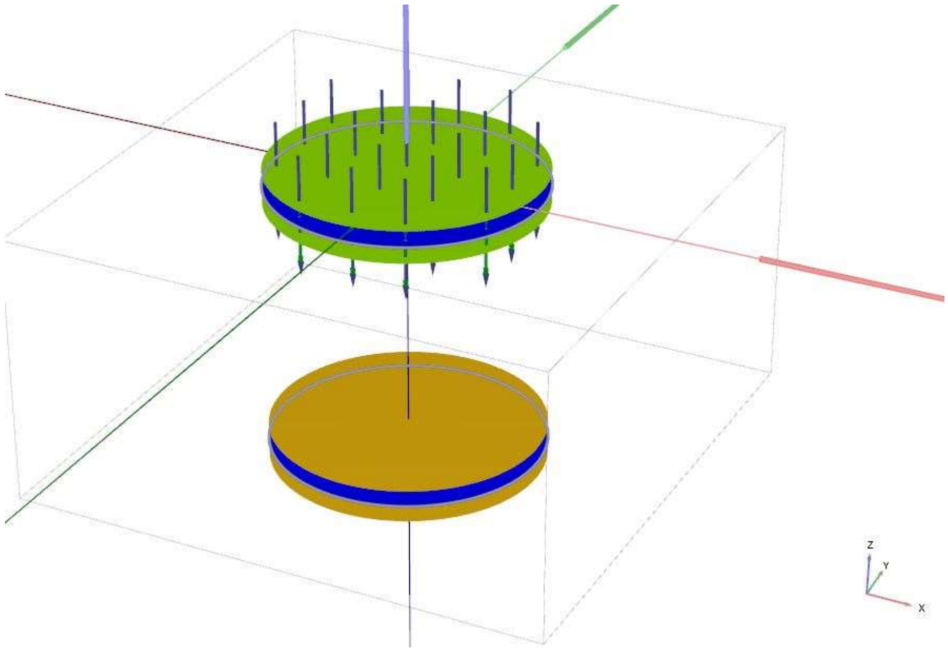

Figure 3.14 The modelled steel plates and interfaces (ø = 10 cm)

To simulate the triaxial stress state two surface loads are used which are activated in the isotropic loading stage to represent the confining pressure. After the isotropic loading the prescribed displacements are activated at the top plate and will deform the sample to a maximum value of one centimetre.

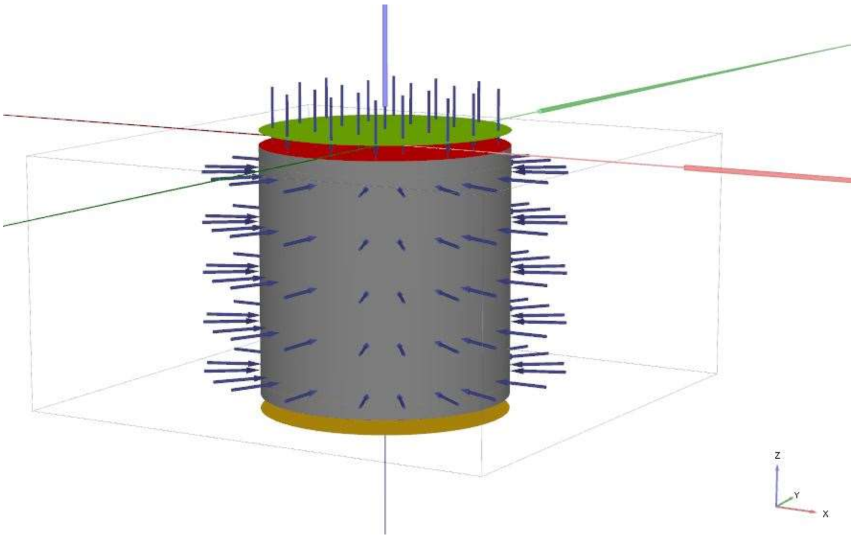

Figure 3.15 The 3D triaxial test model (h and d = 10cm)

To measure the acting stress state and the deformation a stress point and a node, centred on the top of the soil volume are used. For the calculation of the volumetric strains four points are arranged in a circle around the outer perimeter of the soil volume. All triaxial-, and uniaxial tests are calculated under drained conditions.

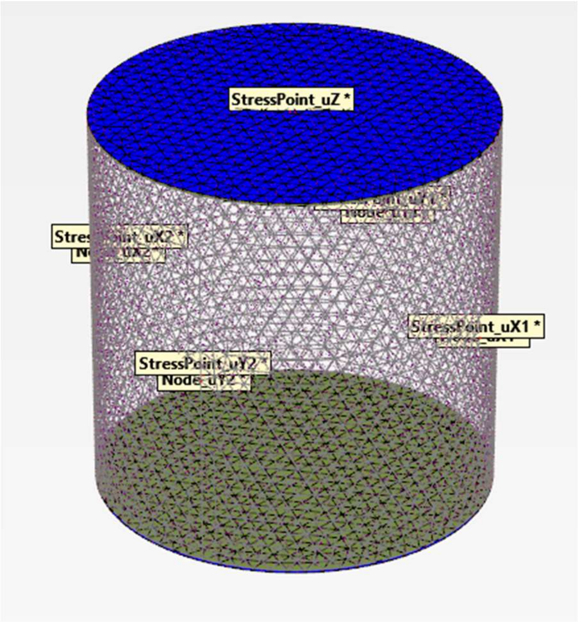

Figure 3.16 Used mesh and measuring stress points and nodes (h and d = 10cm)

3.2.2 Size and Shape Effects

The size and shape of a sample can have an influence on the observed results especially in the softening regime. For the laboratory triaxial tests and the numerical model cylindrical samples are used with varying diameters and heights. The following figure will give an overview on what the geometrical influence on the results can look like.

- Marl: L/D = 1:1 Diameter = 10.0 cm (approx. 4'')
- Mudstone: L/D = 2:1 Diameter = 5.0 cm (approx. 2'')
- Sandstone: L/D = 2:1 Diameter = 3.8 cm (approx.1.5'')

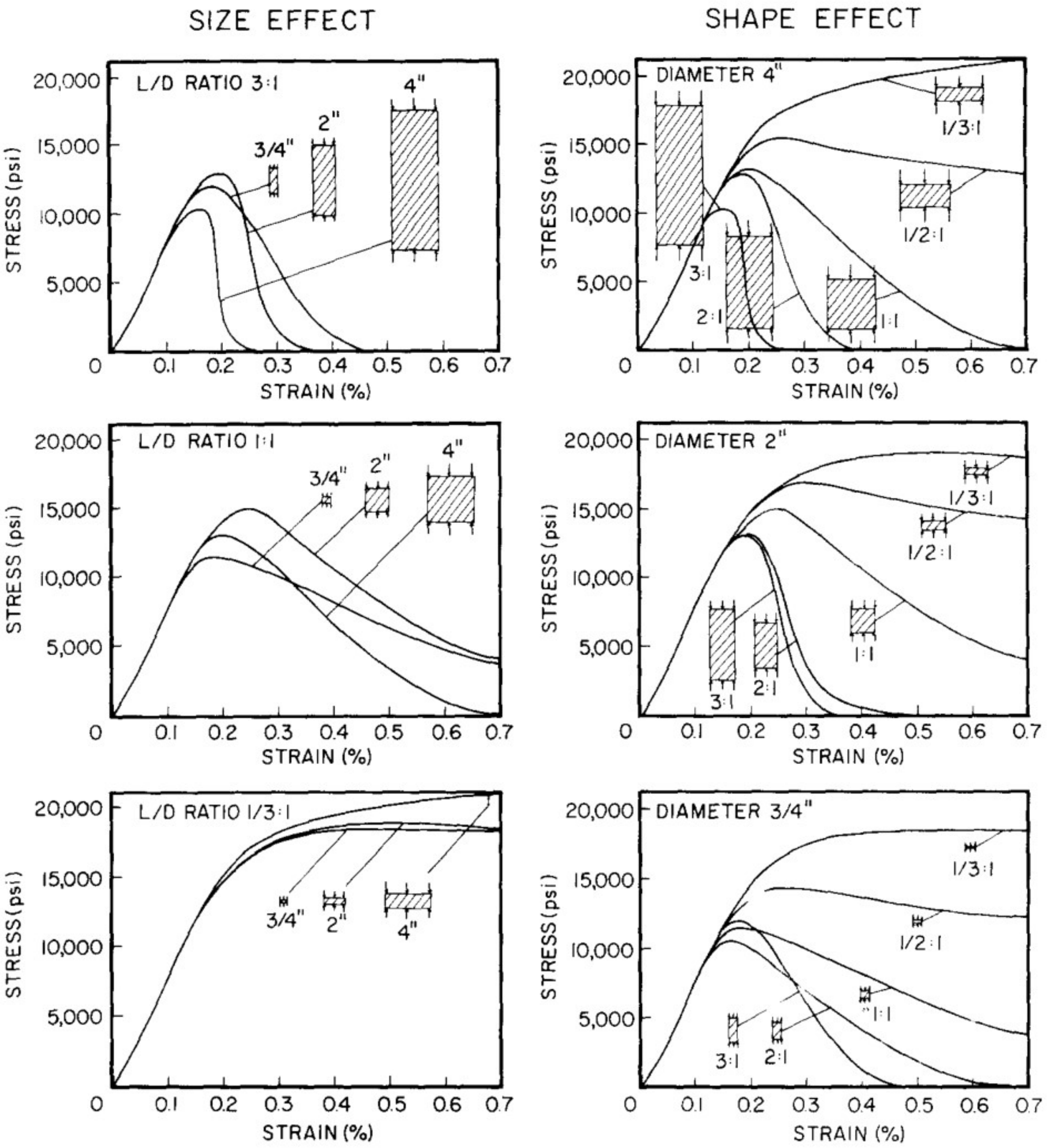

Figure 3.17 Size and shape effects for uniaxial compression observed for marble (Read, et al., 1984)

3.2.1 Feasibility study

As a first trial of the model and the main target of simulating the softening behaviour for HSSR materials, a uniaxial compression test is simulated on concrete. The input parameters are taken from (Schädlich, et al., 2016) and are shown in the table below.

Table 3.6 Parameter set for an uniaxial test on concrete

Concrete								
E_{28} [Gpa]	φ [°]	ν [-]	f_c [kPa]	ε_{cp} [-]	f_{c0n} [-]	f_{cfn} [-]	f_{cun} [-]	Gc [kN/m]
28	37	0.2	22000	-0.0007	0.15	0.2	0.2	1.722

The main goal of this feasibility study is to obtain a working 3D model, as introduced in 3.2.1 and a steady calculated post peak behaviour. The successful simulation of the uniaxial test for concrete in Figure 3.18 shows that a simulation of the softening regime in 3D using the Concrete Model is possible. The next step is the simulation of HSSR material using this model set up with the calculated parameters from 3.1 for marl, mudstone, and sandstone. The results of this drained uniaxial-, and triaxial test are shown in 4.1.

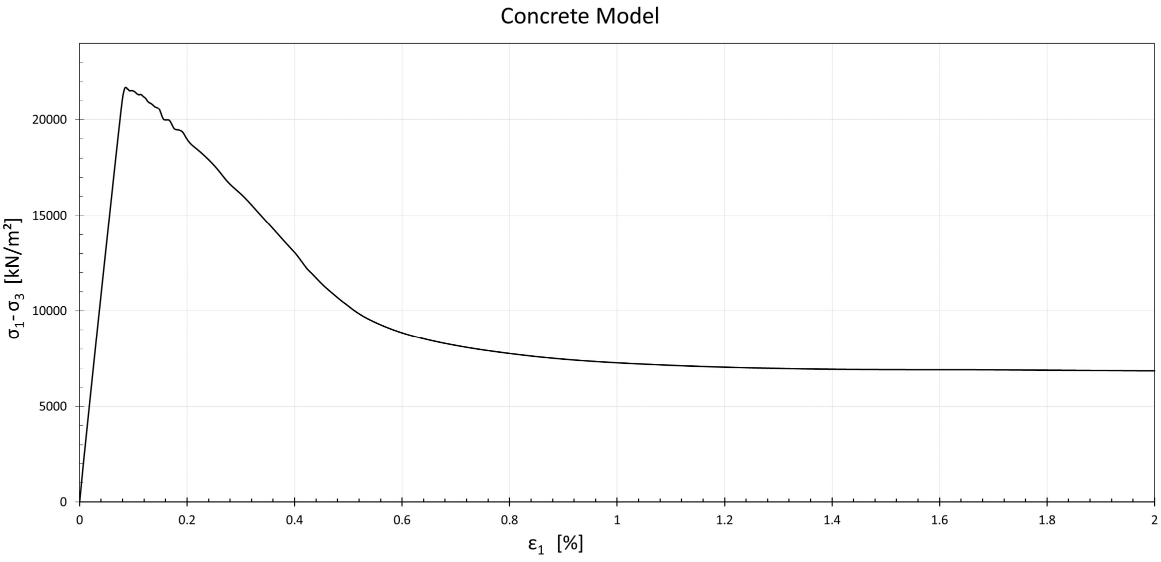

Figure 3.18 Simulation of an uniaxial test on concrete

3.2.2 Mesh dependency

To investigate the influence of the mesh on the calculation results a mesh dependency study is done. Therefore the mesh of a uniaxial test (marl) is refined in several steps from Mesh_1.0 (37 Elements) to Mesh_0.04 (77450 Elements). The reduction of the mesh coarseness parameter in PLAXIS leads to a refined mesh with a higher amount of elements (Table 3.7). The results of this study on the stress/strain behaviour could be observed in Figure 3.19 Plot of the deviatoric stresses over strains for the coarseness determinationFigure 3.19 and for the applied load M_{stage} in Figure 3.20. For all calculations Ten-noded elements are used.

The following table shows the parameter variation for the determination of the mesh dependency.

Table 3.7 Parameters for mesh dependency determination

Mesh Coarseness	Elements	Nodes	Steps	Step at failure
1	37	141	4000	77
0,9	37	141	4000	81
0,8	37	141	4000	86
0,7	37	141	4000	93
0,6	52	186	4000	126
0,5	94	299	4000	147
0,4	132	411	4000	160
0,3	330	850	4000	175
0,2	932	2067	4000	2931
0,1	5940	10773	4000	4000
0,07	15495	25992	4000	4000
0,06	25334	41056	4000	4000
0,05	41687	65931	4000	4000
0,045	57269	88985	4000	4000
0,04	77450	119168	4000	4000

For the determination of the appropriate mesh fineness the results of the coarseness variations are all plotted in one figure to obtain at which degree of fineness the resulting curves in the q over u_z space are getting constant. The corresponding number of elements for the meshes are shown in Table 3.7.

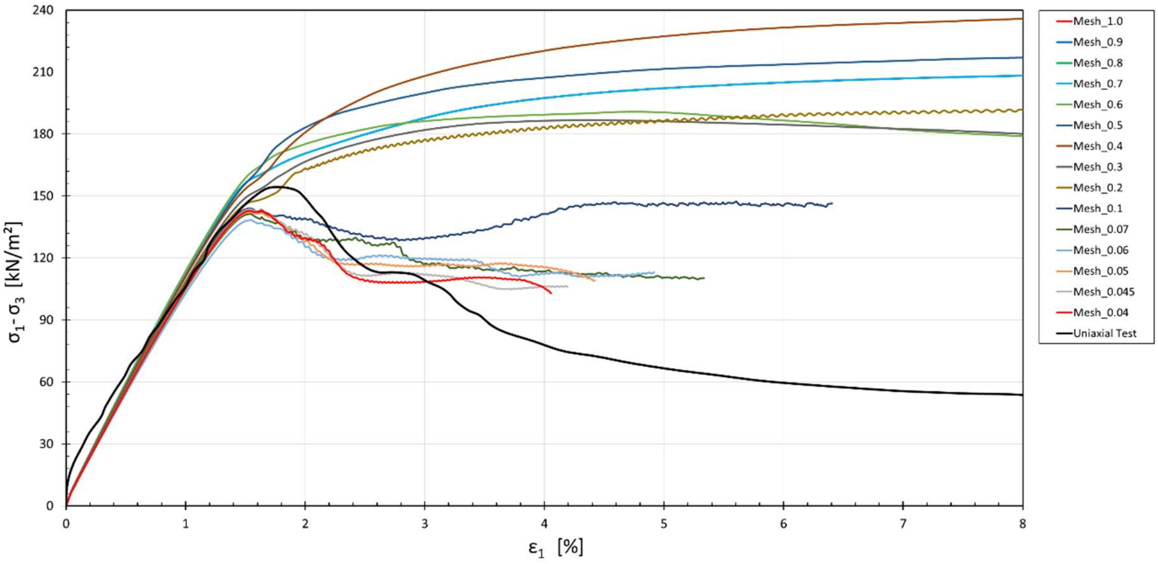

Figure 3.19 Plot of the deviatoric stresses over strains for the coarseness determination

The highest drop of M_{stage} can be observed between Mesh 0.3 and 0.2. From this point on the influence of the mesh fineness on the applied load is getting neglectable.

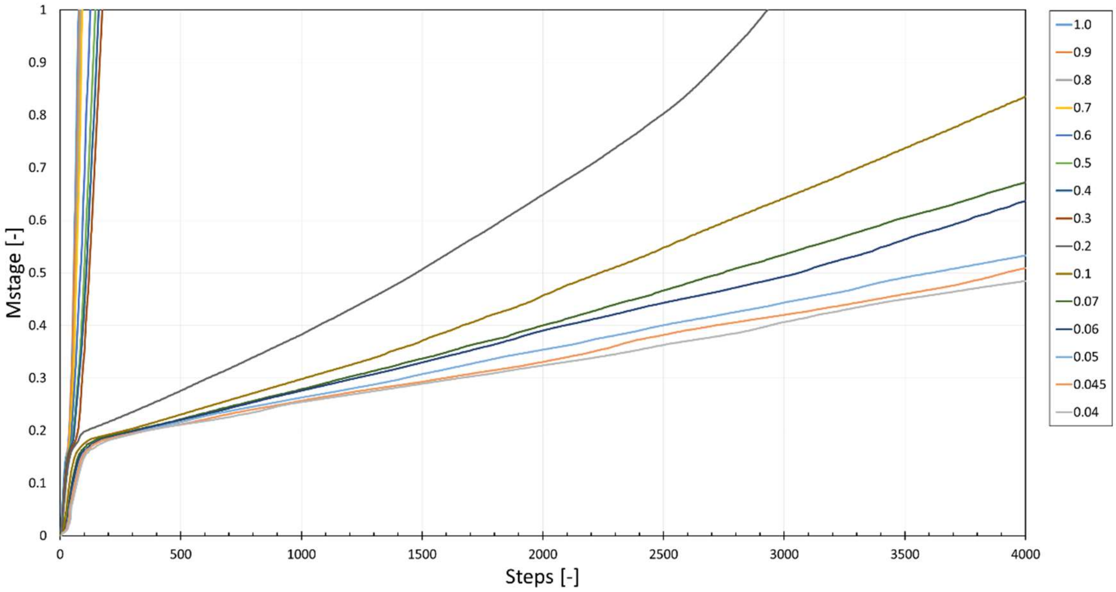

Figure 3.20 Plot of M_{stage} over steps for the coarseness determination

3.2.3 Shear band development depending on mesh fineness

Beside the fit of laboratory- and simulated stress/strain curves the development of the shear band in the sample is also an important indicator for the quality and plausibility of the results. However, the shear band development is highly influenced by the mesh fineness and must represent the real failure mechanism. Therefore, the following figures show the incremental deviatoric stresses in the sample with respect to the mesh fineness illustrated in Table 3.7.

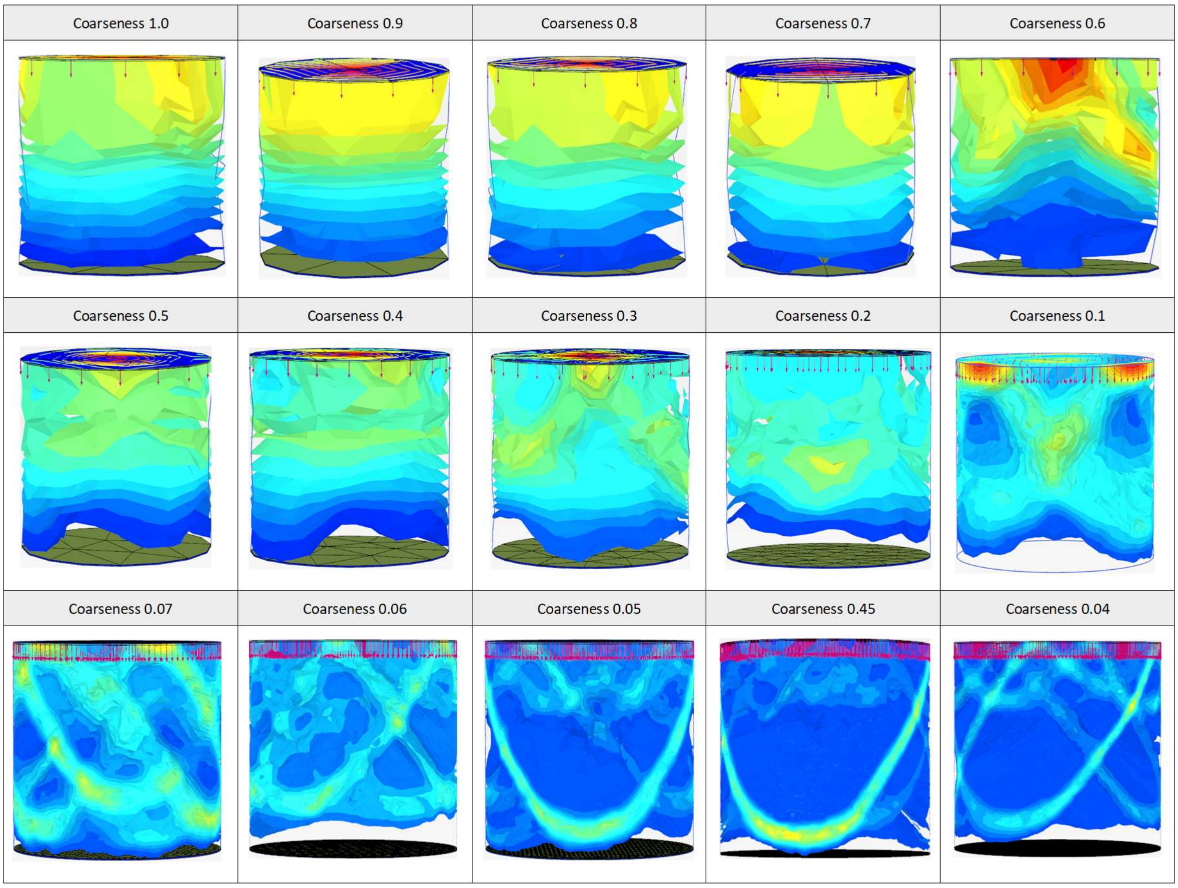

Figure 3.21 Developement of the shear band with increasing mesh fineness (marl)

The shear band starts to develop with a mesh coarseness factor below 0.2 (~1000 elements). Beyond this degree of fineness, the shear band gets more discretised with every mesh refinement step. The shear band quality does not benefit from a further increase of elements beyond 42000 (fineness factor = 0.05). This refinement just causes an enormous increase in calculation time. Therefore, a fineness factor of 0.05 leads to the best combination of shear band development and computation effort.

4 Results

This chapter shows the results of the 3D simulations in Plaxis where uniaxial and triaxial compression tests are simulated. In addition a case study is conducted to observe the behaviour of the Concrete Model on a real boundary value problem.

4.1 Parameter Study

The results of the parameter study on marl, sandstone, and mudstone are illustrated with respect to several confining pressure stages (drained triaxial tests). In addition, the influence of the parameter variation on the stress/strain behaviour and the softening regime is shown.

The herein introduced Standard G_c Variation (3.1.6) is applied to the materials, which means that the strength in compression parameter sets for the Top, Intermediate, and Residual Failure Strength are applied. In addition to the results of the Standard G_c Variation the following parameter are investigated using only the Top Failure Strength principle:
The dilatancy angle ψ and the fitting parameter a are varied to observe the influence on the volumetric behaviour and the shift of the plastic peak strain. All dough a decoupled variation of the fracture energy G_c and the failure strength f_{cfn} is physically not recommended (3.1.6) a variation of f_{cfn} with fixed fracture energy is illustrated in (4.1.6). This variation should outline the influence of the failure strength on the softening regime. Finally, the residual strength f_{cun} and its influence on Zone IV (residual level) is shown.

4.1.1 Standard G_c variation for marl

In this chapter the influence of the three different fracture energy definitions can be observed for marl in four different confining pressure stages. The real laboratory test results from the laboratory are shown in the following graphs from Figure 4.1 to Figure 4.4 as a solid black line, while the numerical results are given as variations of dashed lines. All results are mapped in a deviatoric stress-strain area.

The uniaxial compression test for marl in the figure below shows a very stiff initial behaviour up to 10 kPa. After that, the stress/strain curve increases linearly to a value of 130 kPa where the hardening starts. The test finally reaches a peak value of 154 kPa and then shows a ductile softening behaviour down to a residual value of 50 kPa.

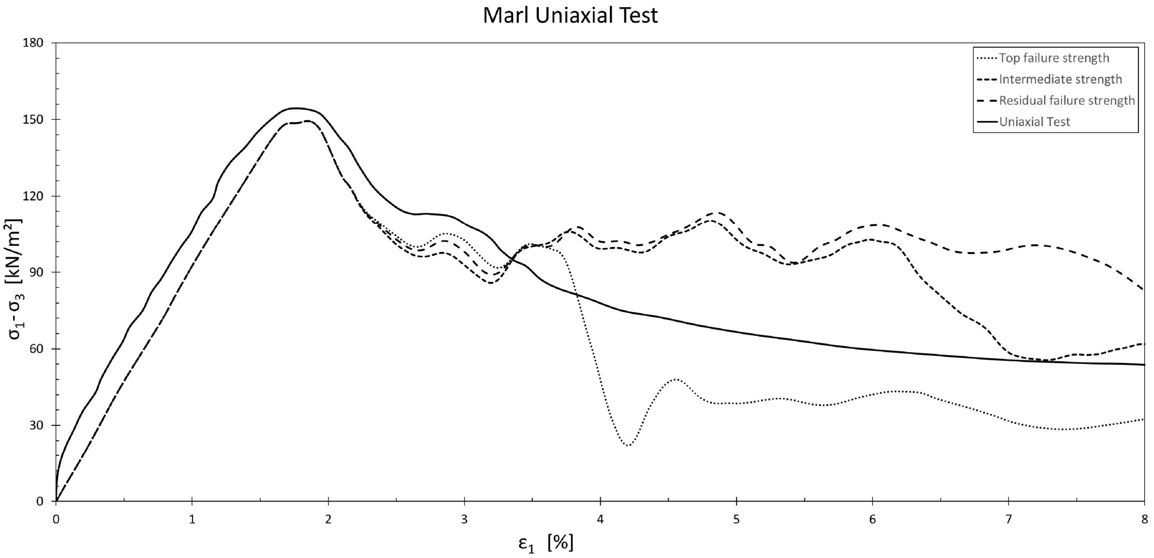

Figure 4.1 Fracture energy variation for the uniaxial test (marl)

The numerical results represent the pre-peak behaviour very well. The used E_{50} of 10.200 kPa gives a good approximation of the real stress/strain behaviour. Also the peak strain and strength show a good convergence. The Top Failure Strength variation shows a sudden drop at 3.5 % deformation while the other two parameter variations are above the laboratory test results. The Intermediate Failure Strength variation drops at 6 % which is not a good approximation for the beginning of the residual state, but the residual strength is reached. In addition, the residual failure strength stays more or less constant and overestimates the residual strength.

Figure 4.2 shows a triaxial test for marl with 50 kPa confining pressure. As in the previous case, the initial stiffness of up to 10 kPa is much higher than in the following hardening part. The test reaches a peak strength of around 250 kPa after which a ductile softening starts, until it developes a constant residual strength of 150 kPa.

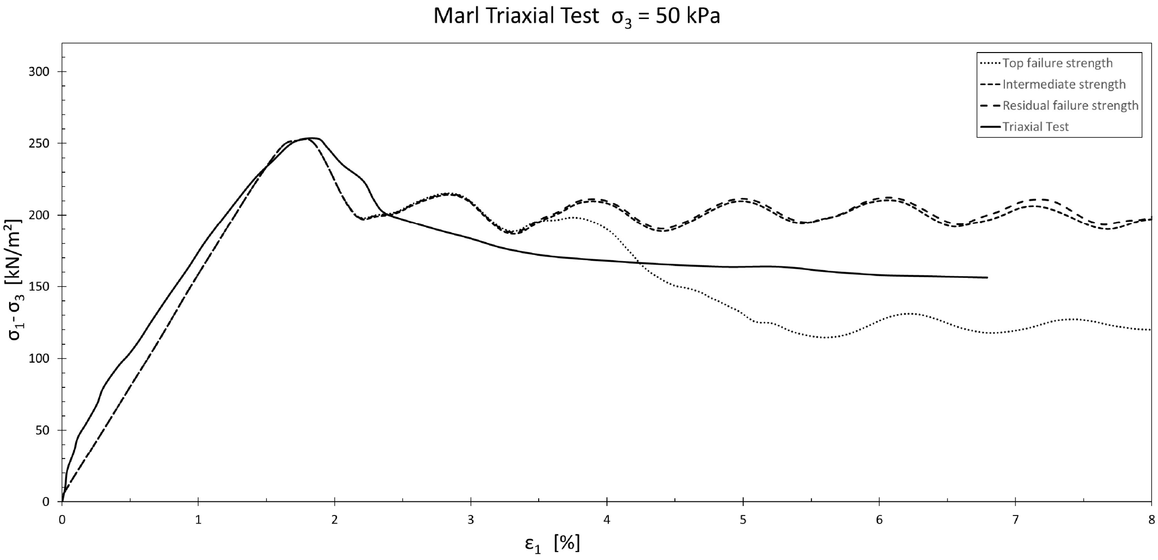

Figure 4.2 Fracture energy variation for the triaxial test with 50 kPa confining pressure (marl)

For the numerical analysis an E_{50} value of 18.000 kPa is used which approximates the pre peak behaviour quite well. Again, the peak strength and strain show a good convergence. All three variations have the same softening behaviour until at 3.5 % deformation the Top Failure Strength variation shows a drop and keep a constant residual strength, underestimating the real test result. The other two variations seem to have an identic constant oscillation in the residual state, in contrast to variation one overestimating the residual value.

In the graph below, two triaxial tests of marl are pictured with 100 kPa confining pressure. This test series shows significant difference in its stiffness development. Therefore, the used E_{50} in the numerical analysis represents an average value The peak strength is constant in both cases, but the peak strain is shifted due to the difference in stiffness. Both show a ductile softening with a constant residual state but with a slightly different residual strength.

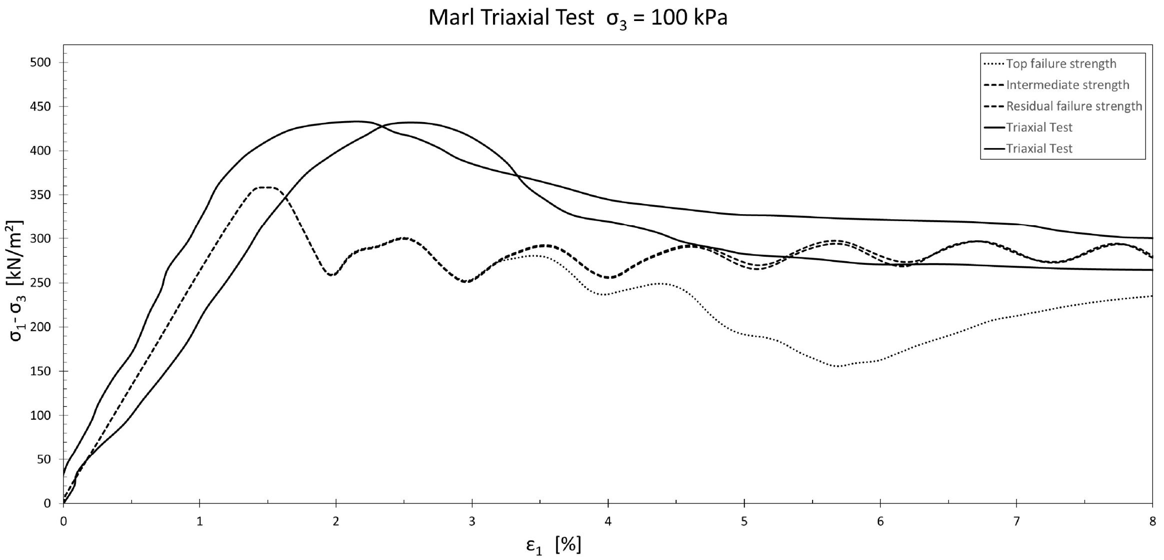

Figure 4.3 Fracture energy variation for the triaxial test with 100 kPa confining pressure (marl)

All three numerical variations in Figure 4.3 show a good approximation of the pre peak behaviour using an interpolated E_{50} of 31.000 kPa. The underestimation of the peak strength and strain could be explained by the assumed friction angle for marl of 32°, which is underestimated for the 100 kPa test series, as it could be seen in Figure 3.5. All three variations have the same softening behaviour until the Top Failure Strength variation shows a drop at 3.5 % deformation and underestimates the residual state. The other two variations seem to have an identic constant oscillation in the residual state, approximating the two real residual values.

In Figure 4.4, a triaxial test for marl with 200 kPa confining pressure is presented. After the hardening part, the stress/strain behaviour shows a plateau in the peak area. After that the softening regime starts with a kink and reaches a constant residual value of 450 kPa.

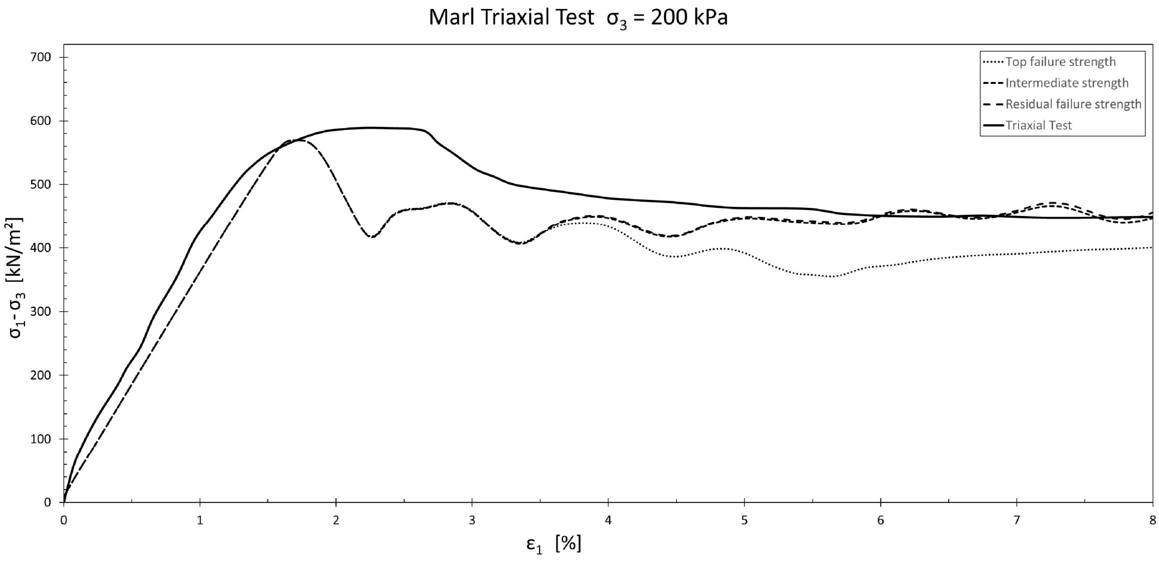

Figure 4.4 Fracture energy variation for the triaxial test with 200 kPa confining pressure (marl)

The approximation of the numerical simulations for the pre peak area with an E_{50} of 42.000 kPa represent the stress/strain behaviour quite well. The failure strength matches-, but the peak strain does not fit. All three variations follow the same softening regime, which underestimates the peak plateau, until the Top Failure Strength variation starts to decrease at 3.5 % deformation. The Intermediate and Residual Failure Strength variations keep their constant oscillating behaviour and approach the residual value.

4.1.2 Standard G_c Variation for mudstone

In this chapter the influence of the three different fracture energy definitions can be observed for mudstone in six different confining pressure stages. The real laboratory test results from the laboratory are shown in the following graphs from Figure 4.5 to Figure 4.10 as a solid black line, while the numerical results are given as variations of dashed lines. All results are mapped in a deviatoric stress/strain area.

The uniaxial test of the mudstone in the figure below shows a ductile behaviour after 1000 kPa applied stress. After that, the stress/strain curve increases up to a peak value of 26.000 kPa and afterwards rapidly drops to 14.000 kPa where a brittle failure occurs.

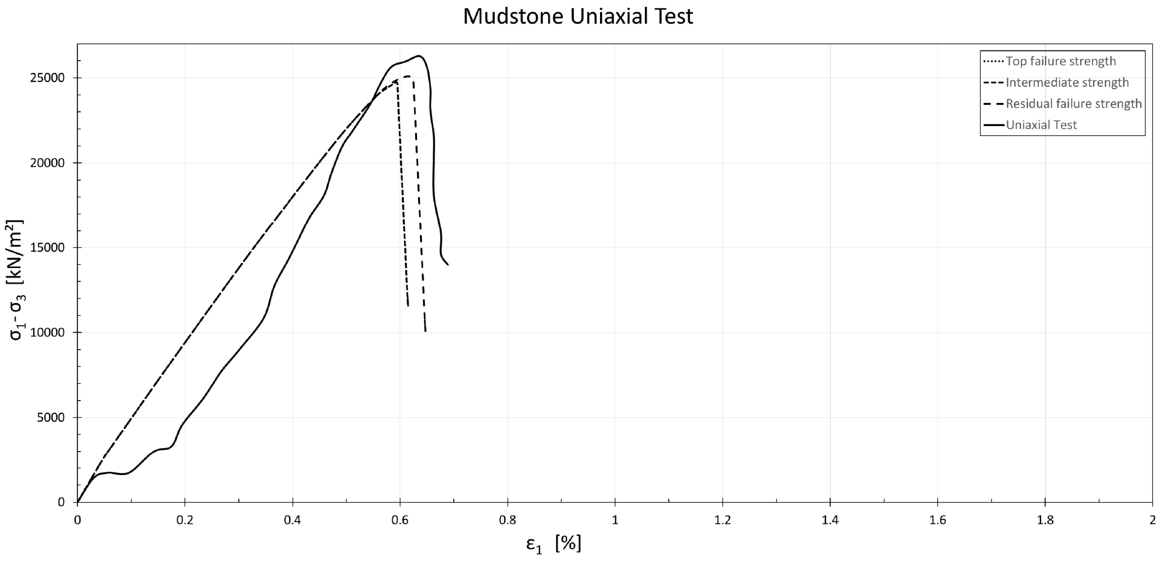

Figure 4.5 Fracture energy variation for the uniaxial test (mudstone)

The numerical analysis fits the laboratory test results pre-peak quite well, neglecting the strain-delay after the initial part. The peak strength as well as the peak strain are slightly underestimated. All three variations show the characteristic rapid down drop, but proceed to a different failure level than the real test. The Residual Failure Strength variation seems to approximate the real test result the best because of its higher G_c value.

The Figure 4.6 below show the triaxial test result for mudstone using 10.000 kPa confining pressure. In opposite to the uniaxial test before, there is now delay in the pre peak area. The post peak behaviour shows a fully developed softening part with a residual strength of around 38.000 kPa.

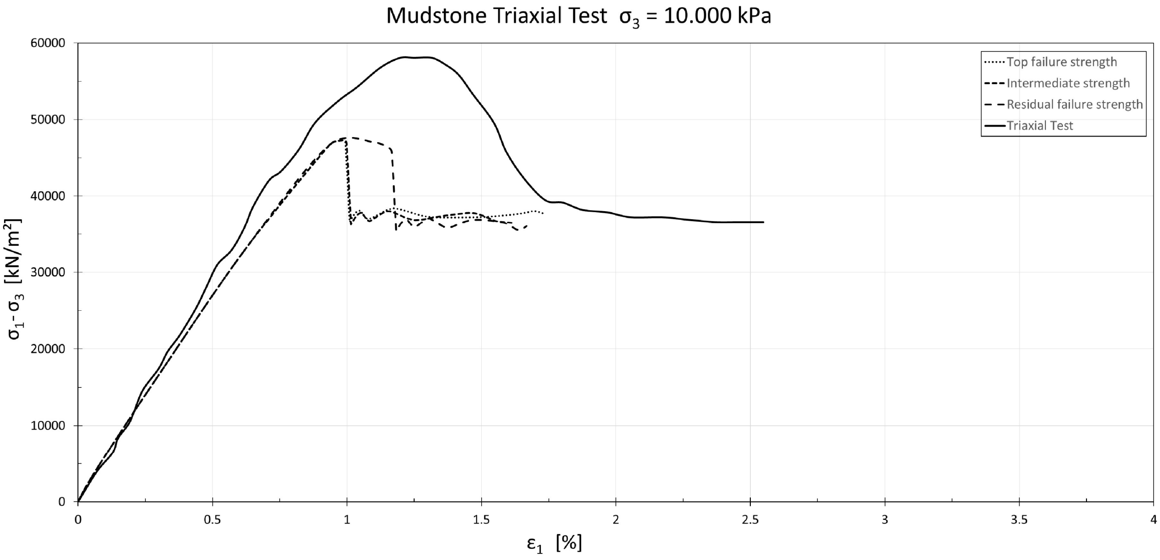

Figure 4.6 Fracture energy variation for the triaxial test with 10.000 kPa confining pressure (mudstone)

In the pre peak regime the numerical variations show a proper approximation of the stress/strain curve by using an E_{50} of 6.1 GPa. The underestimation of the peak strength and strain could be explained by the assumed friction angle for mudstone of 32°, which is underestimated for the 10.000 kPa test series, as it could be seen in Figure 3.6. All three variations keep the same constant residual strength, which fits quite well to the original one. Also, here the Residual Failure Strength variation with its higher value for G_c seems to be the better approximation.

The following graph shows a triaxial test of mudstone, using 20.000 kPa confining pressure. The pre peak behaviour seems to increase linear elastic until a short hardening part before the peak takes place. After the material reaches the peak strength, the softening part continues until the residual strength of 50.000 kPa is reached.

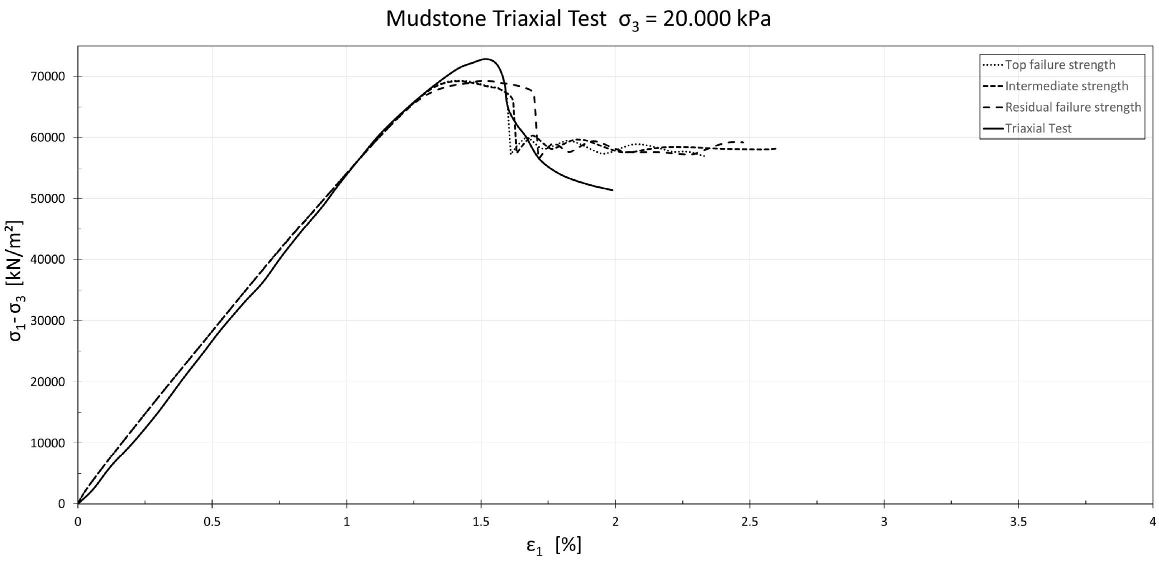

Figure 4.7 Fracture energy variation for the triaxial test with 20.000 kPa confining pressure (mudstone)

All three numerical variations in Figure 4.7 show a very good approximation for the pre peak area. Only the peak strength is underestimated slightly, whereas for the peak strain the analysis shows acceptable values. All variations softens to a residual value of 58.000 kPa which is slightly overestimating the real test behaviour.

The triaxial test result for mudstone using 30.000 kPa confining pressure shows also a highly linear elastic behaviour in the pre peak area until the peak strength is reached. After that softening takes place as expected. The mudstone in this confining pressure stage shows a distinct softening behaviour until the residual value of 70.000 kPa.

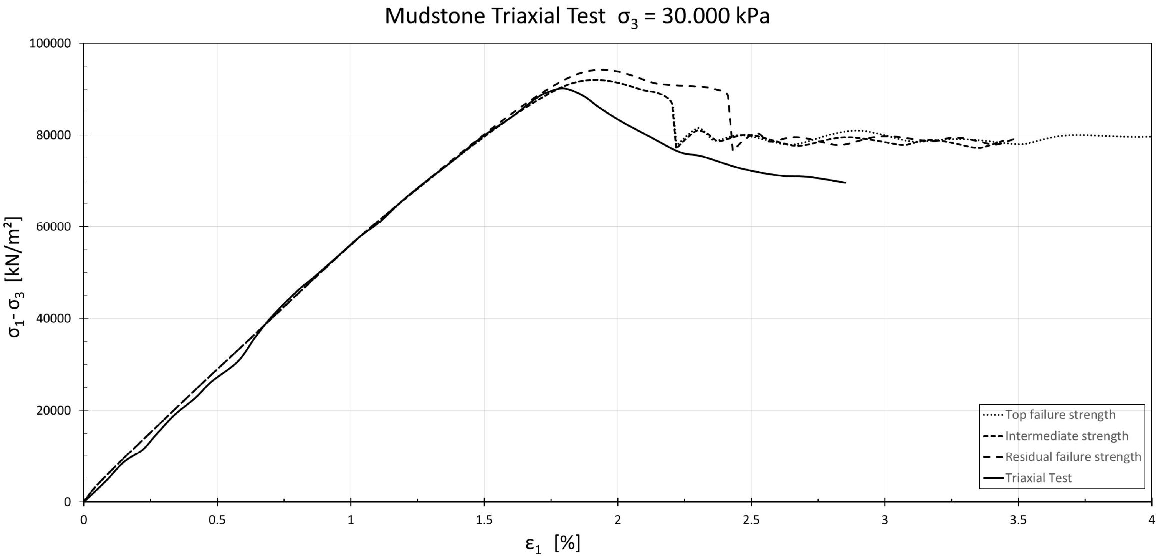

Figure 4.8 Fracture energy variation for the triaxial test with 30.000 kPa confining pressure (mudstone)

For the numerical results in the graph above, the approximation of the pre peak regime seems to fit well. According to the chosen friction angle for mudstone the failure strength is slightly overestimated. All three variations show an increased peak strain as well as an overestimation of the fracture energy. All calculations soften to a residual value of 80.000 kPa, which is slightly overestimating the real residual strength.

The figure below represents a triaxial test for mudstone conducted with 40.000 kPa confining pressure. After the small hardening part prior the peak strength is reached, the softening occurs to a residual strength of 90.000 kPa.

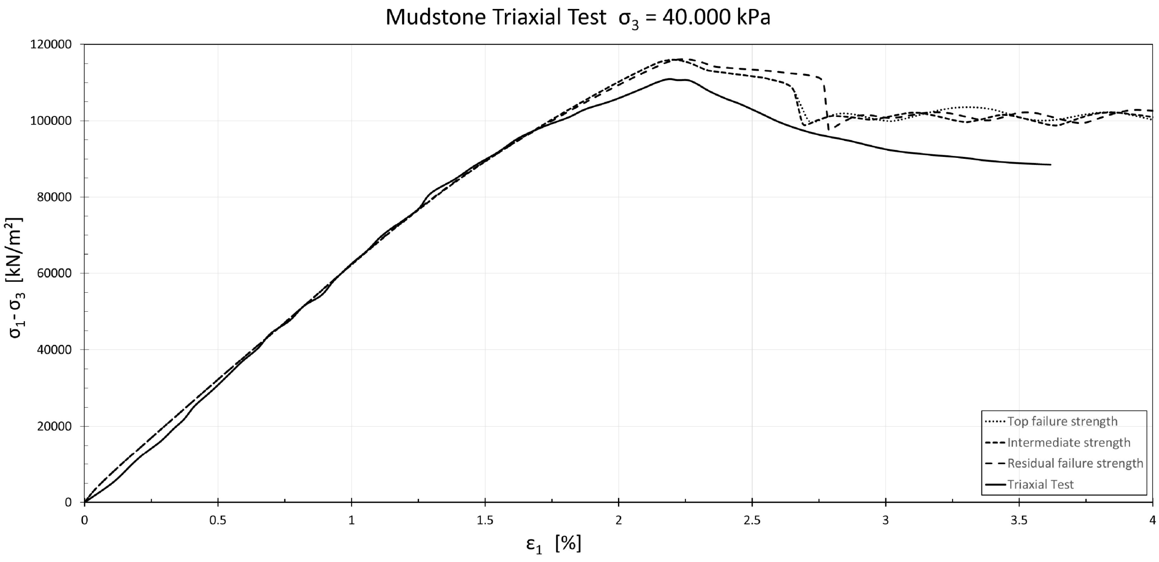

Figure 4.9 Fracture energy variation for the triaxial test with 40.000 kPa confining pressure (mudstone)

As it can be seen in Figure 4.9, the pre peak behaviour is approximated very well by the numerical results. The peak strength is slightly overestimated, but the peak strain seems to be on point. All three results overrate the fracture energy and the residual strength which is kept constant but is slightly to high (10.000 kPa).

The last graph in this chapter, shows the triaxial test for mudstone using 50.000 kPa confining pressure. After the peak strength is reached, a very ductile softening behaviour can be observed, which finally softens to a residual value of 110.000 kPa.

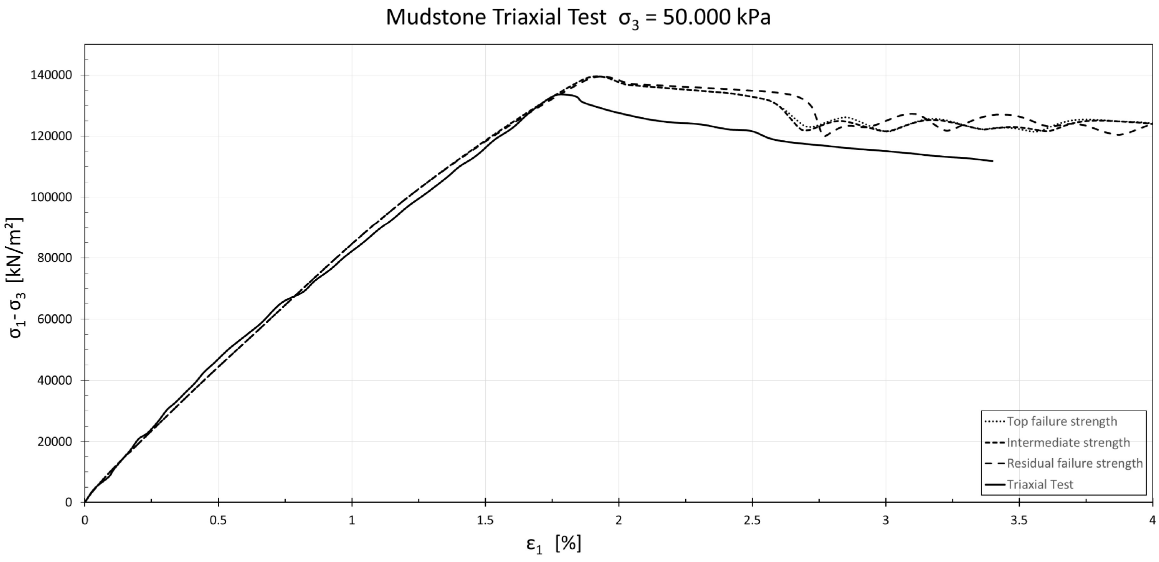

Figure 4.10 Fracture energy variation for the triaxial test with 50.000 kPa confining pressure (mudstone)

The numerical variations for the mudstone shown in the figure above approximate the pre-peak behaviour very good. Due to the chosen friction angle for mudstone from Figure 3.6 the peak strength is slightly overestimated. However, the fracture energy seems to be overestimated for all three variations. Taking into account the overestimated peak strength, the following calculation would fit well.

4.1.3 Standard G_c variation for sandstone

In this section the influence of the three different fracture energy definitions can be observed for sandstone in four different confining pressure stages. The real test results from the laboratory are shown in the following graphs from Figure 4.11 to Figure 4.14 as a solid black line, while the numerical results are given as variations of dashed lines. All results are mapped in a deviatoric stress/strain area

The uniaxial test for sandstone in the figure below shows a very ductile pre peak behaviour, and a brittle failure mode in the post peak regime on the other side.

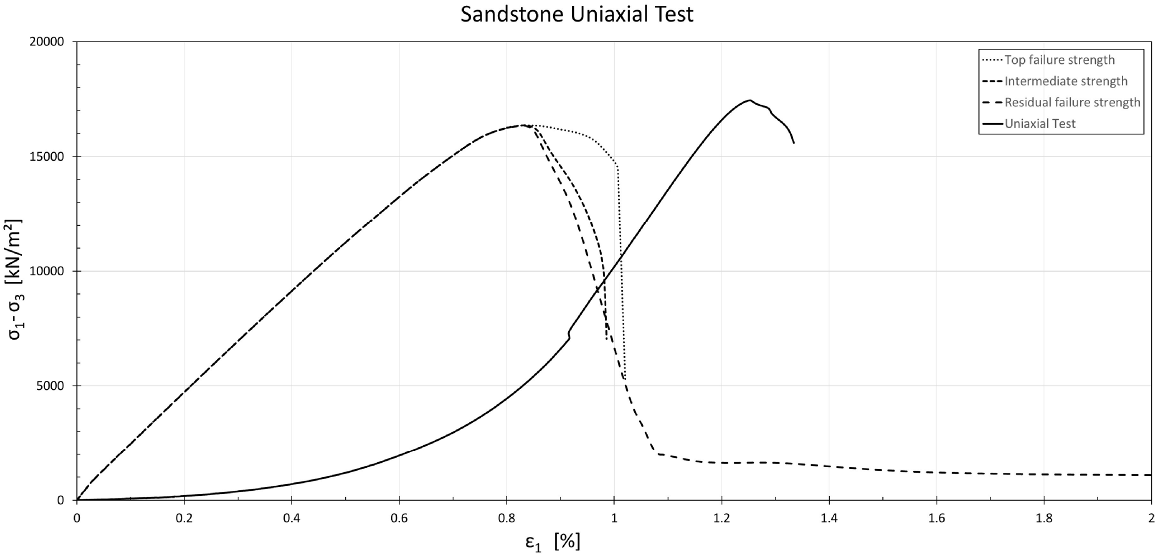

Figure 4.11 Fracture energy variation for the uniaxial test (sandstone)

Because of the high influence from the normalized uniaxial parameters on the further ongoing calculations of the sandstone, the first 0.55 % of the real test are neglected to generate a more realistic parameter set for the triaxial conditions. This leads to the right shift of the peak strain and a higher E_{50} of 2.96 GPa. Therefore, the numerical analysis in Figure 4.11 is not representative for the real test result.

The triaxial test for sandstone using 2.000 kPa confining pressure in the figure below shows much less ductile influence in the initial part than the uniaxial test. In this test, almost linear softening behaviour could be obtained and after that, a constant residual value of about 1.000 kPa takes place.

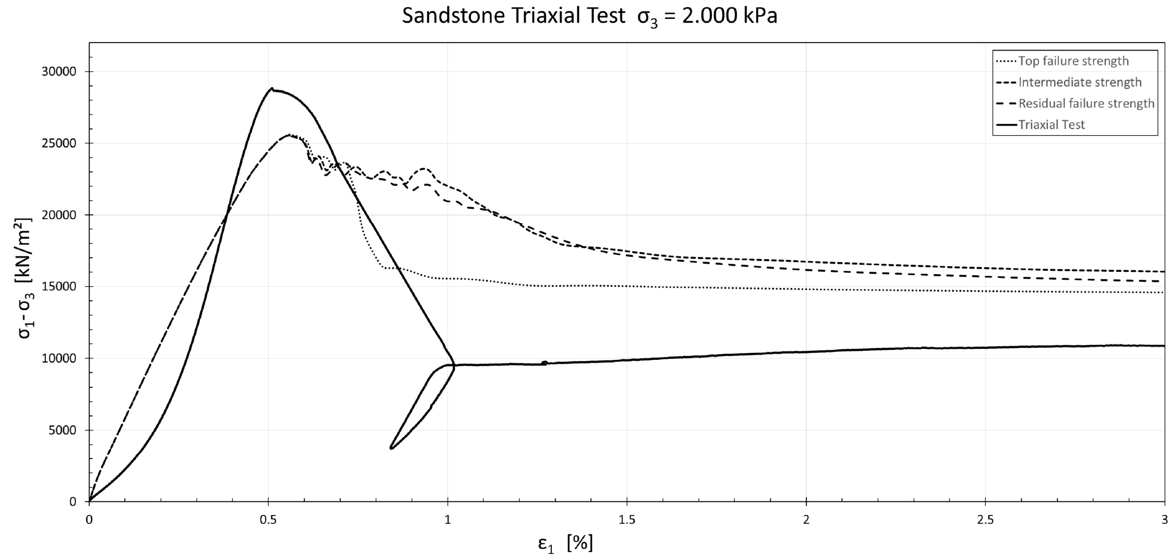

Figure 4.12 Fracture energy variation for the triaxial test with 2.000 kPa confining pressure (sandstone)

All three numerical variations show the same pre peak behaviour and an underestimation of the peak strength, which is not explainable by the chosen friction angle. The Intermediate and the Residual Failure Strength variation show a constant decrease in the softening regime, overestimating G_c. The Top Failure Strength variation seems to adopt the real test result softening path for a while, but then overrates the residual strength like the other two.

The following graph shows the triaxial test for sandstone using 5.000 kPa confining pressure. Again, a more ductile initial part can be observed. The softening regime behaves in a more quadratic relation than the test before, but also shows a constant residual behaviour with a value of around 24.000 kPa.

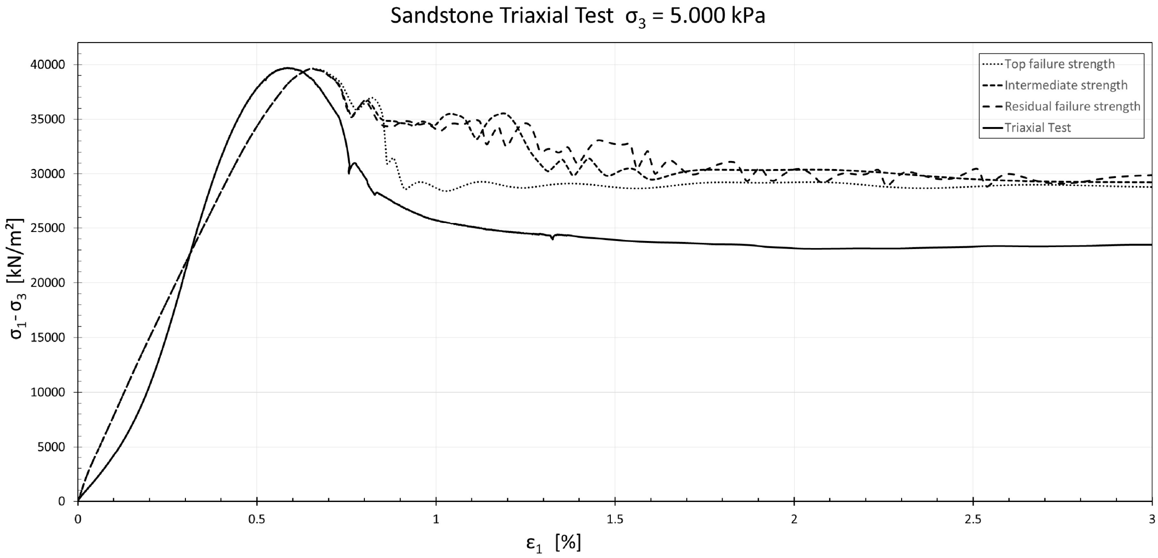

Figure 4.13 Fracture energy variation for the triaxial test with 5.000 kPa confining pressure (sandstone)

The numerical variations in Figure 4.13 approximate the real test result in the pre peak area not that well, but because of the delay in the initial part of the real test result, a better approximation is not possible yet. The peak strength is reached precisely, but the peak strain is slightly overestimated. However the Intermediate and the Residual Failure Strength variation show a constant decrease in the softening regime, overestimating G_c. The Top Failure Strength Variation again adopt the real test result softening path partially, but then overrate the residual strength similar to the test before.

The last graph in this chapter shows the triaxial test result for sandstone using 10.000 kPa confining pressure. As the other two triaxial tests this calculation shows initially a small ductile path. In the post peak area, the softening takes place linear, while the residual strength stays constant at a value of 35.000 kPa.

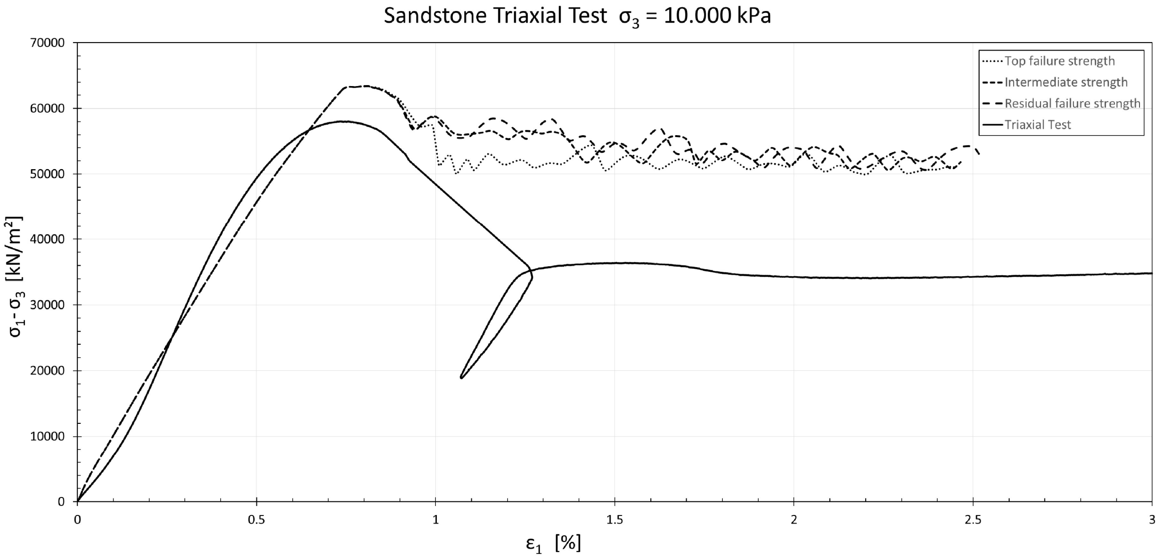

Figure 4.14 Fracture energy variation for the triaxial test with 10.000 kPa confining pressure (sandstone)

In Figure 4.14, all three variations overestimate the peak strength as well as the peak strain, which could be explained by the chosen friction angle from Figure 3.4 a slightly too low E_{50} of 11.8 GPa. While the Intermediate and the Residual Failure Strength variation show a constant decrease in the softening regime, overrating G_c, the Top Failure Strength variation shows a sudden drop down at 1% deformation. All three variations overestimate than the residual strength with 50.000 kPa.

4.1.4 Variation of the dilatancy angle ψ

For the variation of ψ in Figure 4.15 the parameter variation seems to have no influence on the pre peak behaviour. Only after the softening is finished, the influence of ψ become observed. At first the deviatoric stresses tend to increase with increasing ψ but then at around 5% deformation the residual strength seems to decrease with increasing ψ.

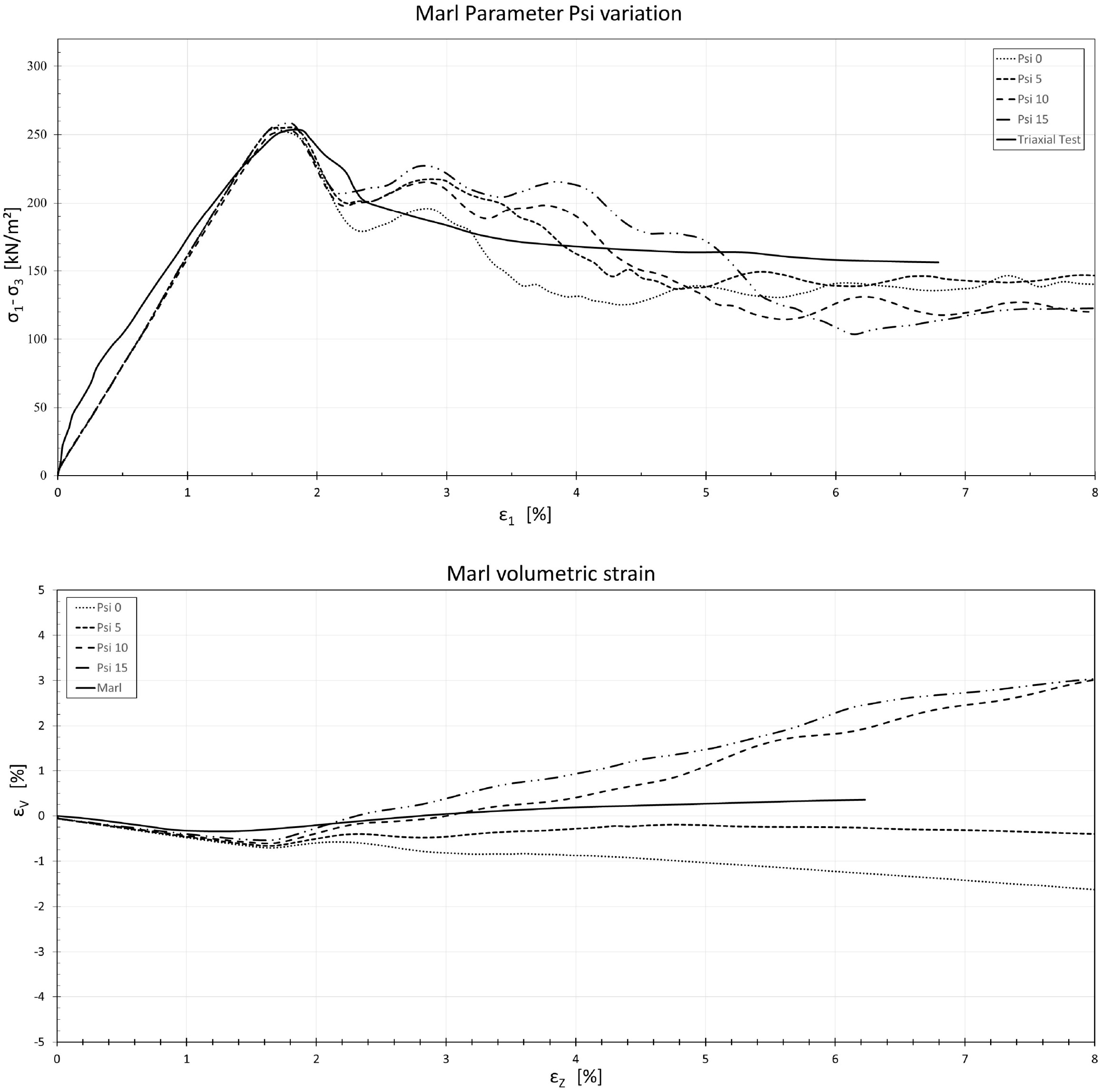

Figure 4.15 Parameter Ψ variation for marl using 50 kPa confining pressure

The influence of Psi for mudstone in Figure 4.16 seems to be very low. As opposed to the observed behaviour for marl there is no influence on the stress state, but with increasing Ψ the drop down to the residual state gets shifted. After that no change in the residual state can be observed. For the comparison of the volumetric strains, no laboratory test data is available.

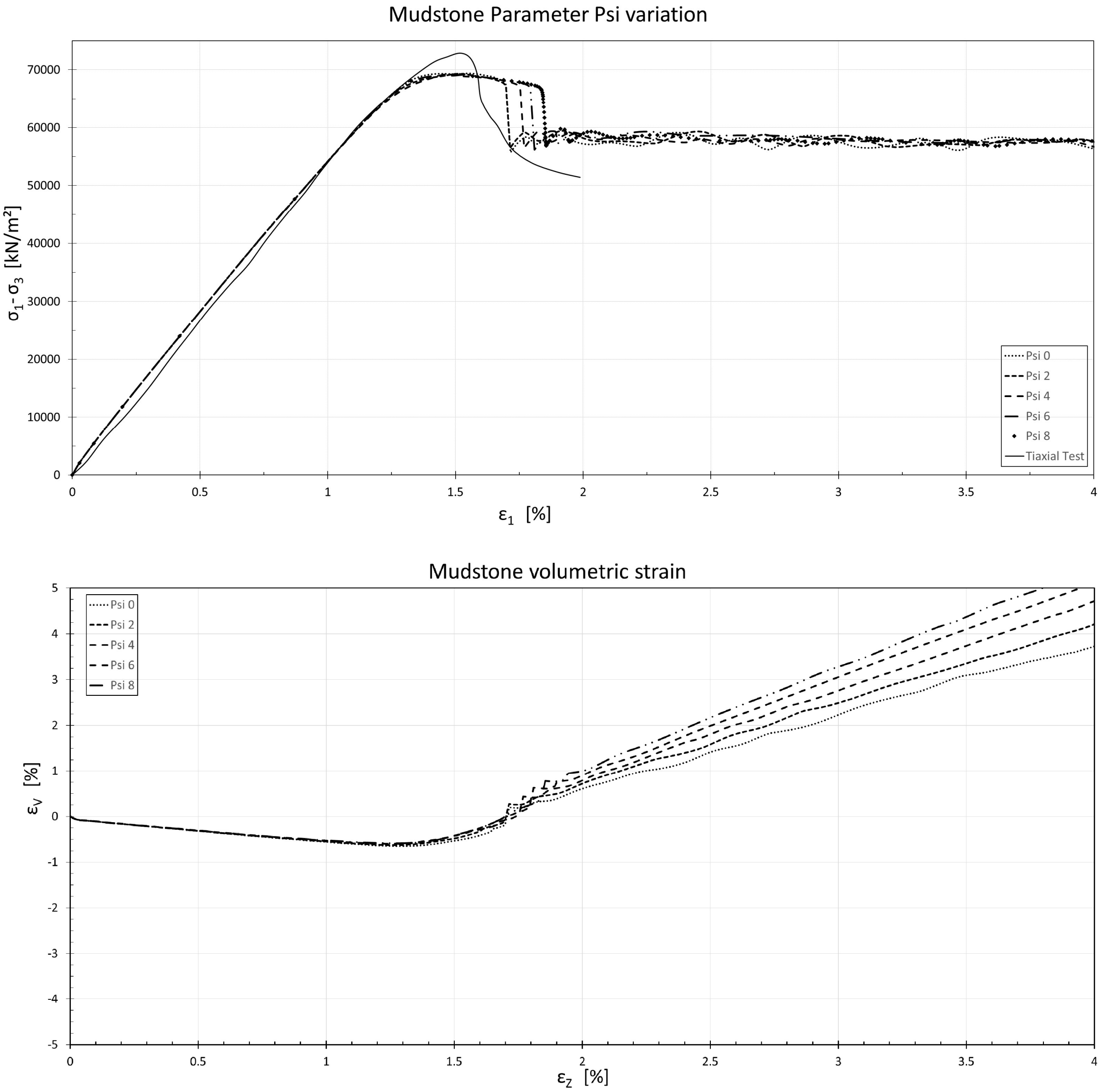

Figure 4.16 Parameter Ψ variation for mudstone using 20.000 kPa confining pressure

For the sandstone, the post peak area increases with Ψ as well as the residual strength rises with Ψ. From a numerical point of view also the oscillations in the residual state are reducing with increasing Ψ.

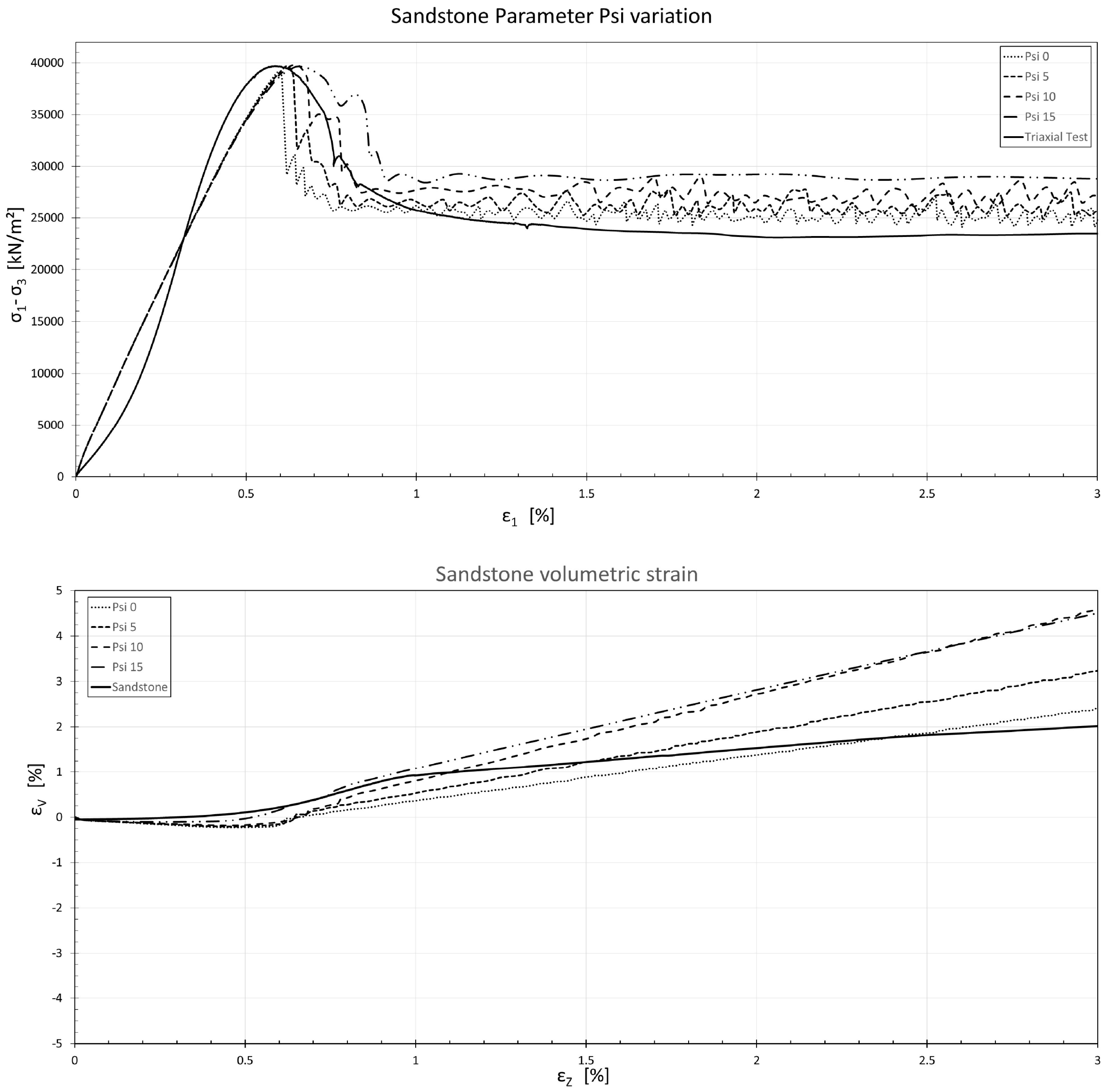

Figure 4.17 Parameter Ψ variation for sandstone using 5.000 kPa confining pressure

4.1.5 Variation of parameter a

In the following graphs from Figure 4.18 to Figure 4.20 the influence of the parameter a can be observed. The parameter variation is done for all three investigated materials using the triaxial results from marl with 50 kPa, mudstone with 20.000 kPa and sandstone with 5.000 kPa confining pressure. Only the parameter a is changed, for all other input parameters the Top Failure Strength definition is chosen. The laboratory test results are shown as a solid black line, while the numerical results are given as variations of dashed lines. All results are mapped in a deviatoric stress/strain area.

In Figure 4.18 the influence of the parameter a on the peak strain is less than expected. Also no difference between zero and one can be observed. A further increase of a produces just a slight shift of the peak strain to the right. The main influence of a seems to manifest in the residual state, where an increasing residual strength with increasing parameter a can be observed.

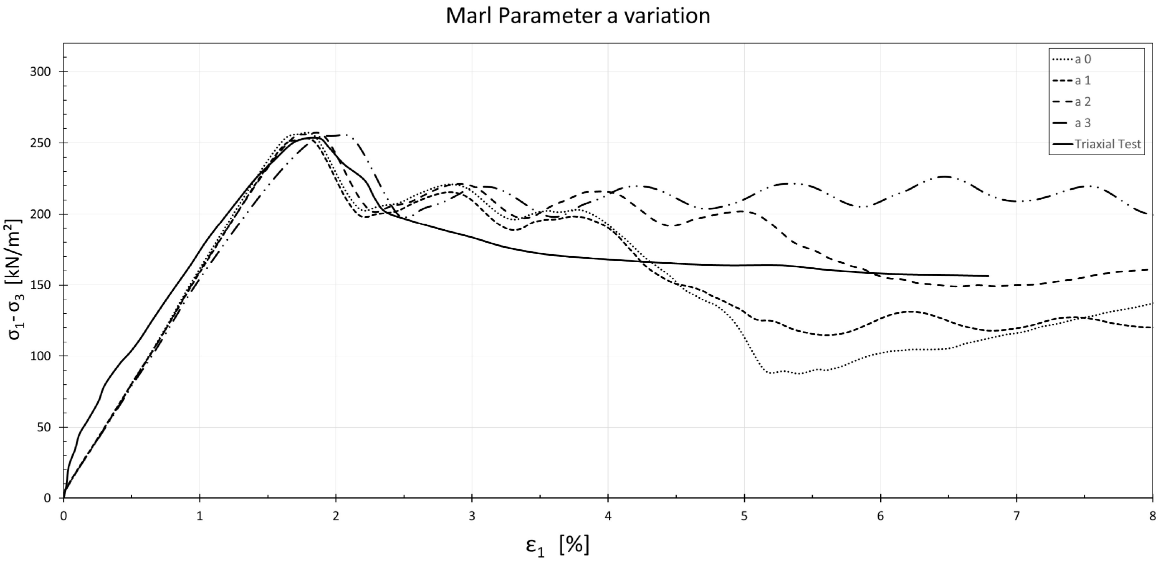

Figure 4.18 Parameter a variation for marl using 50 kPa confining pressure

For the parameter a variation on mudstone in Figure 4.19 the results show the expected behaviour. With increasing parameter a, the peak strain gets shifted to the right and a more ductile behaviour in the softening area can be observed. No influence on the residual strength is shown. Like the marl variation before, no difference between the values zero and one is observed.

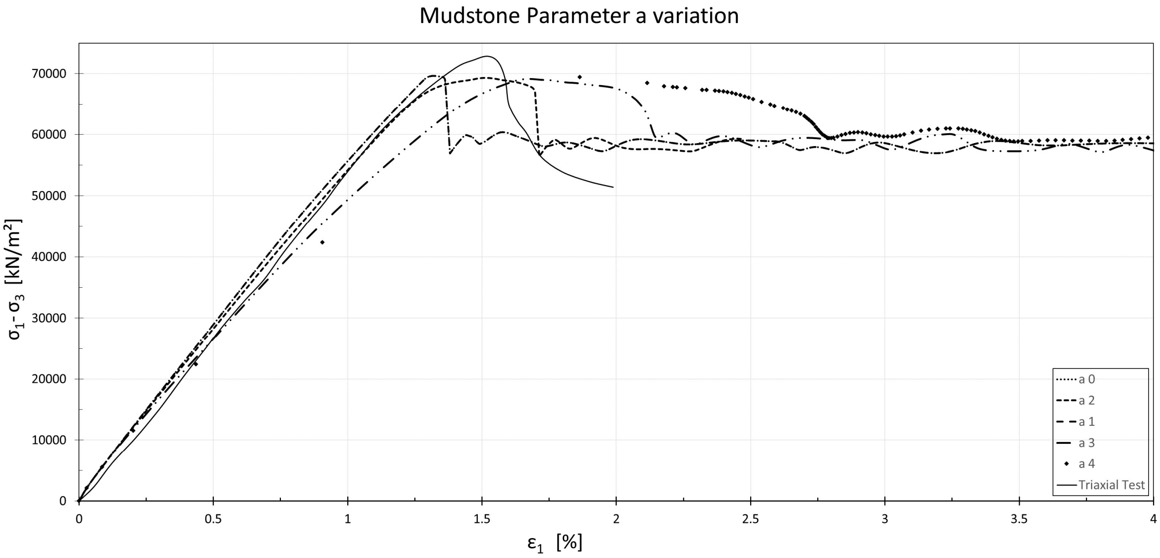

Figure 4.19 Parameter a variation for mudstone using 20.000 kPa confining pressure

Illustrated in Figure 4.20 a seems to have less influence than expected. The values zero, one and two show nearly the same behaviour. Only for a value of a of three a small shifting can be observed.

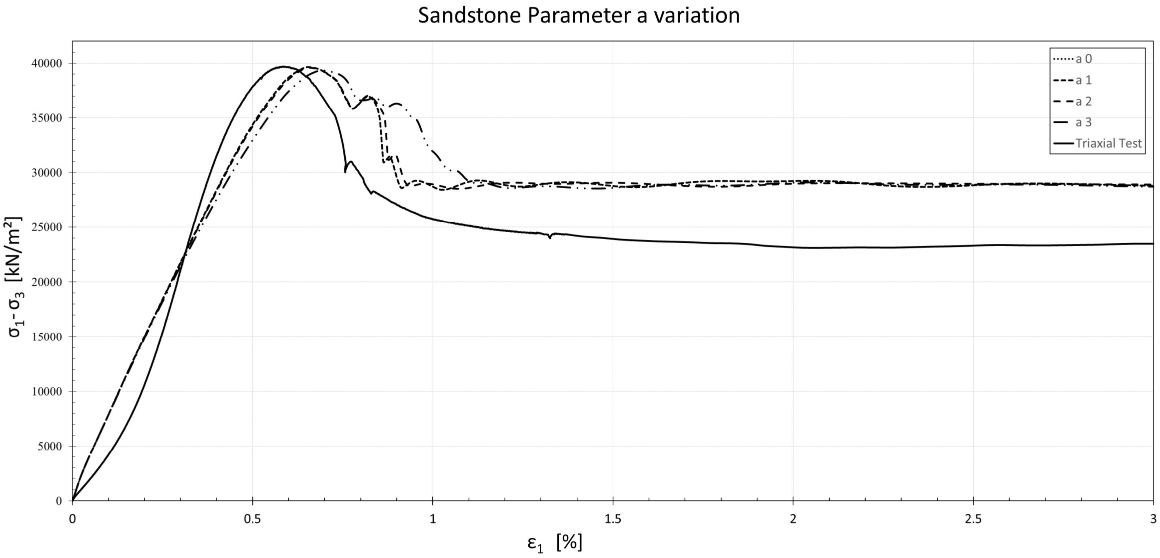

Figure 4.20 Parameter a variation for sandstone using 5.000 kPa confining pressure

4.1.6 Variation of the failure strength f_{cfn}

In the following graphs from Figure 4.21 to Figure 4.23 the influence of the parameter f_{cfn} can be observed. The parameter variation is done for all three investigated materials using the triaxial results from marl with 50 kPa, mudstone with 20.000 kPa and sandstone with 5.000 kPa confining pressure. Only the parameter f_{cfn} is changed, for all other input parameters the Top Failure Strength definition is chosen. The laboratory test results are shown as a solid black line, while the numerical results are given as variations of dashed lines. All results are mapped in a deviatoric stress/strain area.

The variation of f_{cfn} in the figure below shows no influence until 2 % deformation is reached. After that the residual regime increases with increasing failure strength. On the other hand side the final residual strength decreases with increasing f_{cfn}.

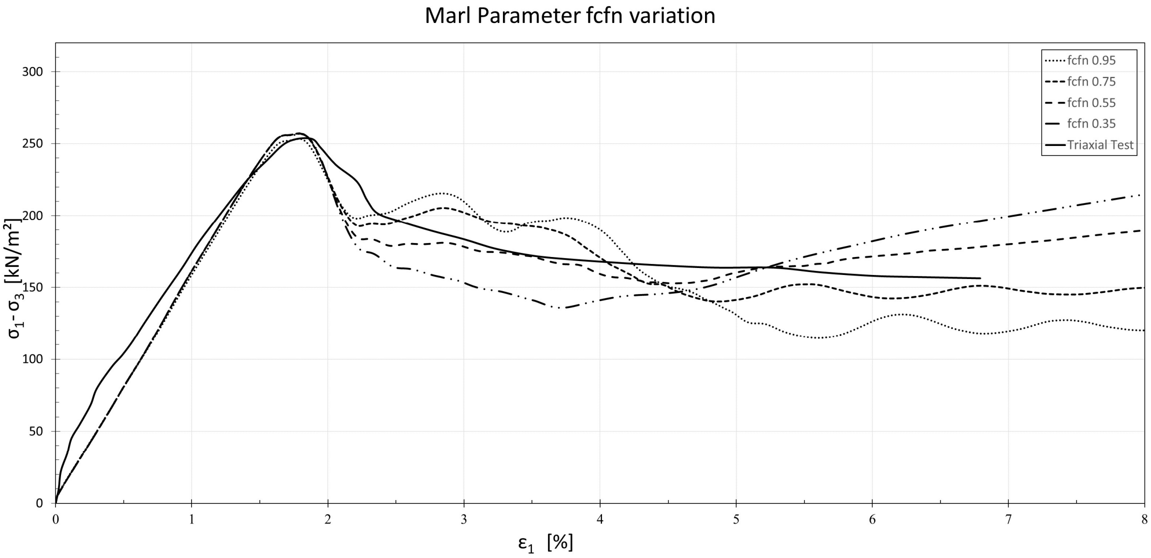

Figure 4.21 Parameter f_{cfn} variation for marl using 50 kPa confining pressure

As it can be seen in the graph below, with decreasing failure strength the linear softening part after the peak is decreasing. The residual strength stays constant through all variations.

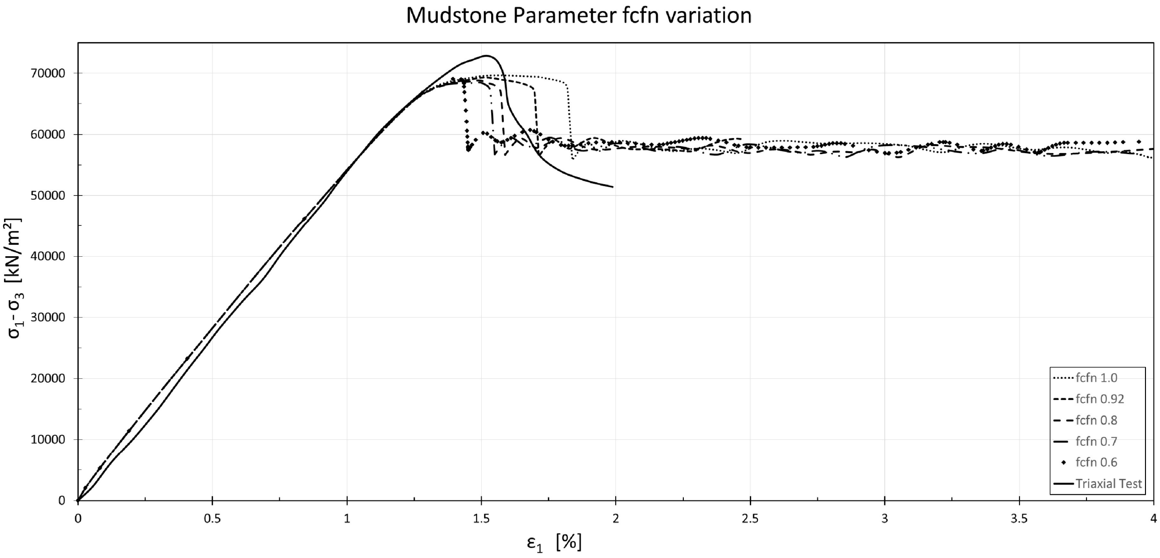

Figure 4.22 Parameter f_{cfn} variation for mudstone using 20.000 kPa confining pressure

Also, in Figure 4.23 shrinkage of the softening part can be observed with decrease of the failure strength. The residual strength of sandstone remains constant through all variations of f_{cfn}.

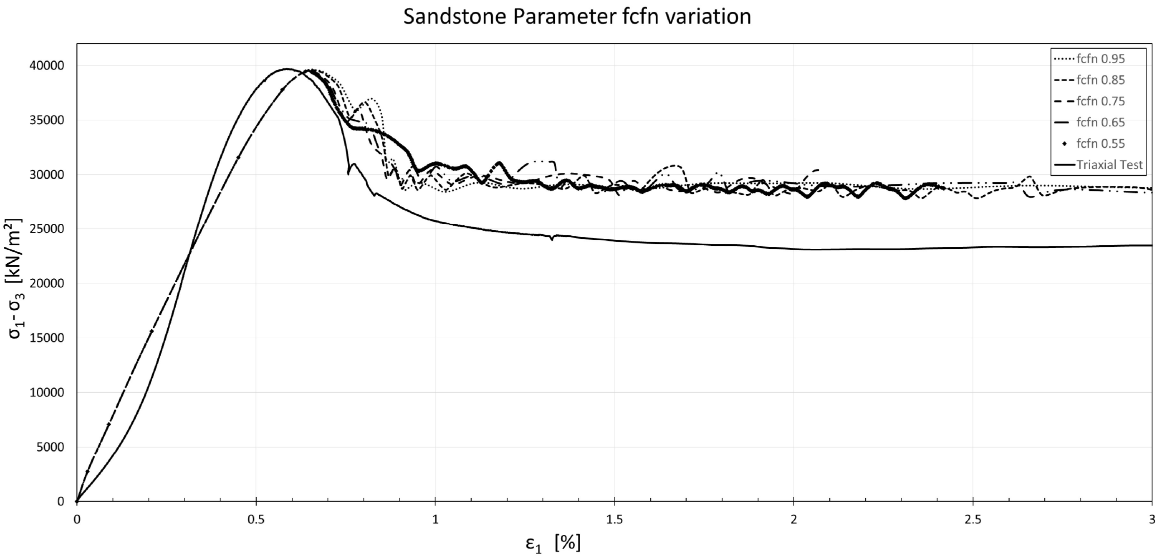

Figure 4.23 Parameter f_{cfn} variation for sandstone using 5.000 kPa confining pressure

4.1.7 Variation of the residual failure strength f_{cun}

In the following graphs from Figure 4.24 to Figure 4.26 the influence of the parameter f_{cun} can be observed. The parameter variation is done for all three investigated material using the triaxial results from marl with 50 kPa, mudstone with 20.000 kPa and sandstone with 5.000 kPa confining pressure. Only the parameter f_{cun} is changed, for all other input parameters, the Top Failure Strength definition is chosen. The laboratory test results are shown as a solid black line, while the numerical results are given as variations of dashed lines. All results are mapped in a deviatoric stress/strain area.

The parameter variation for the residual strength of marl is shown in the graph below. An influence of f_{cun} is observable from 3.5% deformation. With increasing f_{cun} the residual strength also increases until the residual strength is equal to the failure strength f_{cfn} with 0.95.

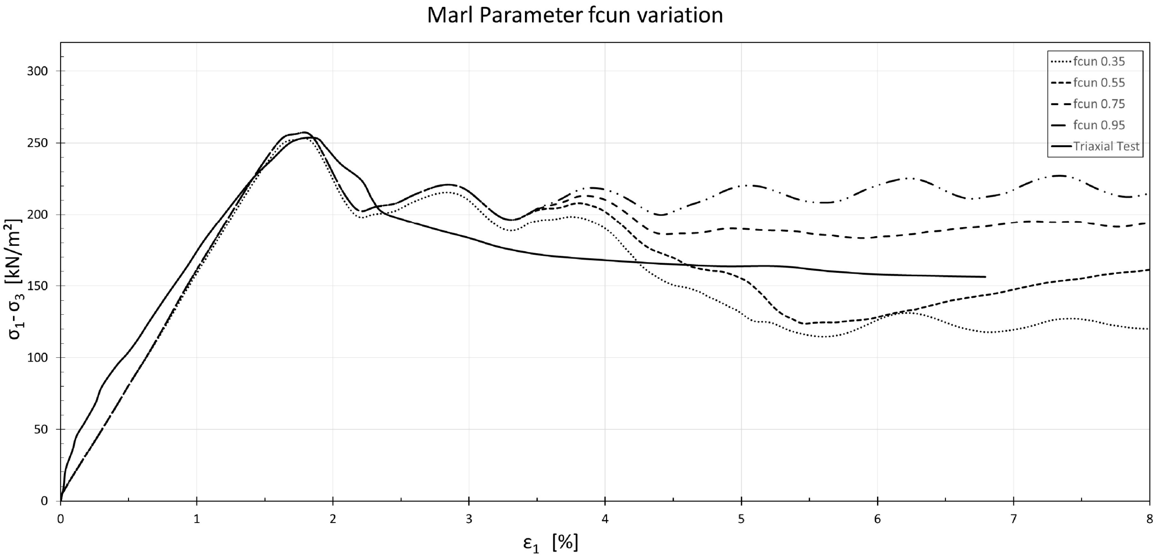

Figure 4.24 Parameter f_{cun} variation for marl using 50 kPa confining pressure

The residual strength study for mudstone in Figure 4.25 shows the significant influence of the parameter f_{cun}. From 0.92, which is equal to the failure strength, reducing f_{cun} leads to a stepwise decreasing residual strength.

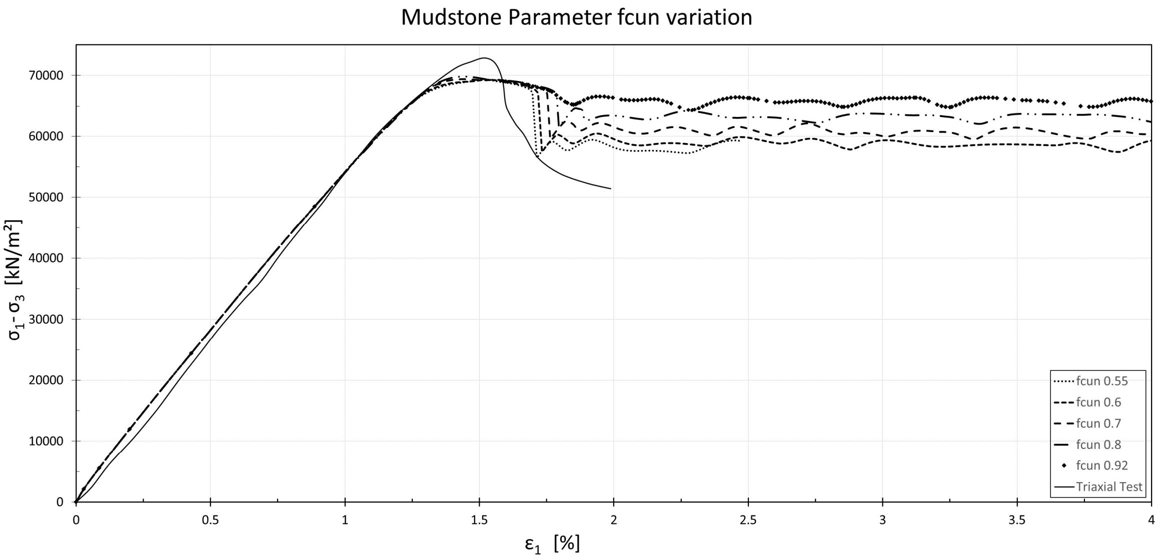

Figure 4.25 Parameter f_{cun} variation for mudstone using 20.000 kPa confining pressure

Also, the sandstone variation for f_{cun} shows the expected behaviour of a stepwise decreasing residual strength with decreasing f_{cun}. Furthermore, no influence in the pre peak is visible.

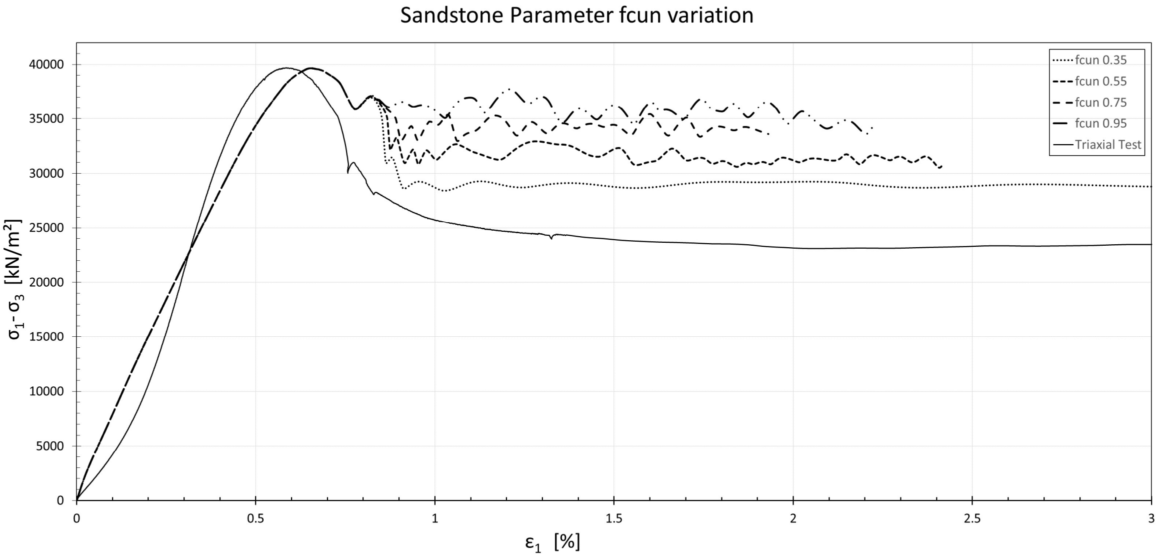

Figure 4.26 Parameter f_{cun} variation for sandstone using 5.000 kPa confining pressure

4.2 Case Study

This chapter deals with the applicability of the Concrete Model on a realistic boundary value problem. The example of a building pit excavation in marl, shown in Figure 4.27, is used as a case study to apply the Concrete Model in practice. Marl is chosen as the investigated material because its Hardening Soil parameter are already known and will be used as a reference for an additional HS calculation. The Case study is divided into three phases:

- Initial Phase: To derive the initial stress state the K_0 procedure is used.
- Phase 2: The volume of the building pit is excavated.
- Phase 3: Additional load (prescribed vert. displacement) onto a plate.

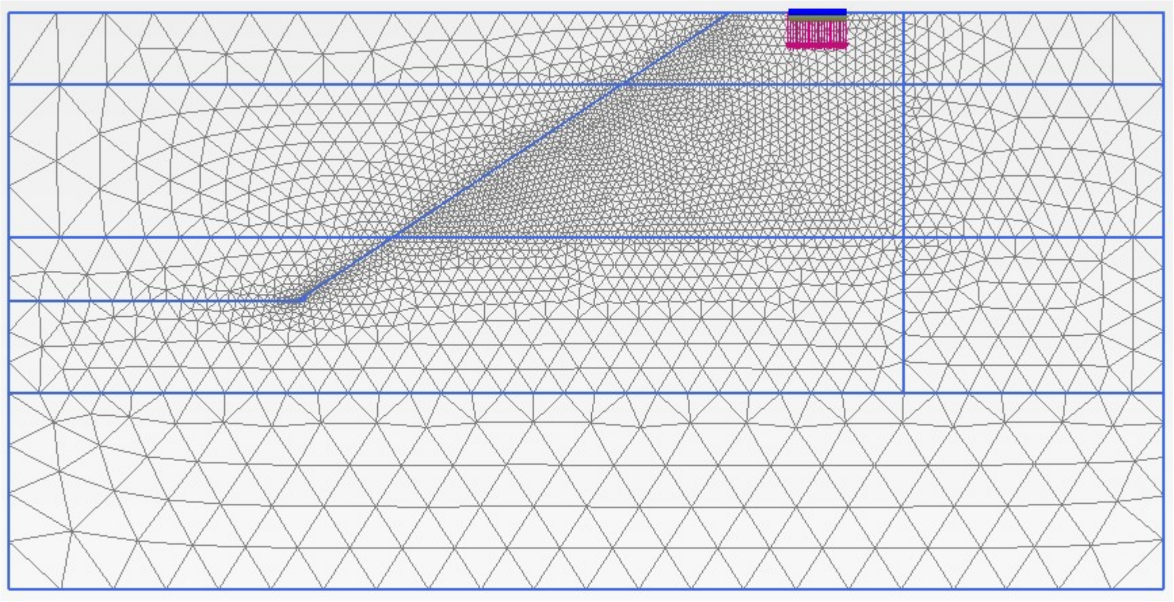

Figure 4.27 Used Mesh for the case study

The prescribed displacement is applied on a rigid plate (linear elastic) with a length of two metres situated next to the slope of the excavation (Figure 4.27, blue).

The average element size A_{el} can be used to derive the equivalent element length L_{eq} (3.1.5). The parameters used for the Top-, Intermediate-, and Residual Failure Strength are illustrated in the table below.

Table 4.1 Fracture energy for the case study

Strength in Compression Parameter							
	f_c [kPa]	ε_{cp} [-]	f_{cfn} [-]	ε_{cf} [-]	f_{cun} [-]	g_c [kN/m²]	G_c [kN/m]
Top Failure strength	154	0.01811	0.95	0.021	0.35	0.434	0.217
Intermediate Failure strength	154	0.01811	0.7	0.031	0.35	1.687	0.843
Residual Failure strength	154	0.01811	0.35	0.051	0.35	3.292	1.645

As a reference and also to obtain differences in the model behaviour, an additional simulation is done using the Hardening Soil Model with the same mesh and model set up.

Table 4.2 Hardening Soil parameters for marl (p_{ref} = 100 kPa)

Hardening Soil Parameters							
φ'	ψ	c'	E_{oed}^{ref}	E_{50}^{ref}	E_{ur}^{ref}	m	ν_{ur}
[°]	[°]	[kPa]	[kPa]	[kPa]	[kPa]	[-]	[-]
32	10	44	15000	30000	100000	0.9	0.25

The Concrete Model is not able to provide a stress depending stiffness like the HS model. Therefore, the layered model below is using four different depth related stiffnesses to simulate the stiffness increase with depth.

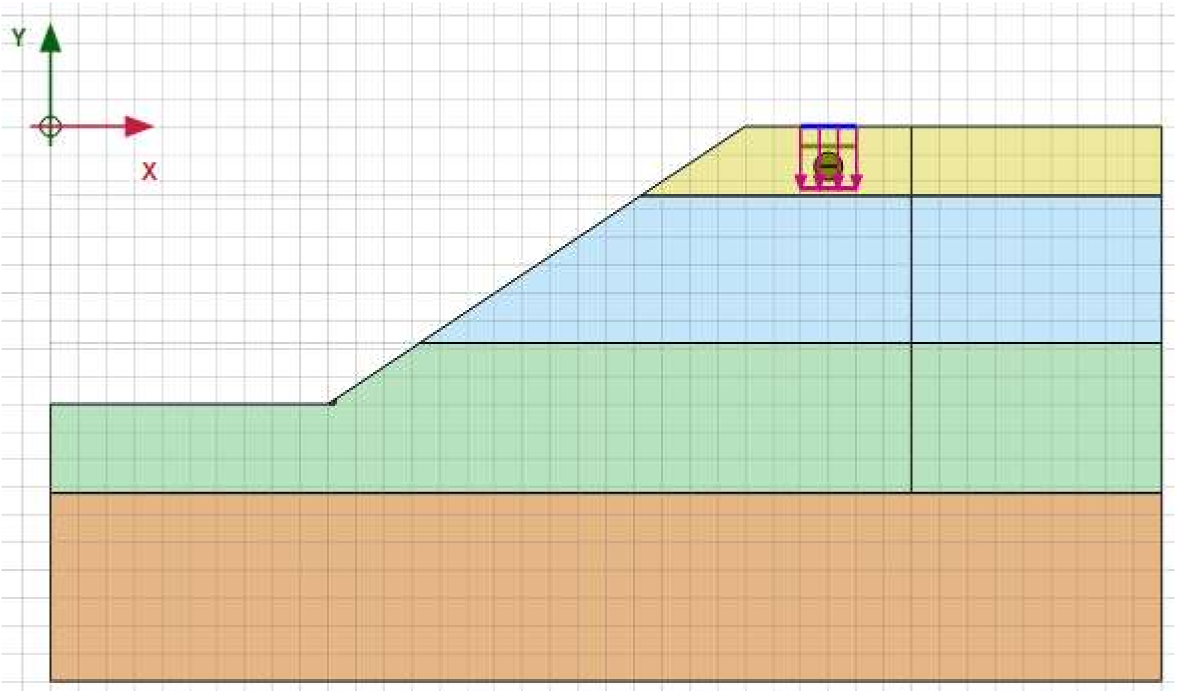

Figure 4.28 Subdivided ground model for the CM using different stiffness

The following figures (Figure 4.29 to Figure 4.36) show the incremental strains as well as the plastic point history for the Hardening Soil parameter set and the Top, Intermediate and Residual Failure Strength definition set.

The Hardening Soil simulation (perfectly plastic material behaviour) shows a relatively thick shear band. The ground below the plate indicates shallow failure which is displayed by local stress peaks at the edges of the plate.

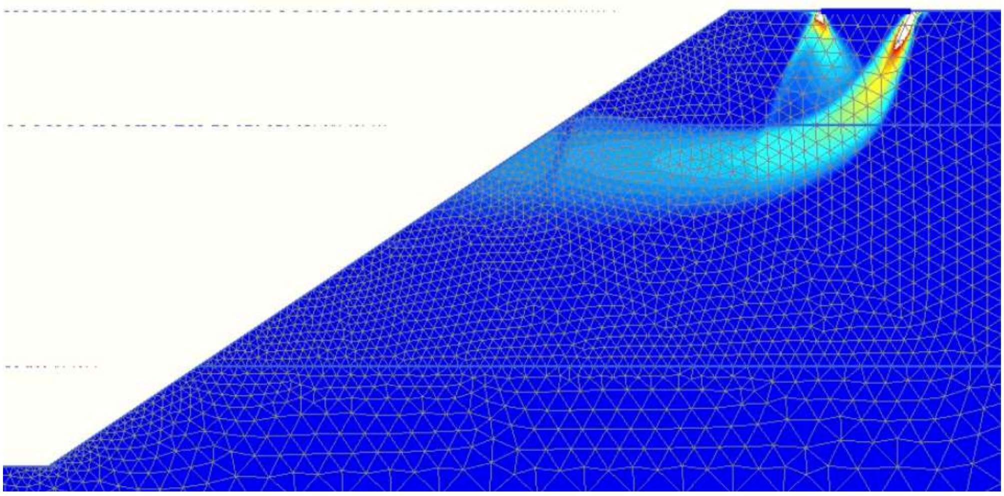

Figure 4.29 Shear band for the Hardening Soil parameter set

The plastic point history shows a big plastic zone development under the plate which finally results in failure. Plasticity does not only occur in the area of the expected shear plane the soil plasticises along the whole slope.

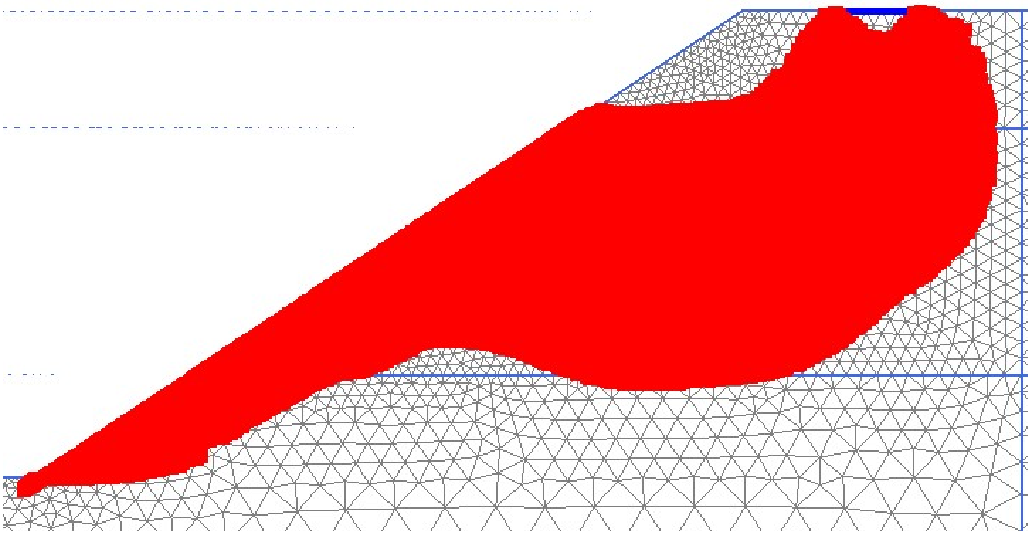

Figure 4.30 Plastic point history for the Hardening Soil parameter set

The Top Failure Strength parameter set gives a clear, thin, and shallow shear band. The incremental displacement plot shows no stress peaks at the edges of the plate. It seems that the failure mechanism follows the border of changing stiffness between two layers. Probably the very low fracture energy and the brittle failure definition (Top Failure Strength, 3.1.6) guides the slope failure mechanism.

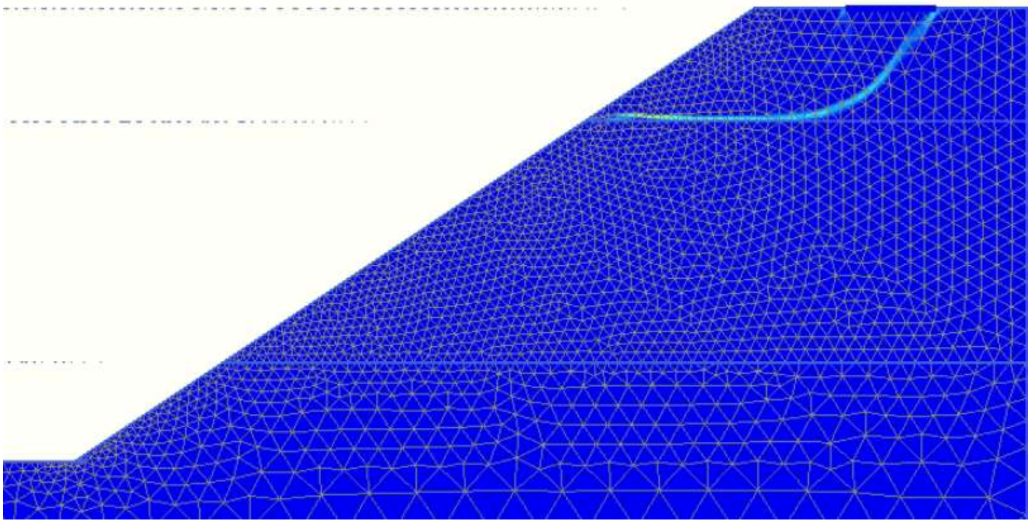

Figure 4.31 Shear band for the Top Failure parameter set

The plastic point history for the Top Failure Definition shows that during the loading procedure three different failure mechanisms or planes are developing. Initially, the system produces a base failure, but during loading two shear bands are developing towards the excavation surface.

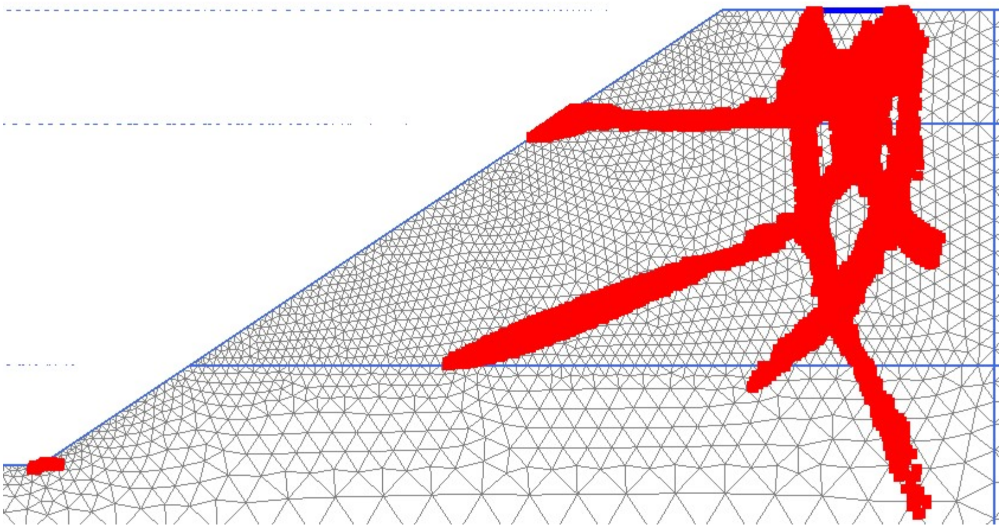

Figure 4.32 Plastic point history for the Top Failure parameter set

The Intermediate Failure Strength parameter set gives a very clear shear band and the expected slope failure occurs. In this case no significant influence of the stiffness change could be observed. This difference to the shallow behaviour before is discussed in detail in section 5.3.4

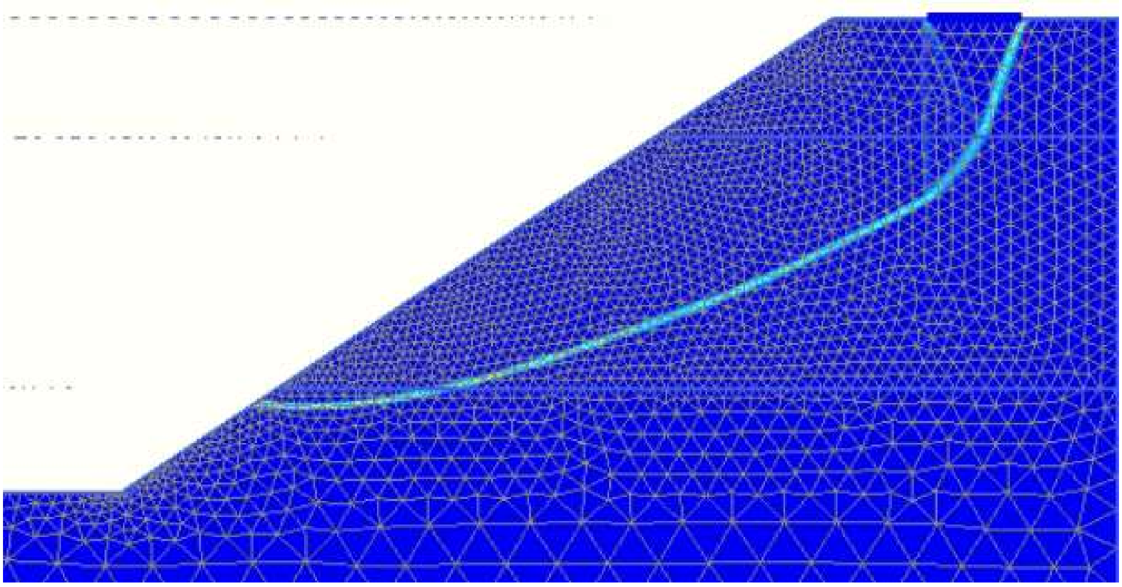

Figure 4.33 Shear band for the Intermediate Failure parameter set

Also here the plastic failure point history shows that at first a local failure under the plate is developing, but later on the failure mechanism develops downwards the slope. As opposed to the Top Failure definition, the failure mechanism develops in a deeper stratum, because of the higher amount of fracture energy.

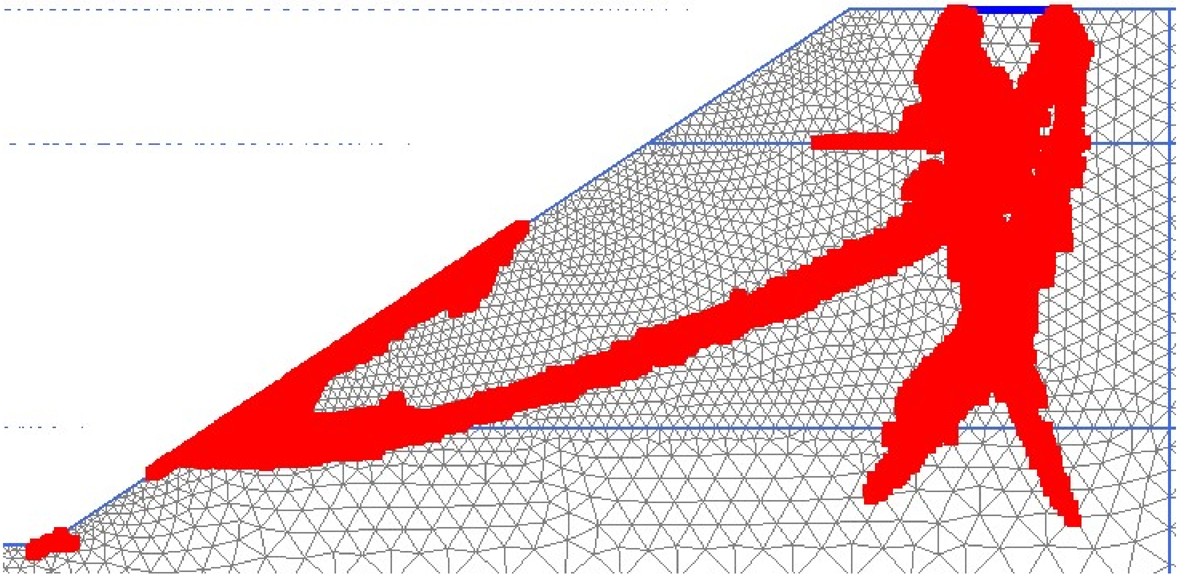

Figure 4.34 Plastic point history for the Intermediate Failure parameter set

The Residual Failure Strength definition delivers a shear band, which seems to go along the stiffness border similar to the Top Failure Strength mode. A variation of this calculation where the stiffness differences are neglected is shown in section 5.3.4.

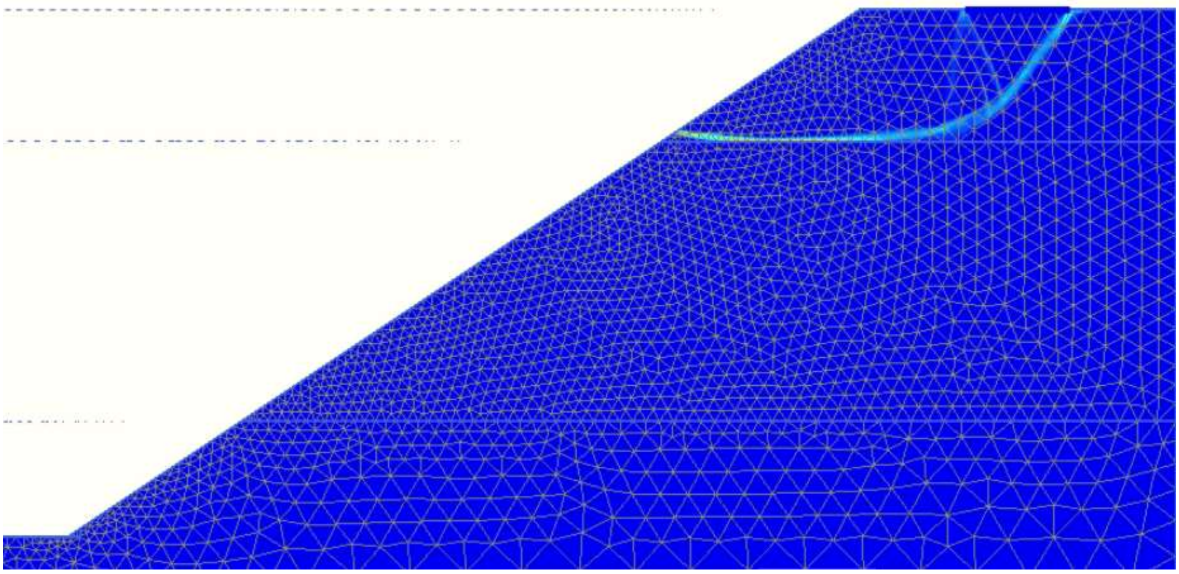

Figure 4.35 Shear band for the Residual failure parameter set

The plastic failure history is similar to the cases before, developing a local failure under the plate. But the leading failure mechanism is a upper slope failure, where else the deeper mechanism is not fully developed at this time.

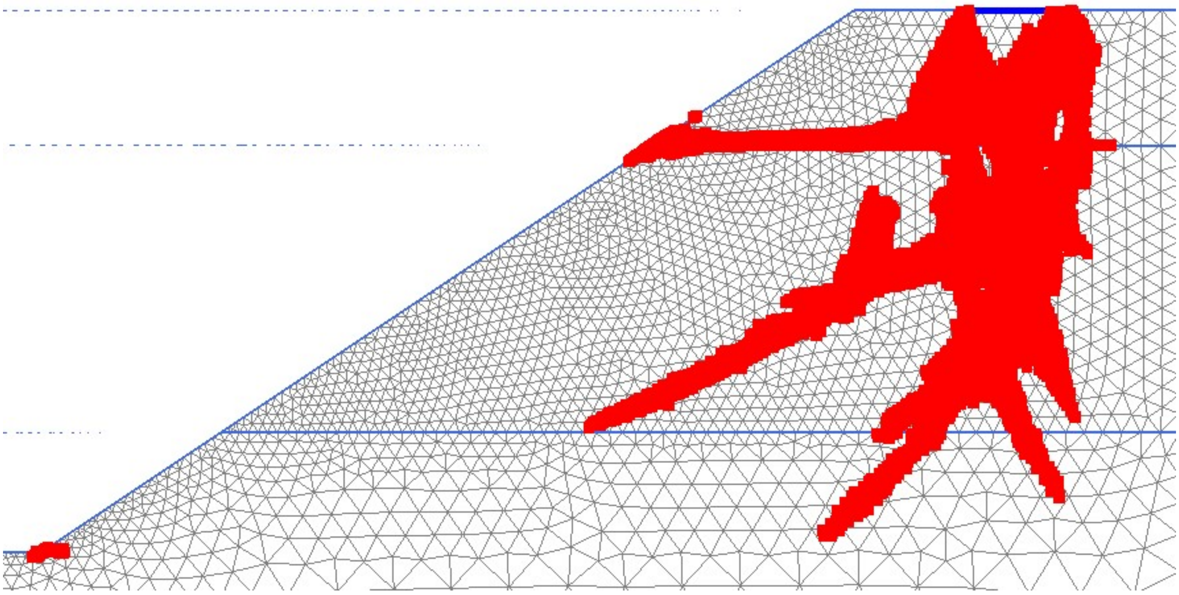

Figure 4.36 Plastic point history for the Residual Failure parameter set

The plot below shows the resulting settlements under the plate. All three Concrete Model definitions show a good approximation of the pre peak area. The Intermediate and the Top Failure definition seem to reach the peak strength exactly, whereas the Residual Failure Strength graph overestimates the peak strength a little. All three show a stress release after the peak and a much lower residual strength as the Hardening Soil Model. The observable “softening” of the HS Model has no mechanical background. Furthermore this depends on numerical issues which are discussed in section 5.3.5.

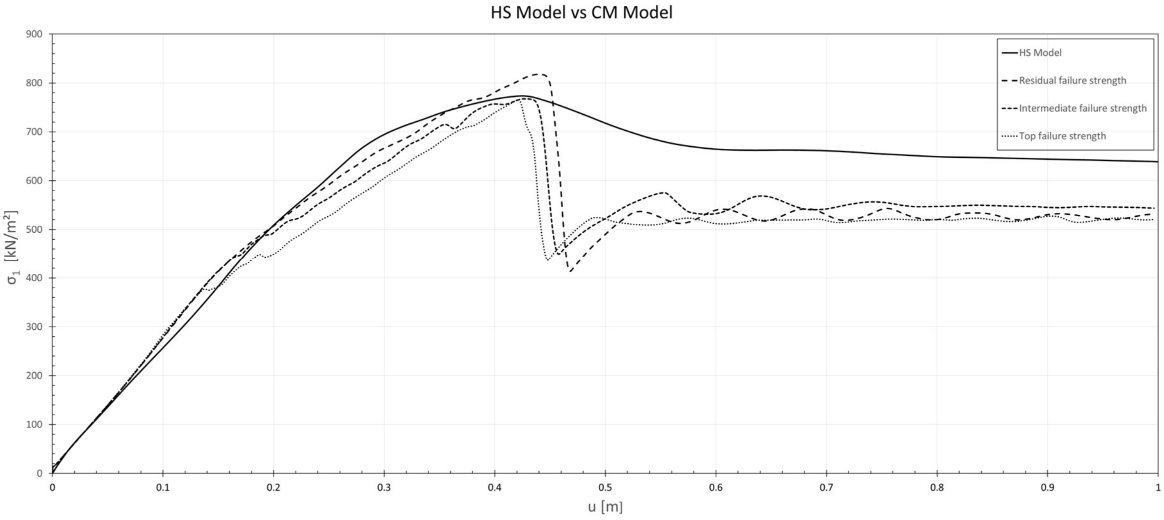

Figure 4.37 Calculation results of the case study

The results of the calculations using the Concrete Model shows a softening behaviour as expected. The definition of the G_c variations seem to fit in the case study, because the Residual Failure Strength definition shows more deformation was well as a higher fracture energy amount, whereas the Top Failure definition shows a smaller amount of fracture energy.

5 Discussion

The last chapter summarises the results and findings of this thesis and gives a short outlook on the topics still in need of further research.

5.1 Interpretation

The summarised interpretation for the Standard G_c Variations for marl, mudstone, and sandstone as well as the special parameter variations for the dilatancy angle ψ, the fitting parameter a, the failure strength f_{cfn}, and the residual failure strength f_{cun} are discussed here. In addition, the comparison of the Hardening Soil and the Concrete Model calculations of the case study is evaluated.

5.1.1 Parameter Study Interpretation

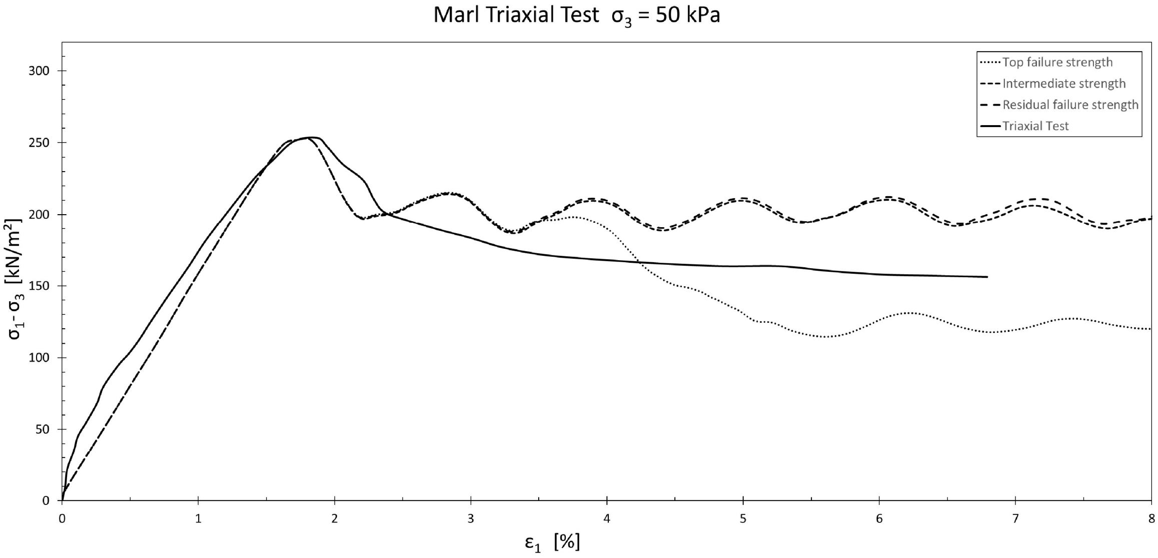

Figure 5.1 Representative stress/strain curve for the Standard G_c Variation (marl)

All three Standard G_c Variations for marl show a good approximation of the pre peak behaviour. Except for the triaxial simulation using 100 kPa confining pressure the peak strength is reached in all simulations which can be explained by the misfit of the Mohr circle at 100 kPa confinement (Figure 3.5). Generally, the post peak softening behaviour is represented very well in all three variations. In all cases the residual strength level is overestimated slightly from the Top Failure Variation and the Intermediate Failure Variation.

The Top Failure Strength shows a drop down in the residual state. For the modelling of the marl the Intermediate Strength Variation is recommended because of the best approximation of the stress/strain behaviour through all stages.

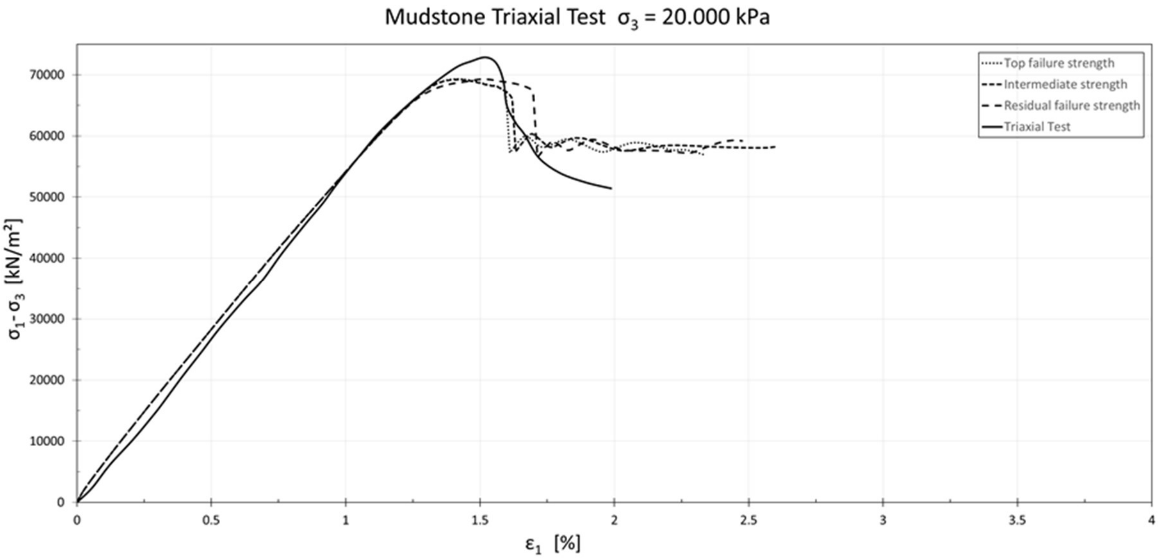

Figure 5.2 Representative stress/strain curve for the Standard G_c Variation (mudstone)

The Standard G_c Variation for mudstone represents the pre peak area very well. Except for the confining pressure stage of 10 MPa (Figure 3.6 Mohr circles for mudstone) all other simulations approximate the peak strength in a suitable way. The mudstone test series clearly shows the development of the post peak softening regime from an initial elastic-brittle to a nearly perfectly-plastic behaviour with increasing confining pressure (as described in Figure 1.6). As expected, the brittle mudstone behaviour with its high UCS is represented best by the Top Failure Strength and the Intermediate Strength definition. The Residual Strength Definition is overrating the fracture energy G_c through all stages. Generally, the residual state is slightly overestimated by all definitions in all stages. This indicates that the residual strength f_{cun} have to be reduced to a lower value (investigated in 4.1.7) The mudstone parameter variations show less oscillations in the residual state than any other material.

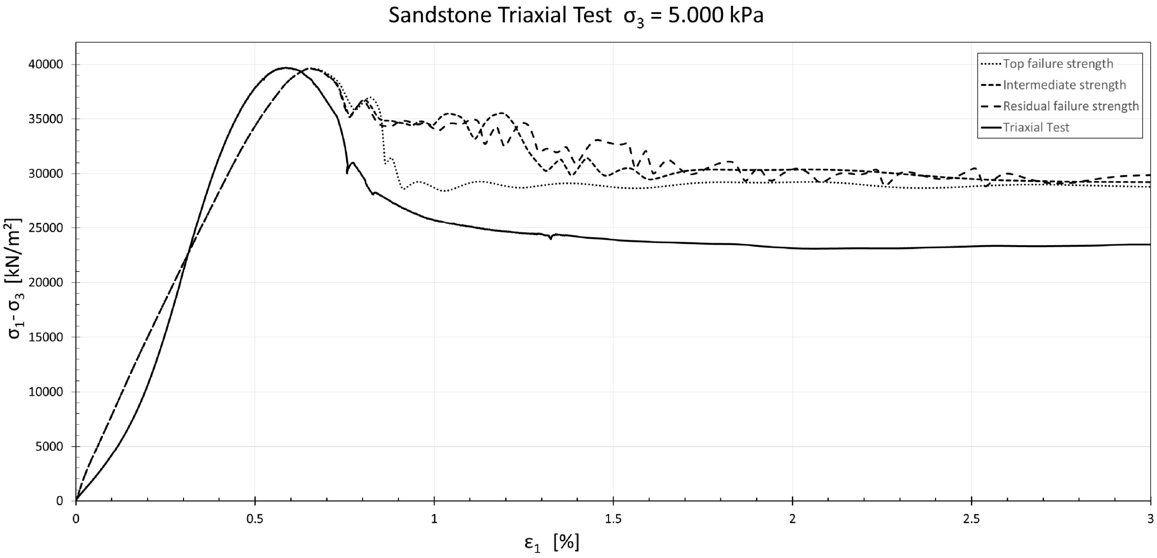

Figure 5.3 Representative stress/strain curve for the Standard G_c Variation (sandstone)

The sandstone Standard G_c Variation does not represent the pre peak stress/strain behaviour well. All original material results show a delay at the initial phase/stress onset which is caused by the high amount of porosity for sandstone (Figure 4.11). Using the standard settings of the Concrete Model it is not possible to reproduce this delayed pre peak behaviour. The peak strength is over-, and underestimated which is visible in Figure 3.4. Through all stages the Top Failure Strength Definition delivers the most suitable approximation of the softening regime. Post peak oscillations are not observable for this definition. This can be caused by the right combination of fracture energy and failure strength which leads to a stable solution. However, the Intermediate-, and the Residual Strength Definition are overestimating the softening regime which is explainable by the high UCS and the tendency to brittle behaviour which mainly represents the Top Failure Definition.

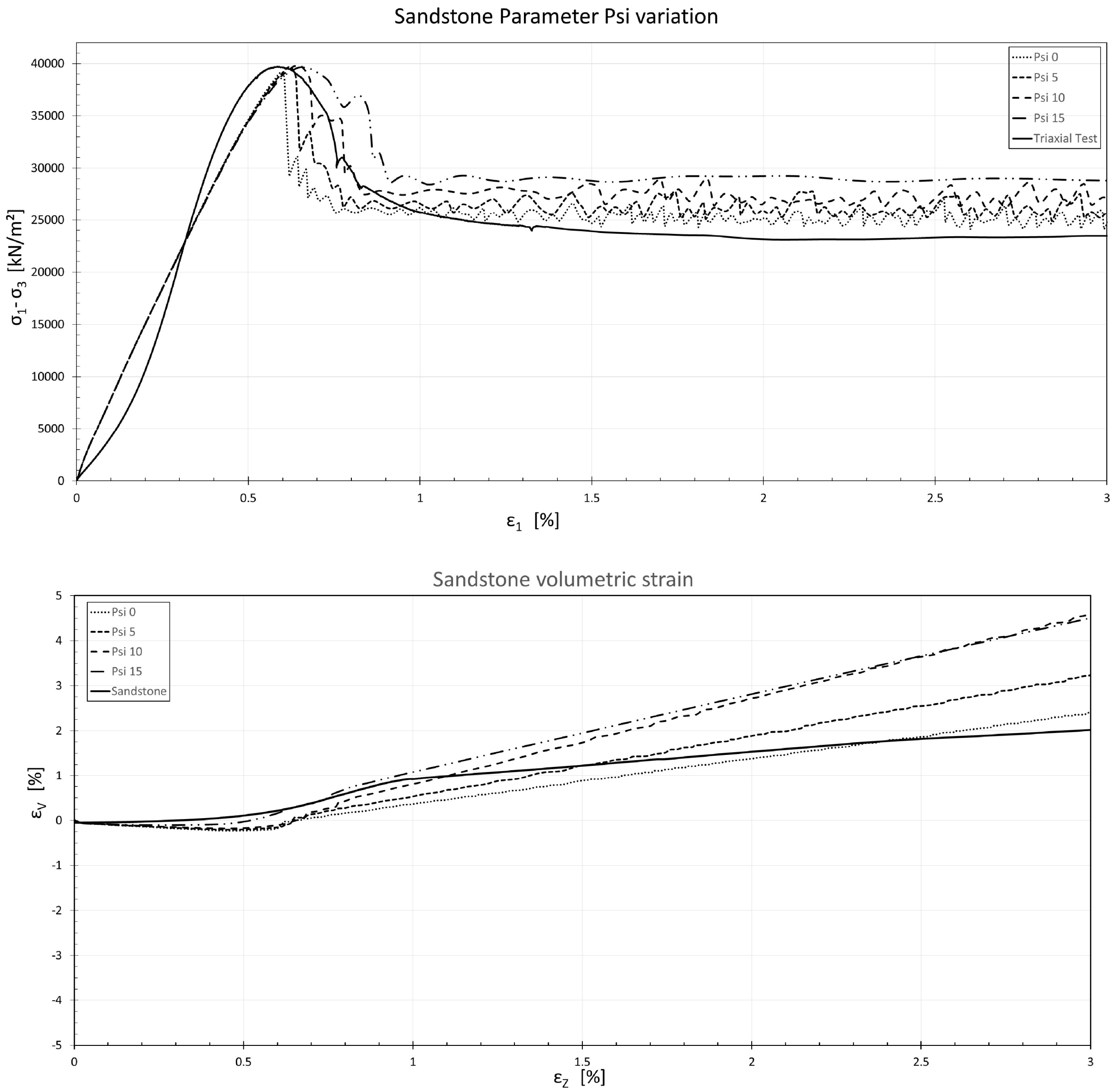

Figure 5.4 Representative stress/strain and volumetric strain curve for the Ψ variation (sandstone)

The parameter variation of the dilatancy angle ψ has no influence on the pre peak behaviour and the peak strength. The post peak regime changes from brittle to more ductile behaviour as it would be expected with increasing ψ. In addition, the residual level is also increasing with increasing dilatancy angle. From a numerical point of view, the oscillations in the residual state are reducing with increasing Ψ as well. The reason why this is stabilising the numerical calculations is not figured out by now.

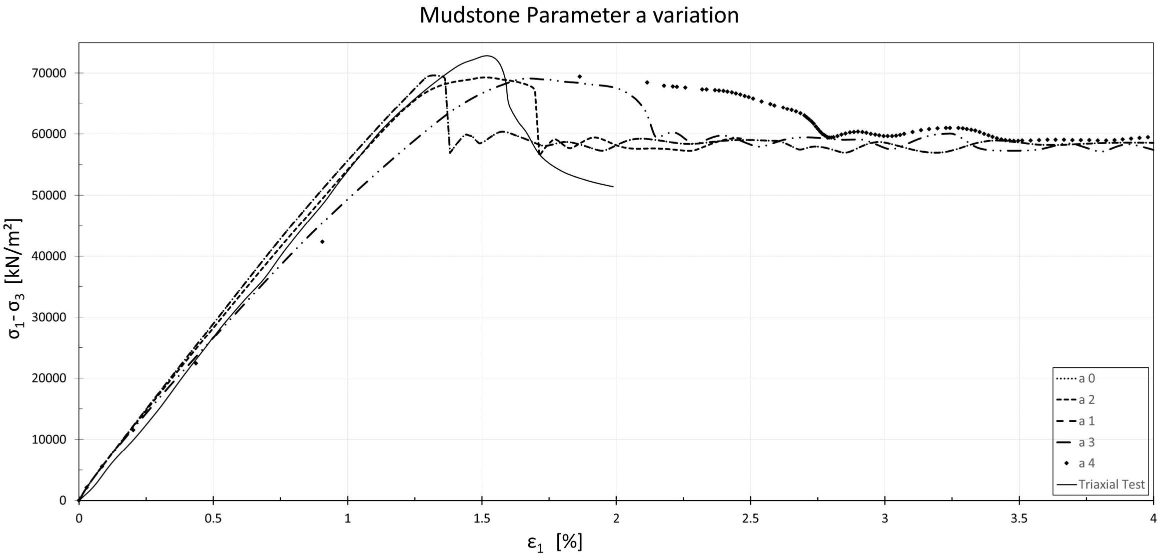

Figure 5.5 Representative stress/strain curve for the parameter a variation (mudstone)

Parameter a as a fitting parameter guides the shifting of the peak strain through increasing confining pressure stages. The influence of this is only observable for the mudstone variation. For the marl and sandstone variations the variation of a only leads to undesired changes in the residual state. Per definition there should be a difference between 0 and 1 as an input parameter for a, but this is not observable. This is discussed in detail in 5.3.6.

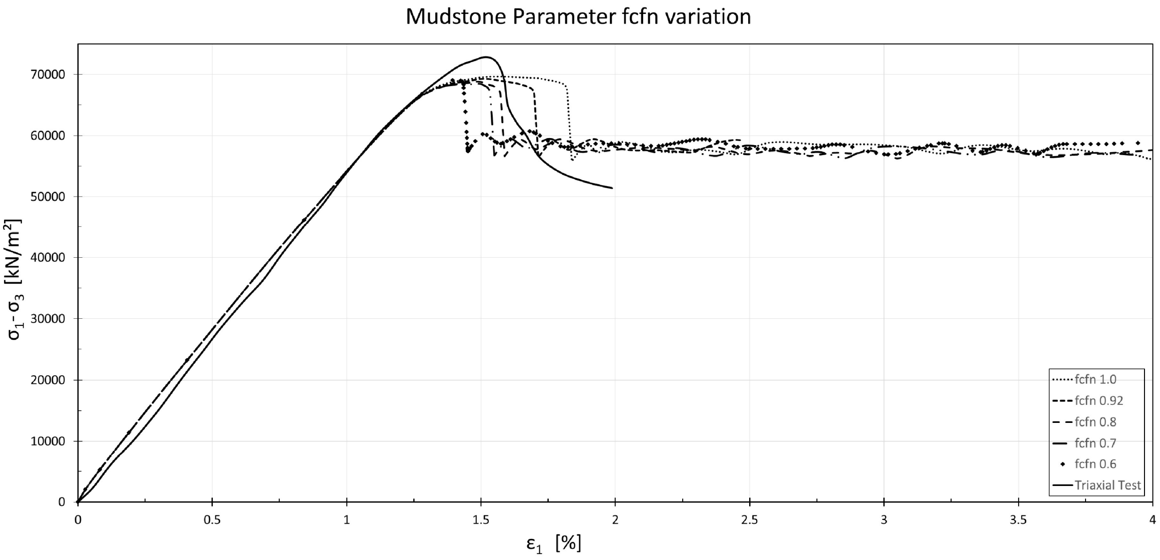

Figure 5.6 Representative stress/strain curve for the f_{cfn} variation (mudstone)

For the variation of the failure strength f_{cfn} the fracture energy G_c is kept constant to neglect its influence on the post peak behaviour. If the fracture energy would be adapted for the current failure strain, the post peak behaviour would tend to increase the softening area Zone II with decreasing failure strength. The constant G_c in this variation forces the stress/strain post peak behaviour to react in the opposite way to ensure that the "equilibrium" of failure strength and fracture energy in Zone II is fulfilled. This study should show that it is not allowed to variate these two parameters independently, because of their direct coupling (3.1.6).

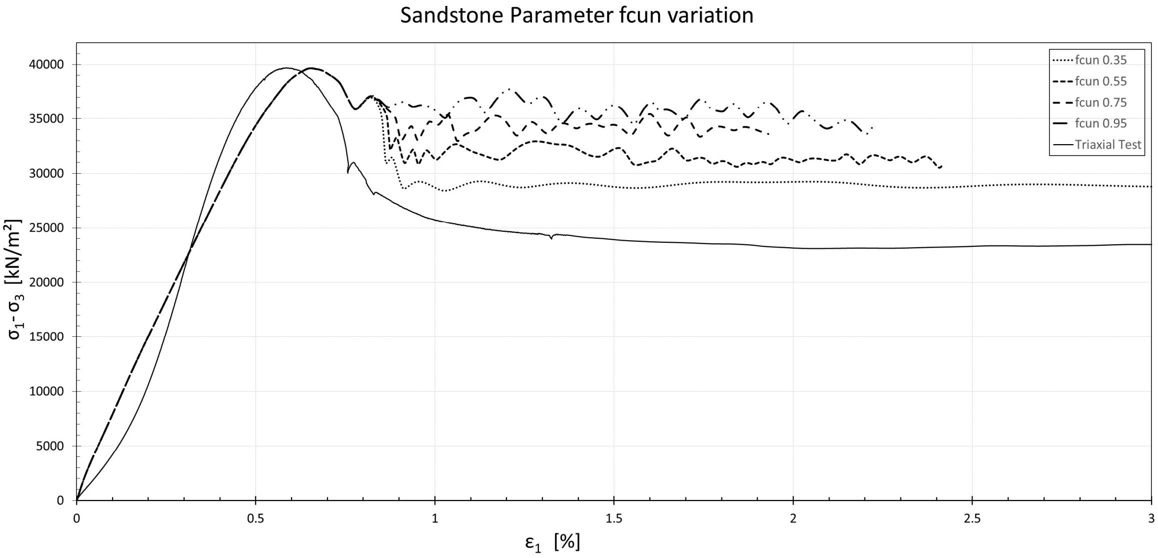

Figure 5.7 Representative stress/strain curve for the f_{cun} variation (mudstone)

The influence of the residual strength parameter f_{cun} is clearly observable in all variations. From assuming a nearly perfectly plastic behaviour where f_{cun} and f_{cfn} are equal (0.95) the residual state is decreasing with decreasing residual strength. Where the influence of the parameter is visible is defined at the end of Zone III. The same behaviour is shown for the mudstone variation. Only the marl variation does not deliver a constant residual state.

5.1.2 Case Study Interpretation

The goal of the case study is to investigate the applicability of the Concrete Model on a boundary value problem. Therefore, an excavation is calculated using the three Standard G_c Variation parameter sets of marl. In addition, a calculation is done using the Hardening Soil Model to compare the findings. The figure below shows the stress/deformation behaviour of a stress point right under the plate where the load is applied. The Intermediate and the Top Failure definition seem to reach the peak strength exactly, whereas the Residual Failure Strength graph overestimates the peak strength by a slight amount. All three variations of the Concrete Model successfully developed the expected post peak softening. The definition for the G_c variations seem to fit in the case study, because the Residual Failure Strength definition shows more deformation as well as a higher fracture energy, whereas the Top Failure definition shows a smaller amount of fracture energy.

The post peak behaviour obtained from the Hardening Soil Model cannot be considered as strain-softening because the HS Model assumes a perfectly plastic failure mode and is generally not able to model softening. More likely, this problem is cased by numerical reasons which are also visible in the 3D simulation of a triaxial compression with the HS Model section (5.3.5).

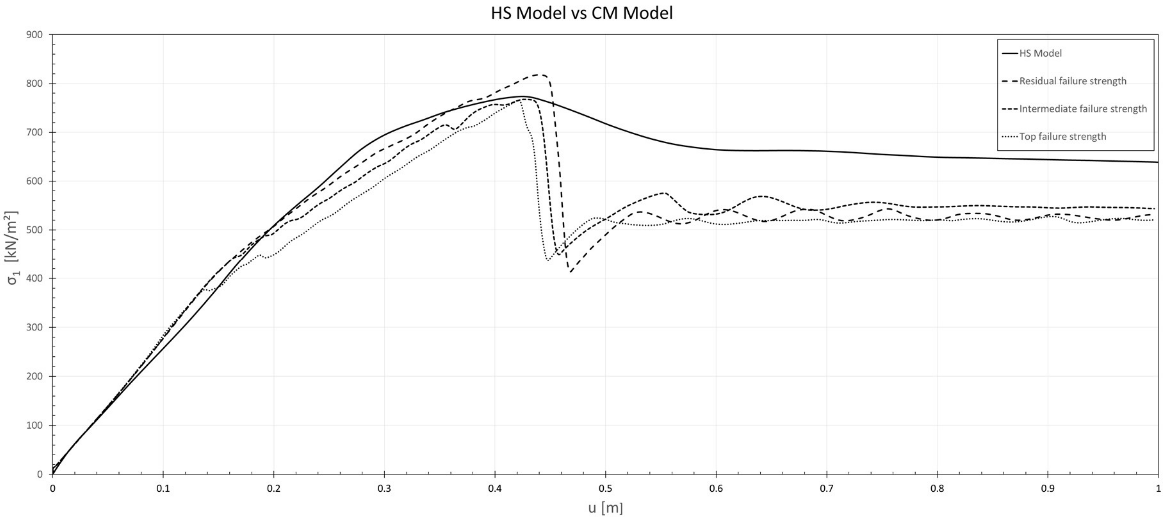

Figure 5.8 Case study result (deformation under the plate)

Considering the results of the case study, it is possible to use the Concrete Model in a boundary value problem for representing HSSR material behaviour. The Model is able to represent the non-linear hardening part, the estimated peak strength, and a proper strain-softening behaviour.

5.2 Conclusion

The main target of this thesis was to approximate the main mechanical features of HSSR material including non-linear hardening and strain-softening by utilizing the Concrete Model. Therefore, several assumptions had to be made for the parameter determination to guarantee the comparability of the materials which are described in detail in subchapter (3.1). The main problem of the Concrete Model is that it is not able to represent stress dependent stiffness at all. Therefore, the elastic modulus must be adapted on the currently acting stress situation. This is done for the drained triaxial compression simulations as well as for the case study. In both cases a comparison of the calculation results with the reference values shows a suitable approximation of the non-linear pre peak area. This proves that the secant modulus at 50% for deviatoric loading (E_{50}) can be used for representing HSSR stiffness behaviour utilizing the Concrete Model (3.1.1). The strength in compression parameters which are used in this model to represent the post peak behaviour is usually not determined for HSSR materials. Therefore, the Standard G_c Variation (3.1.6) is introduced in this thesis to represent the special characteristics of HSSR. The invented Top-, Intermediate-, and Residual Failure Strength variation is able to represent the post peak behaviour from brittle to ductile in a sufficient way. This is shown by the numerical uniaxial and triaxial test series (4.1) where this method is applied on marl, mudstone, and sandstone. In all cases the post peak strain-softening developes successfully and proves the validity of this method. Generally, the results of the numerical simulated laboratory tests approximate the real material behaviour in a sufficient way. However, there is still a slight overestimation of the residual state through all test series. Several simulations show an over- or underestimation of the peak strength which can be explained by the determination of the friction angle using Mohr circles (3.1.4). The Concrete Model uses a Mohr Coulomb failure criterion but especially for rock-like materials with a higher UCS a Hoek Brown failure envelope would approximate the material behaviour in a more precisely way (Figure 1.5). How to avoid the oscillations appearing in the post peak area caused by numerical problems, is not clear yet, but it is possible to control them using the right combination of desired iterations and maximum load fractions per step. Compared with the Hardening Soil Model, the results of the case study confirm the applicability of the Concrete Model for engineering boundary value problems. All three Standard G_c Variations deliver a good approximation of the peak strength and show a proper strain-softening. To simulate the stress dependent stiffness it is necessary to use a layered model set up with pre calculated depth related stiffnesses to guarantee realistic deformations.

The following three tables show the recommended parameter sets for marl, mudstone, and sandstone based on the simulation results gathered in this thesis

Table 5.1 Recommended parameters for marl

Marl					
Confining	[kPa]	0	50	100	200
Elastic Parameters					
E_{28}	[kPa]	10200	18000	31000	42000
ν	[-]	0.25	0.25	0.25	0.25
Strength in compression					
$f_{c,28}$	[kPa]	154	154	154	154
f_{c0n}	[-]	0.05	0.05	0.05	0.05
f_{cfn}	[-]	0.7	0.7	0.7	0.7
f_{cun}	[-]	0.35	0.35	0.35	0.35
$g_{c,28}$	[kN/m²]	1.687	1.687	1.687	1.687
$G_{c,28}$	[kN/m]	0.0968	0.0968	0.0968	0.0968
φ_{max}	[°]	32	32	32	32
ψ	[°]	10	10	10	10
Ductility					
ε_{cp}^{p}	[-]	-0.003012	-0.003012	-0.003012	-0.003012
a	[-]	1	1	1	1

Table 5.2 Recommended parameters for mudstone

Mudstone							
Confining	[MPa]	0	10	20	30	40	50
Elastic Parameters							
E_{28}	[MPa]	5480	6000	6100	6100	6757	9695
ν	[-]	0.25	0.25	0.25	0.25	0.25	0.25
Strength in compression							
$f_{c,28}$	[kPa]	26274	26274	26274	26274	26274	26274
f_{c0n}	[-]	0.1	0.1	0.1	0.1	0.1	0.1
f_{cfn}	[-]	0.92	0.92	0.92	0.92	0.92	0.92
f_{cun}	[-]	0.55	0.55	0.55	0.55	0.55	0.55
$g_{c,28}$	[kN/m²]	5.044	5.044	5.044	5.044	5.044	5.044
$G_{c,28}$	[kN/m]	0.241	0.241	0.241	0.241	0.241	0.241
φ_{max}	[°]	32	32	32	32	32	32
ψ	[°]	2	2	2	2	2	2
Ductility							
ε_{cp}^{p}	[-]	-0.0015655	-0.0015655	-0.0015655	-0.0015655	-0.0015655	-0.0015655
a	[-]	2	2	2	2	2	2

Table 5.3 Recommended parameters for sandstone

Sandstone					
Confining	[MPa]	0	2	5	10
Elastic Parameters					
E_{28}	[MPa]	2960	7795	9925	11840
ν	[-]	0.25	0.25	0.25	0.25
Strength in compression					
$f_{c,28}$	[kPa]	17452	17452	17452	17452
f_{c0n}	[-]	0.05	0.05	0.05	0.05
f_{cfn}	[-]	0.95	0.95	0.95	0.95
f_{cun}	[-]	0.35	0.35	0.35	0.35
$g_{c,28}$	[kN/m²]	8.508	8.508	8.508	8.508
$G_{c,28}$	[kN/m]	0.336	0.336	0.336	0.336
φ_{max}	[°]	45	45	45	45
ψ	[°]	15	15	15	15
Ductility					
ε_{cp}^{p}	[-]	-0.0066341	-0.0066341	-0.0066341	-0.0066341
a	[-]	0	0	0	0

5.3 Lessons learned and open questions

Several challenges were faced while working on this thesis. The problems encountered, solved and topics which need further investigation are mentioned below.

5.3.1 3D model set up

Remote scripting was used to produce the triaxial test in PLAXIS. In the first run the soil body was directly modelled as a volume element and then split into surfaces to create the top and bottom plate. Interfaces were modelled at this surfaces between the specimen and the plates. The following calculations showed that there appeared several problems like no shear band development, odd shear bands or results which were not plausible.

The solution of this problem is to create the soil body by extruding a surface. In addition, the plates as well as the interfaces are separate surfaces with individual properties. After that, the shear band development and deformation history match the expectations.

5.3.2 Oscillations

Most results show several kinds of oscillations after reaching the residual state. To overcome this problem some of the numerical control parameters should be changed. By applying very small and equal steps the effect of upscaling or downscaling can be reduced. Generally recommended combinations for the min. and max. iterations in such situations are 2/2 or 3/3 (HS Model). The mudstone and sandstone calculations are less influenced by the chosen iteration procedure and the best results are still derived with 6/60 (standard setting PLAXIS). The best results for the marl are derived with 6/6. The tolerated error is constant for all calculations with 0.01.

The post peak oscillations can also be influenced by the maximum load fraction per step. For the case study this parameter was downsized to $5 * 10^{-4}$ to reduce the unstable stress/strain behaviour. The uniaxial and triaxial tests are less affected by this parameter.

5.3.3 Uniaxial and triaxial failure mode

The figures below show the different failure modes of the investigated materials. For mudstone and sandstone a very clear shear band develops in triaxial conditions which is characteristic for the high and narrow sample sizes. The marl with their stocky dimensions develop several shear bands parallel until the authoritative failure mode occurs. The uniaxial compression results show no classic shear banding. For the mudstone a spalling like failure mode appears while marl and sandstone show an intensive vertical compression. These failure modes are not expected under uniaxial compression. A change of the model set up or the loading conditions cannot change this behaviour.

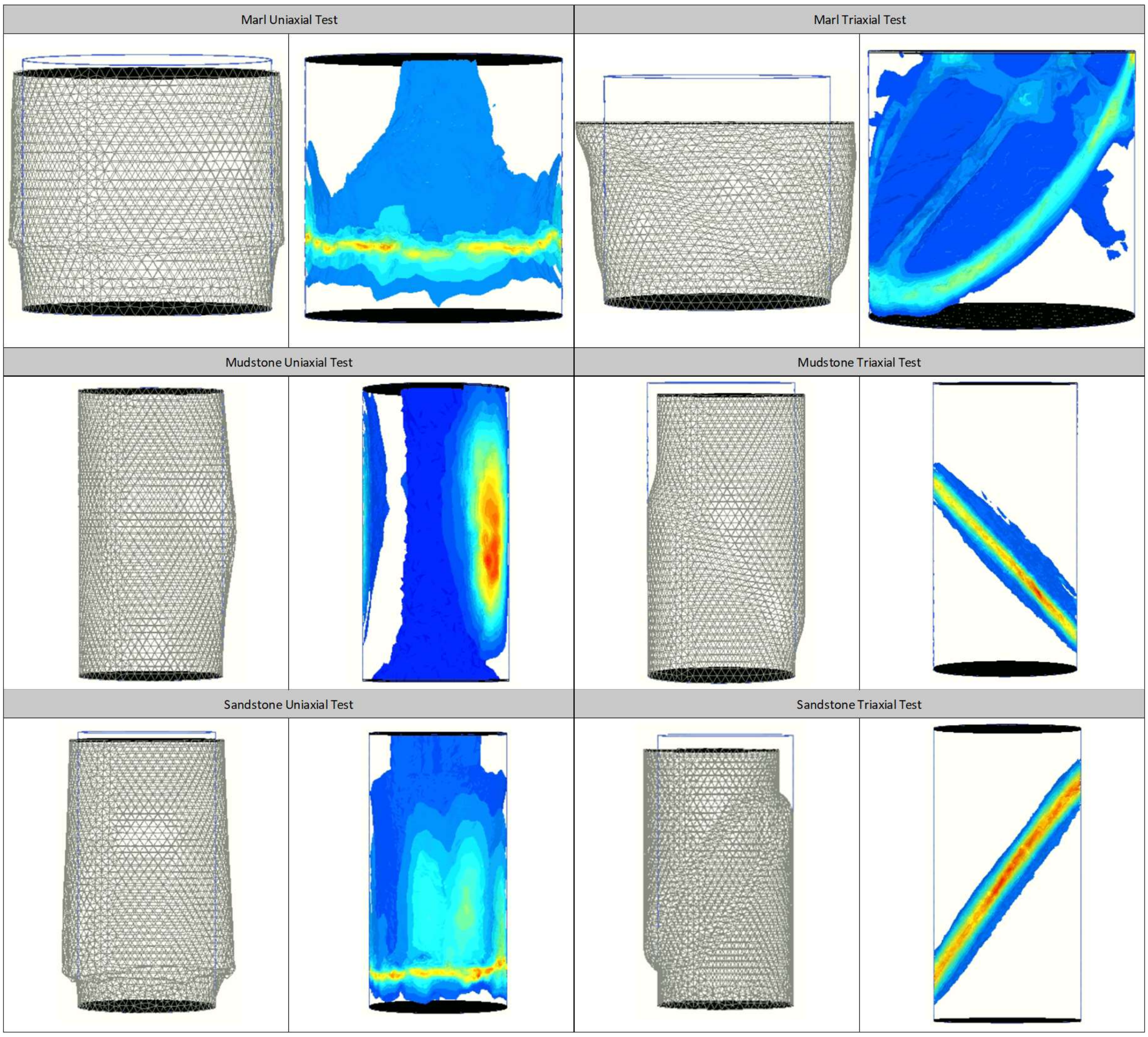

Figure 5.9 Shear band development under uniaxial- and triaxial compression

5.3.4 Influence of a homogeneous stiffness distribution

The failure mechanism of the slope (case study) is influenced by the rapid stiffness change of the layered model. To obtain if differences occur in the development of the shear surface, the model set up is changed. Therefore, the layers are removed-, and the stiffness is distributed homogeneously and constant in the whole model. The chosen elastic modulus with a reference pressure of 100 kPa is chosen as a represent value for this situation.

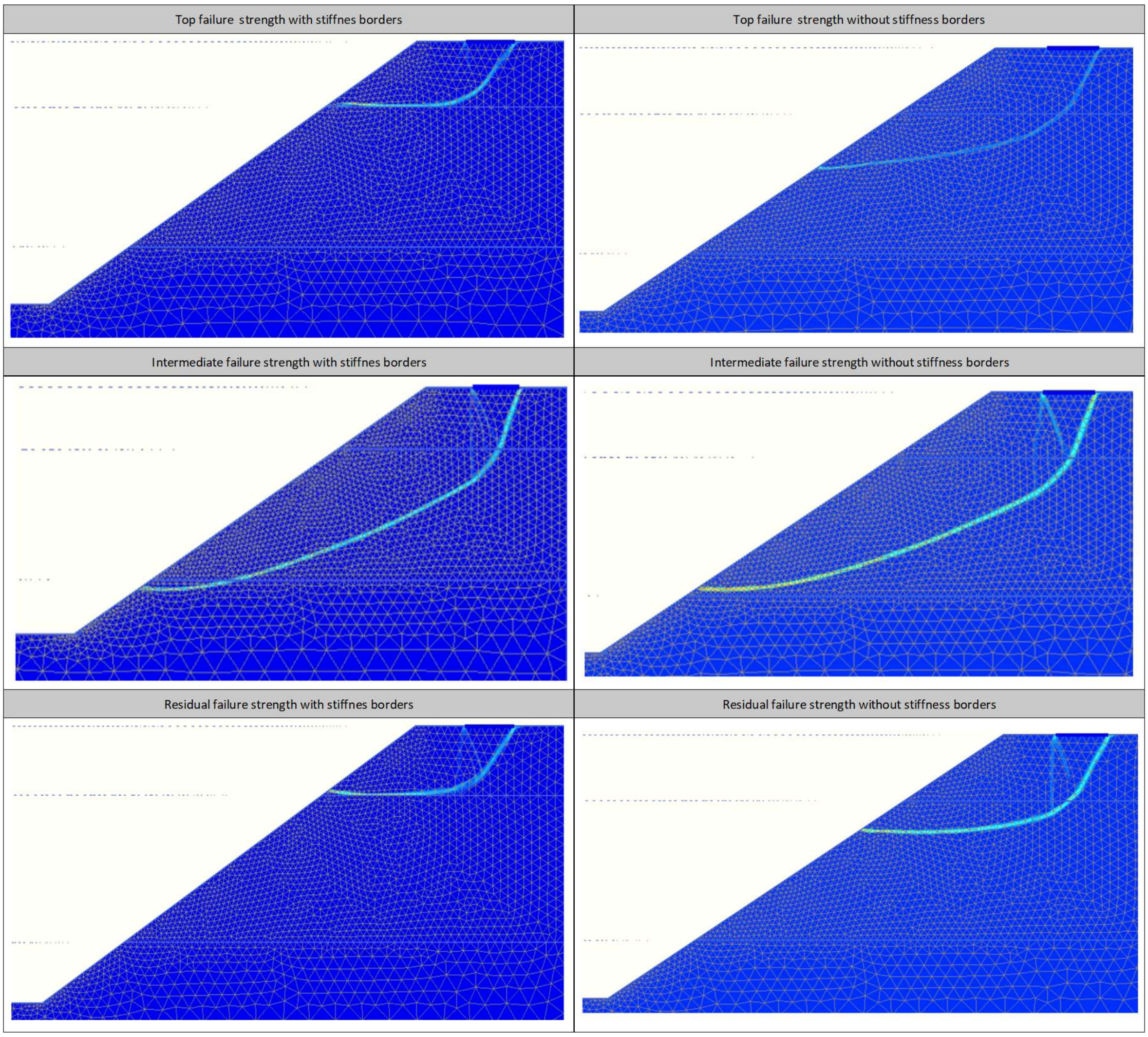

Figure 5.10 Influence of stiffness borders on shear band development

For the Top Failure and the Residual Failure Strength definition the stiffness change seems to have an impact on the resulting shear surface. The failure in both cases is shallower than with the Intermediate parameters but can develop more clearly. The Intermediate Failure Strength parameter set causes the same failure mechanism as in the layered model before.

5.3.5 Hardening Soil triaxial test simulation

The observed “strain-softening” in the case study (Figure 4.37) modelled with the Hardening Soil Model is generally not possible. This mechanical behaviour is not implemented. This undesired post peak behaviour is additionally investigated in a drained triaxial test (marl) using 50 kPa confining pressure. The Hardening Soil Model shows strain-softening in a similar way to the case study. After consultation of several experts this is caused by numerical problems of the material model or the test set up and should be investigated further.

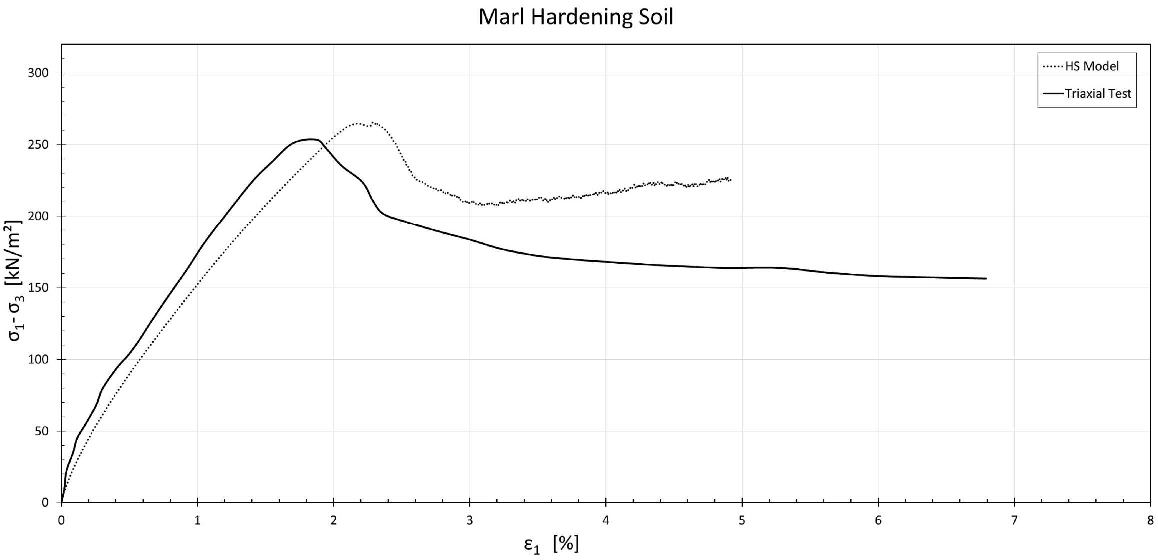

Figure 5.11 3D simulation of a drained triaxial compression test using the Hardening Soil Model (50 kPa confining pressure, marl)

5.3.6 General remarks

The shifting of the peak strain with increasing deviatoric stresses (parameter a), is only observable for the mudstone. For the marl and the sandstone simulation, no influence of this parameter is observable. In addition, according to formula (2.1) there should be a difference using zero or one for the calculations which is not observable in any simulation.

For the prescribed displacements in the triaxial simulations a value of one centimetre is used. Changing this value leads to different results in the softening regime. Using lower values for the displacements causes an earlier drop of the stress state in the post peak area. Further changes and investigations of the load fraction per step could solve this problem but is not part of this thesis.

For the triaxial loading situation and the case study, E_{50} seems to be the right elastic modulus. For other simulations, E_{oed} or E_{ur} may be a better approximation which depends on the boundary problem situation.

5.4 Outlook

The applicability of the Concrete Model for modelling HSSR material is investigated in this thesis, but still there are open questions left and there is room for improvement. Overall there are four major topics left which require further research:

- All simulations are simulated under compression. Therefore, the focus of the parameter determination was on the strength in compression parameters. Generally tension is also acting in a triaxial test because of the shearing failure. Several pre studies have shown that the influence of the Concrete Model tensile parameters in this simulations have a neglactable influence on the results. In addition, no information for the tensile behaviour was available for the investigated materials. Therefore, no information about the behaviour in the tensile stress state and the applicability of this model for HSSR material is investigated.

- The oscillations in the post peak area are manageable but cannot be removed at the moment. The numerical reasons which causes this problems should be a topic for further research.

- The time dependent parameters are neglected in this study, but the possibility to model the creep behaviour may be a task for ongoing investigations in comparison with the soft soil creep model.

- The shifting of the peak strain which is guided by parameter a is not observable for all investigated materials. In addition, several cases show an influence in the post peak behaviour which is not considered for this parameter. The detailed influence of this fitting parameter should be investigated by further studies.

Further studies on HSSR material utilizing the Concrete Model have to focus on self-generated parameter sets. Therefore, it will be advantageous to use laboratory tests from the same institution which wants to model the material. Values and parameters taken from the literature can cause uncertainties if they are not derived with respect to the Concrete Model.

6 Bibliography

Aschaber, Matthias. 2017. *Entwicklung und Anwendung eines Dreiphasenmodells für Beton.* Innsbruck : LEOPOLD–FRANZENS–UNIVERSITÄT INNSBRUCK, 2017.

Berre, Toralv. 2011. Triaxial Testing of Soft Rocks. *Geotechnical Testing Journal.* 2011, Bd. 34, 1.

E. Hoek, E.T. Brown. 1997. Practical estimates of rock mass strength. *International Journal of Rock Mechanics and Mining Sciences.* 1997, Bd. 8, 34.

Huang, Xing, et al. 2017. *Experimental Study on the Dilatancy and Fracturing Behavior of Soft Rock Under Unloading Conditions.* Iran Unuversity of Science and Technology : Iran Unuversity of Science and Technology , 2017. 10.1007/s40999-016-0144-9.

Kanji, Milton Assis. 2014. *Critical issues in soft rocks.* Journal of Rock Mechanics and Geotechnical Engineering : Elsevier B.V, 2014.

Kanji, Milton, He, Manchao und Ribeiro e Sousa, Luis. 2020. *Soft Rock Mechanics and Engineering.* Cham : Springer, 2020. 978-3-030-29476-2.

Majid Mirahmadi, Mohsen Soleiman Dehkordi. 2018. Application of the Cohesion Softening-Friction Softening and the Cohesion Softening-Friction Hardening Models oveyance Tunnel in Iranf Rock Mass Behavior to Estimate the Specific Energy of TBM, Case Study: Amir-Kabir Water Con. *Geotechnical and Geological Engineering.* 2018, 37.

Marcher, Thomas. 2003. *Nichtlokale Modellierung der Entfestigung dichter Sande und steifer Tone.* Stuttgart : P.A.Vermeer, 2003. 3-921837-50-2.

PLAXIS. 2019. *PLAXIS Material Models Manual.* s.l. : PLAXIS, 2019.

Plinninger, Ralf J., Spaun, Georg und Nickmann, Marion. 2012. *Geotechnische Aspekte der Beprobung und Untersuchung veränderlich fester Gesteine.* Deutschland : ResearchGate, 2012. 258769174.

Read, H.E. und Hegemier, G.A. 1984. *Strain Softening of Rock, Soil and Concrete - A Review Article.* North Holland : Elsevier Science Publishers B.V, 1984. 0167-6636.

Renani, Hossein Rafiei und Martin, C.Derek. 2019. *Factor of safety of strain-softening slopes.* Chinese Academy of Science : Journal of Rock Mechanics and Geotechnical Engineering, 2019. 1674-7755.

Schädlich, Bert und Schweiger, Helmut. 2016. *Shotcrete Model Implementation, validation and application.* Graz University of Technology : Computational Geotechnics Group, 2016.

Schneider, Martin. 2010. *An Advanced Transient Concrete Model for the Determination of Restraint in Concrete Structures Subjected to Fire and the Fire Resistance of Concrete*

Tunnel Sections. Wien : Vienna University of Technology, 2010.

Schütz, R., Potts, D.M und Zdravkovic, L. 2011. *Advanced constitutive modelling of shotcrete: Model formulation and calibration.* Computers and Geotechnics 38 : Elsevier, 2011.

Schütz, Reinhard. 2010. *Numerical Modelling of Shotcrete for Tunnelling.* London : Imperial College London, 2010.

Skempton, A. W. 1964. *Long-Term Stability of Clay Slopes.* s.l. : ICE Publishing, 1964. 0016-8505.

Smith, Sandra. 2017. *Retrospective Analysis of Mine Seismicity: Glencore, Kidd Mine.* Sudbory, Ontario : Laurentian University, 2017. 10.13140.

Stephen G. Wright, Jorge G. Zornberg, Jennifer E. Aguettant. 2007. *The Fully Softened Shear Strength of High Plasticity Clays.* Austin, Texas : The University of Texas at Austin, 2007.

Vakili, Abouzar. 2016. An improved unified constitutive model for rock material and guidelines for its application in numerical modelling. *Computers and Geotechnics.* s.l. : Elsevier, 2016.

Wang Ruijie, Li Chong , Xu Jinhai , Pan Lijin. 2018. Development and verification of large deformation model considering stiffness deterioration and shear dilatation effect in FLAC 3D. *International Journal of Mining Science and Technology.* 2018, 28.

7 Appendix

The following phyton code was used to generate the test set up in PLAXIS using the reote scripting function.

```
########################################################################################################################
# Author:       Stefan Stauder
# Modyfied by:  Christian Wallner
# Date:         16.02.2020
# Description:  Remote Scripting of a triaxial-test with different confining pressures
# Comments:     [NONE]
########################################################################################################################

import numpy as np
import pickle

#### Define the path to the scripting libraries ########################################################################
plaxis_path  = r'C:\Program Files\Plaxis\PLAXIS 3D\python\Lib\site-packages'
import imp

found_module = imp.find_module('plxscripting', [plaxis_path])
plxscripting = imp.load_module('plxscripting', *found_module)

from plxscripting.easy import *

#### Port info

####Alienhirn1
#localhostport        = 10000
#localhostport_output = 10001

####Alienhirn2
#localhostport        = 10002
#localhostport_output = 10003

####Superhirn
localhostport        = 10011
localhostport_output = 10010

####mani
#localhostport        =  10003#Mani PC
#localhostport_output =  10000#Mani PC

#localhostport        =  10005 #Stefan PC
#localhostport_output =  10000 #Stefan PC

#localhostport        =  #Studien Ass. PC
#localhostport_output =  #Studien Ass. PC

#### Connect to PLAXIS application with password chosen in the server settings
#s_i, g_i = new_server('localhost', localhostport, password = 'DX$ExZZETBX~y%F5')               #Alienhirn
#s_o, g_o = new_server('localhost', localhostport_output, password = 'DX$ExZZETBX~y%F5')            #Alienhirn

```

```
#s_i, g_i = new_server('localhost', localhostport, password = '9Ft7e2L/^AKfCeS%')               #Mani PC
#s_o, g_o = new_server('localhost', localhostport_output, password = '9Ft7e2L/^AKfCeS%')        #Mani PC

#s_i, g_i = new_server('localhost', localhostport, password = 'Vv4whSsf%#TMX<61')                #Stefan PC
#s_o, g_o = new_server('localhost', localhostport_output, password = 'Vv4whSsf%#TMX<61')     #Stefan PC

s_i, g_i = new_server('localhost', localhostport, password = 'mDizf@GHX=s7W?!D')               #Superhirn
s_o, g_o = new_server('localhost', localhostport_output, password = 'mDizf@GHX=s7W?!D')      #Superhirn


#### Model parameters ##################################################################################################
#### Steps for prescribed displacements
No_Steps                =  3000

#### Loads
Vertical_Pressure       = -50
Lateral_Pressure        = -50
Prescribed_Displacement = -0.01

#### Coarseness



#### Output path
output_path = 'M:\\FMT-A\\7600_Numerik Ergebnisse\\Stauder\\Diplomarbeit_Wallner\\'


#### Material parameters ###############################################################################################
#### Probe
MaterialName            = 'CM_50'
Colour                  = 10676870
SoilModel               = 13 # Concrete
DrainageType            = 'Drained'
InterfaceStrength       = 'Rigid'
K0PrimaryIsK0Secondary  = True
K0Determination         = 'Automatic'
Rinter                  = 1
gammaUnsat              = 20.25
gammaSat                = 20.37
nu                      = 0.25
ppE28                   = 30000
fc28                    = 145.717
fc0n                    = 0.05
fcfn                    = 0.43
fcun                    = 0.43
Gc28                    = [0.25]
#Gc28                    = 0.14
phimax                  = 32
concretePsi             = 10
concreteA               = 1
epscpp                  = -0.01193
epscp3                  = -0.01193



#### Plates
MaterialName_plate      = 'Plate'
Colour_plate            = 16711680
```

```
        Elasticity              = 0 # Elastic
        IsIsotropic             = True
        d                       = 0.025
        w                       = 79
        E1                      = 210000000
        E2                      = 210000000
        Nu12                    = 0.2
        G12                     = 87500000
        G13                     = 87500000
        G23                     = 87500000

        #### Bottom Interface
        MaterialName_BottomInterface           = 'Bottom_Interface'
        Colour_BottomInterface                 =  964844
        SoilModel_BottomInterface              =  2
        DrainageType_BottomInterface           = 'Drained'
        DilatancyCutOff_BottomInterface        =  False
        InterfaceStrength_BottomInterface      = 'Rigid'
        K0PrimaryIsK0Secondary_BottomInterface =  True
        K0Determination_BottomInterface        =  'Manual'
        K0Primary_BottomInterface              =  1
        cref_BottomInterface                   =  0.01
        phi_BottomInterface                    =  5
        psi_BottomInterface                    =  0
        gammaUnsat_BottomInterface             =  0
        gammaSat_BottomInterface               =  0
        Rinter_BottomInterface                 =  1
        ninit_BottomInterface                  =  0.3333333333333333
        ck_BottomInterface                     =  1e15
        nu_BottomInterface                     =  0.495
        nuu_BottomInterface                    =  0.495
        Eref_BottomInterface                   =  100e3
        Eoed_BottomInterface                   =  3377926.42140468
        Gref_BottomInterface                   =  33444.8160535117

        #### Top Interface
        MaterialName_TopInterface              = 'Top_Interface'
        Colour_TopInterface                    =  125850
        SoilModel_TopInterface                 =  2
        DrainageType_TopInterface              = 'Drained'
        DilatancyCutOff_TopInterface           =  False
        InterfaceStrength_TopInterface         = 'Rigid'
        K0PrimaryIsK0Secondary_TopInterface    =  True
        K0Determination_TopInterface           = 'Manual'
        K0Primary_TopInterface                 =  1
        cref_TopInterface                      =  0.01
        phi_TopInterface                       =  2.5
        psi_TopInterface                       =  0
        gammaUnsat_TopInterface                =  0
        gammaSat_TopInterface                  =  0
        Rinter_TopInterface                    =  1
        ninit_TopInterface                     =  0.3333333333333333
        ck_TopInterface                        =  1e15
        nu_TopInterface                        =  0.495
        nuu_TopInterface                       =  0.495
        Eref_TopInterface                      =  100e3
        Eoed_TopInterface                      =  3377926.42140468
        Gref_TopInterface                      =  33444.8160535117


        #### Model Generation ##################################################################################################

        s_i.new()   # Start a new project

        #### Set model and element properties
```

```
        g_i.setproperties('ModelType', 'Full', 'ElementType', '10-Noded', 'UnitForce', 'kN')
        g_i.SoilContour.initializerectangular(-0.1, -0.1, 0.1, 0.1)

        #### Assign materials
        probe = g_i.soilmat()
        probe.setproperties('MaterialName', MaterialName,
                            'Colour', Colour,
                            'SoilModel', SoilModel,
                            'DrainageType', DrainageType,
                            'InterfaceStrength', InterfaceStrength,
                            'K0PrimaryIsK0Secondary', K0PrimaryIsK0Secondary,
                            'K0Determination', K0Determination,
                            'Rinter', Rinter,
                            'gammaUnsat', gammaUnsat,
                            'gammaSat', gammaSat,
                            'nu', nu,
                            'ppE28', ppE28,
                            'fc28', fc28,
                            'fc0n', fc0n,
                            'fcfn', fcfn,
                            'fcun', fcun,
                            'Gc28', Gc28[0],
                            'phimax', phimax,
                            'concretePsi', concretePsi,
                            'concreteA', concreteA,
                            'epscpp', epscpp,
                            'epscp3',epscp3)



        plate = g_i.platemat()
        plate.setproperties('MaterialName', MaterialName_plate,
                            'Colour', Colour_plate,
                            'Elasticity', Elasticity,
                            'IsIsotropic', IsIsotropic,
                            'd', d,
                            'w', w,
                            'E1', E1,
                            'E2', E2,
                            'Nu12', Nu12,
                            'G12', G12,
                            'G13', G13,
                            'G23', G23)

        bottom_interface = g_i.soilmat()
        bottom_interface.setproperties('MaterialName', MaterialName_BottomInterface,
                               'Colour', Colour_BottomInterface,
                               'SoilModel', SoilModel_BottomInterface,
                               'DrainageType', DrainageType_BottomInterface,
                               'DilatancyCutOff', DilatancyCutOff_BottomInterface,
                               'InterfaceStrength', InterfaceStrength_BottomInterface,
                               'K0PrimaryIsK0Secondary', K0PrimaryIsK0Secondary_BottomInterface,
                               'K0Determination', K0Determination_BottomInterface,
                               'K0Primary', K0Primary_BottomInterface,
                               'cref', cref_BottomInterface,
                               'phi', phi_BottomInterface,
                               'psi', psi_BottomInterface,
                               'gammaUnsat', gammaUnsat_BottomInterface,
                               'gammaSat', gammaSat_BottomInterface,
```

```
                              'Rinter', Rinter_BottomInterface,
                              'ninit', ninit_BottomInterface,
                              'ck', ck_BottomInterface,
                              'nuu', nuu_BottomInterface,
                              'nu', nu_BottomInterface,
                              'Eref', Eref_BottomInterface,
                              'Gref', Gref_BottomInterface,
                              'Eoed', Eoed_BottomInterface)

       top_interface = g_i.soilmat()
       top_interface.setproperties('MaterialName', MaterialName_TopInterface,
                              'Colour', Colour_TopInterface,
                              'SoilModel', SoilModel_TopInterface,
                              'DrainageType', DrainageType_TopInterface,
                              'DilatancyCutOff', DilatancyCutOff_TopInterface,
                              'InterfaceStrength', InterfaceStrength_TopInterface,
                              'K0PrimaryIsK0Secondary', K0PrimaryIsK0Secondary_TopInterface,
                              'K0Determination', K0Determination_TopInterface,
                              'K0Primary', K0Primary_TopInterface,
                              'cref', cref_TopInterface,
                              'phi', phi_TopInterface,
                              'psi', psi_TopInterface,
                              'gammaUnsat', gammaUnsat_TopInterface,
                              'gammaSat', gammaSat_TopInterface,
                              'Rinter', Rinter_TopInterface,
                              'ninit', ninit_TopInterface,
                              'ck', ck_TopInterface,
                              'nuu', nu_TopInterface,
                              'nu', nu_TopInterface,
                              'Eref', Eref_TopInterface,
                              'Gref', Gref_BottomInterface,
                              'Eoed', Eoed_BottomInterface)

       #### Structures
       g_i.gotostructures()

       #### Creation of the soil volume
       #volume = g_i.cylinder(0.05, 0.1, 0, 0, -0.1, 0, 0, 1)   # radius, height, creation points x2 y2 z2, direction points x3 y3 z3
       #g_i.Soils[0].Material = probe #   Assign probe to the "soil"
       #volume_1 = g_i.Volume_1


       polycurve1 = g_i.polycurve(0, -0.05, 0, 1, 0, 0, 0, 1, 0)
       polycurve1.reset('Arc', 0, 360, 0.05)
       polycurve_1 = g_i.Polycurve_1 #definition of the plate to the polycurve object (including the next line)
       #g_i.plate(polycurve_1)
       g_i.surface(polycurve_1)

       polycurve2 = g_i.polycurve(0, -0.05, -0.1, 1, 0, 0, 0, 1, 0)
       polycurve2.reset('Arc', 0, 360, 0.05)
       polycurve_2 = g_i.Polycurve_2 #definition of the plate to the polycurve object (including the next line)
       #g_i.plate(polycurve_2)
       g_i.surface(polycurve_2)

       surface_1 = g_i.Surface_1 #(Alternative way of use of volumes)
       surface_2 = g_i.Surface_2 #(Alternative way of use of volumes)

       g_i.extrude(surface_1, 0, 0, -0.1)
```

```
        g_i.Soils[0].Material = probe #   Assign probe to the "soil"
        volume_1 = g_i.Volume_1

        #### Decomposition of volume, creates the surfaces
        g_i.decomposesrf(volume_1)
        surfacevolume_1_1 = g_i.Surface_Volume_1_1   # Assigns the surface to the variable surfacevolume_1_1
        surfacevolume_1_2 = g_i.Surface_Volume_1_2
        surfacevolume_1_3 = g_i.Surface_Volume_1_3

        #### Decomposition of volume, creates the surfaces
        #g_i.decomposesrf(volume_2)
        #surfacevolume_2_1 = g_i.Surface_Volume_2_1   # Assigns the surface to the variable surfacevolume_1_1
        #surfacevolume_2_2 = g_i.Surface_Volume_2_2
        #surfacevolume_2_3 = g_i.Surface_Volume_2_3

        #g_i.remove volume_2 from volume_1

        #surface_1 = g_i.Surface_1 #(Alternative way of use of volumes)
        #surface_2 = g_i.Surface_2 #(Alternative way of use of volumes)

        #### Assignment of the Plates
        g_i.plate(surfacevolume_1_1)   # Creates the plate from the surface
        g_i.plate(surfacevolume_1_3)   # Creates the plate from the surface
        g_i.Plates[0].Material = plate   # Assigns the first material to the plate
        g_i.Plates[1].Material = plate   # Assigns the second material to the plate

        #    g_i.delete(surface_1) # enables to delete the surfaces created before
        #    g_i.delete(surface_2) # enables to delete the surfaces created before

        #### Definition of surface loads
        g_i.surfload(surfacevolume_1_1, 'sigz', Lateral_Pressure) # corresponds to 'surfload Polycurve_8 "sigx" 2 "sigy" 5', written on the website
        surfaceload_2 = g_i.surfload(surfacevolume_1_2, 'Distribution', 'Perpendicular', 'sign_ref', Lateral_Pressure)

        #### Definition of Interfaces
        neg_topinterface    = g_i.neginterface(surface_1, 'MaterialMode', 'Custom', 'Material', top_interface)
        pos_topinterface    = g_i.posinterface(surface_1, 'MaterialMode', 'Custom', 'Material', top_interface)
        neg_bottominterface = g_i.neginterface(surface_2, 'MaterialMode', 'Custom', 'Material', bottom_interface)
        pos_bottominterface = g_i.posinterface(surface_2, 'MaterialMode', 'Custom', 'Material', bottom_interface)

        #### Definition of Prescribed Displacement
        surfacedisp = g_i.surfdispl(surfacevolume_1_1, 'Displacement_x', 'Free', 'Displacement_y', 'Free', 'Displacement_z',
                                    'Prescribed', 'Distribution', 'Uniform', 'uz', Prescribed_Displacement)


        #### Meshing and selection of curve points
        g_i.gotomesh()
        g_i.mesh(0.05, 256, True, 1.2, 0.005) # (Coarseness, Max_Core_to_Use, Enhanced_Mesh, Global_SF, Min_Element_Size)
        #g_i.mesh(0.05) # (Coarseness, Max_Core_to_Use, Enhanced_Mesh, Global_SF, Min_Element_Size)

        g_i.selectmeshpoints() # Opens Curve Point Selecter

```

```
          # Indexing CurvePoints: Node1 (CN_1), Node2 (CN_2), ..., NodeX (CN_X), StressPoint1 (CS_1), StressPoint2 (CS_2), ..., StressPointX (CS_X)
        g_o.addcurvepoint('Node', (0,0,0))   # Selects the the node closest to the (X1 Y1 Z1) coordinates
        g_o.CurvePoints[0].Identification.set('Node_uZ')   # Changes the name of the selected point

        g_o.addcurvepoint('Node', (0.05,0,-0.05))
        g_o.CurvePoints[1].Identification.set('Node_uX1')

        g_o.addcurvepoint('Node', (0,0.05,-0.05))
        g_o.CurvePoints[2].Identification.set('Node_uY1')

        g_o.addcurvepoint('Node', (-0.05,0,-0.05))
        g_o.CurvePoints[3].Identification.set('Node_uX2')

        g_o.addcurvepoint('Node', (0,-0.05,-0.05))
        g_o.CurvePoints[4].Identification.set('Node_uY2')

        g_o.addcurvepoint('StressPoint', (0,0,0))   # Selects the the StressPoint closest to the (X1 Y1 Z1) coordinates
        g_o.CurvePoints[5].Identification.set('StressPoint_uZ')

        g_o.addcurvepoint('StressPoint', (0.05,0,-0.05))
        g_o.CurvePoints[6].Identification.set('StressPoint_uX1')

        g_o.addcurvepoint('StressPoint', (0,0.05,-0.05))
        g_o.CurvePoints[7].Identification.set('StressPoint_uY1')

        g_o.addcurvepoint('StressPoint', (-0.05,0,-0.05))
        g_o.CurvePoints[8].Identification.set('StressPoint_uX2')

        g_o.addcurvepoint('StressPoint', (0,-0.05,-0.05))
        g_o.CurvePoints[9].Identification.set('StressPoint_uY2')

        g_o.update()   # Updates and saves the selcected points selected and goes back to the input window
        #    g_i.viewmesh()   # If desired, user can activate the mesh view crossing out the comment sign.

        #### Staged construction
        g_i.gotostages()

        # Boundary conditions
        g_i.Deformations.BoundaryXMin.set(g_i.Phases[:], 'Free')
        g_i.Deformations.BoundaryXMax.set(g_i.Phases[:], 'Free')
        g_i.Deformations.BoundaryYMin.set(g_i.Phases[:], 'Free')
        g_i.Deformations.BoundaryYMax.set(g_i.Phases[:], 'Free')
        g_i.Deformations.BoundaryZMin.set(g_i.Phases[:], 'Fully fixed')
        g_i.Deformations.BoundaryZMax.set(g_i.Phases[:], 'Free')

        # Initial phase
        g_i.Plates.activate(g_i.InitialPhase)
        g_i.Soils.activate(g_i.InitialPhase)

        # Phase 1
        g_i.phase(g_i.InitialPhase)  # Creation of a new phase (g_i.previous_phase)
        g_i.setcurrentphase(g_i.Phase_1)
        g_i.Phase_1.Identification = 'Isotropic Loading'   # Entitles the face
        g_i.Plates.activate(g_i.Phase_1)   # Activates all plates
        g_i.Interfaces.activate(g_i.Phase_1)   # Activates all interfaces
        g_i.SurfaceLoads.activate(g_i.Phase_1)   # Activates all surface loads
        g_i.Phase_1.Deform.ResetDisplacementsToZero = True    # Reset displacements
        g_i.Phase_1.Deform.UseDefaultIterationParams.set(False)
        g_i.Phase_1.Deform.ArcLengthControl = 'Off'
```

```
        g_i.Phase_1.Deform.MaxSteps = No_Steps
        #    g_i.Phase_1.Solver = 'Pardiso (multicore direct)'

        # Phase 2
        g_i.phase(g_i.Phase_1)
        g_i.setcurrentphase(g_i.Phase_2)
        g_i.Phase_2.Identification = 'Prescribed Displacement'
        g_i.Plates.activate(g_i.Phase_2)   # Activates all plates
        g_i.Interfaces.activate(g_i.Phase_2)   # Activates all interfaces
        g_i.SurfaceDisplacements.activate(g_i.Phase_2)
        g_i.Phase_2.Deform.ResetDisplacementsToZero = True
        g_i.Phase_2.Deform.UseDefaultIterationParams.set(False)
        g_i.Phase_2.Deform.ArcLengthControl = 'Off'
        g_i.Phase_2.Deform.MaxSteps = No_Steps
        g_i.Phase_2.MaxStepsStored = 100
        #    g_i.Phase_2.Solver = 'Pardiso (multicore direct)'

        #### Calculation and output ########################################################################################

        for i in range(len(Gc28)):

            g_i.gotostages()

            if i != 0:
                g_i.InitialPhase.ShouldCalculate = True
                g_i.Phase_1.ShouldCalculate = True
                g_i.Phase_2.ShouldCalculate = True

            probe.setproperties('Gc28', Gc28[i])

            g_i.calculate()

            model_path = output_path + MaterialName + '_Gc28_' + str(Gc28[i]) + '.p3dx'
            g_i.save(model_path)   # Save project


```

The following graphs show a preliminary study on a uniaxial test of marl using the PLAXIS Soil Test Tool, to obtain the influence of several parameters in a stress point analysis.

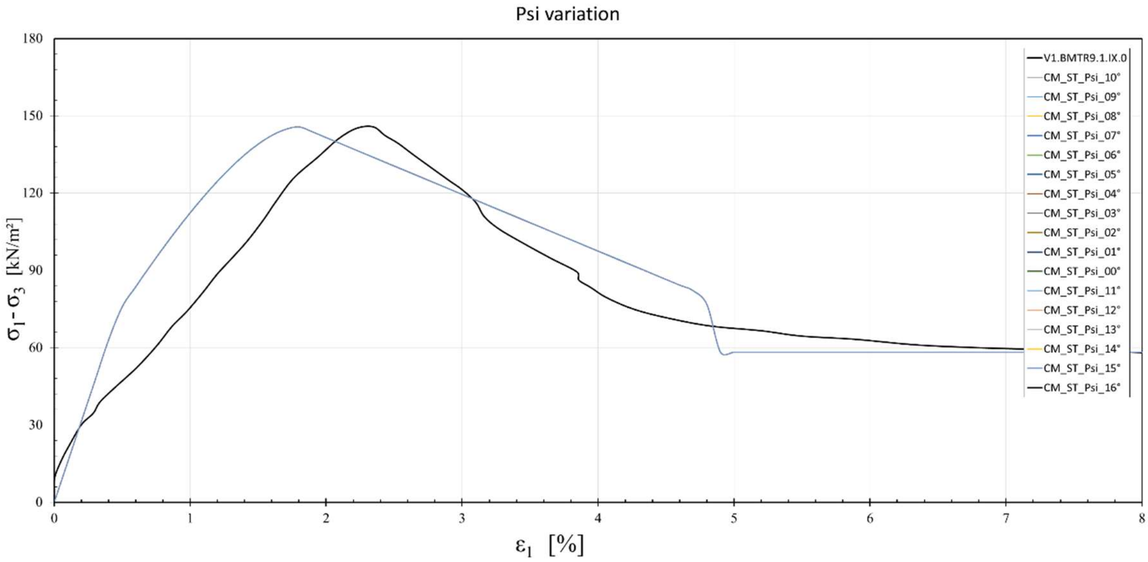

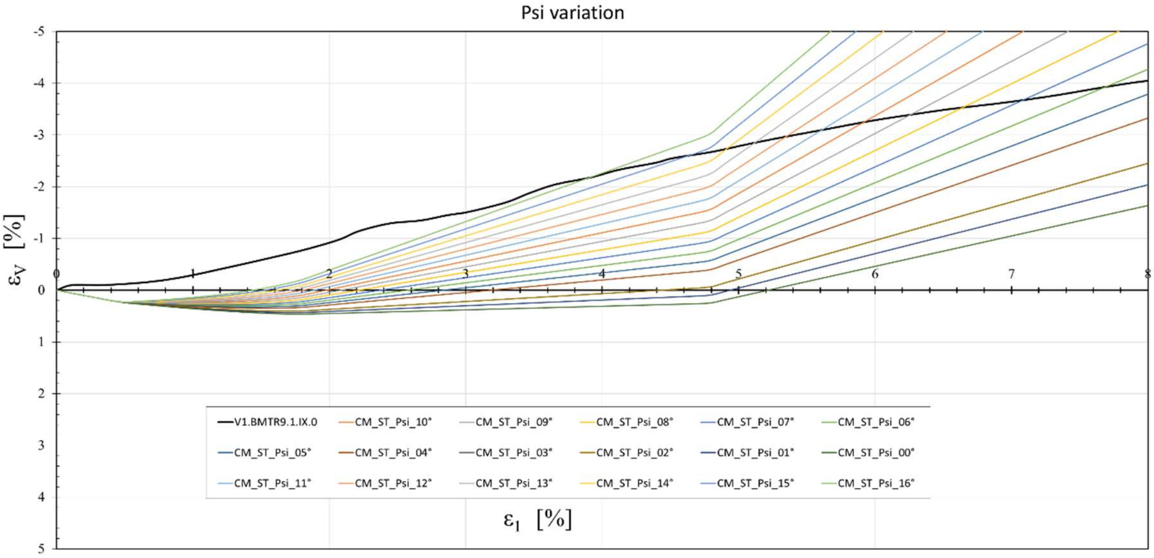

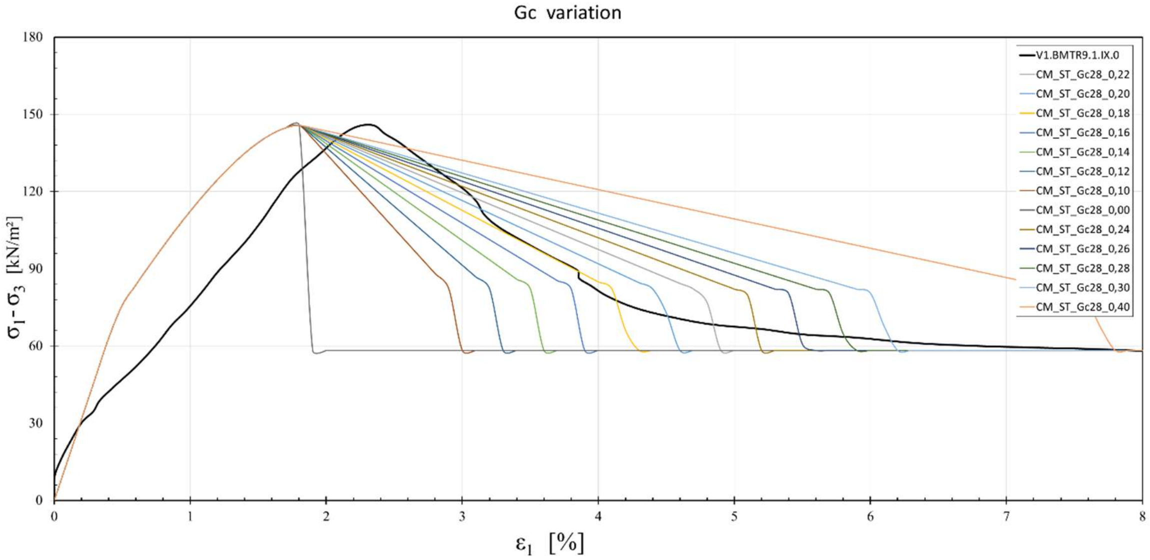
Gc variation
180
150
120
90
60
30
0
$\sigma_1 - \sigma_3$ [kN/m²]
0
1
2
3
4
5
6
7
8
ε_1 [%]
V1.BMTR9.1.IX.0
CM_ST_Gc28_0,22
CM_ST_Gc28_0,20
CM_ST_Gc28_0,18
CM_ST_Gc28_0,16
CM_ST_Gc28_0,14
CM_ST_Gc28_0,12
CM_ST_Gc28_0,10
CM_ST_Gc28_0,00
CM_ST_Gc28_0,24
CM_ST_Gc28_0,26
CM_ST_Gc28_0,28
CM_ST_Gc28_0,30
CM_ST_Gc28_0,40

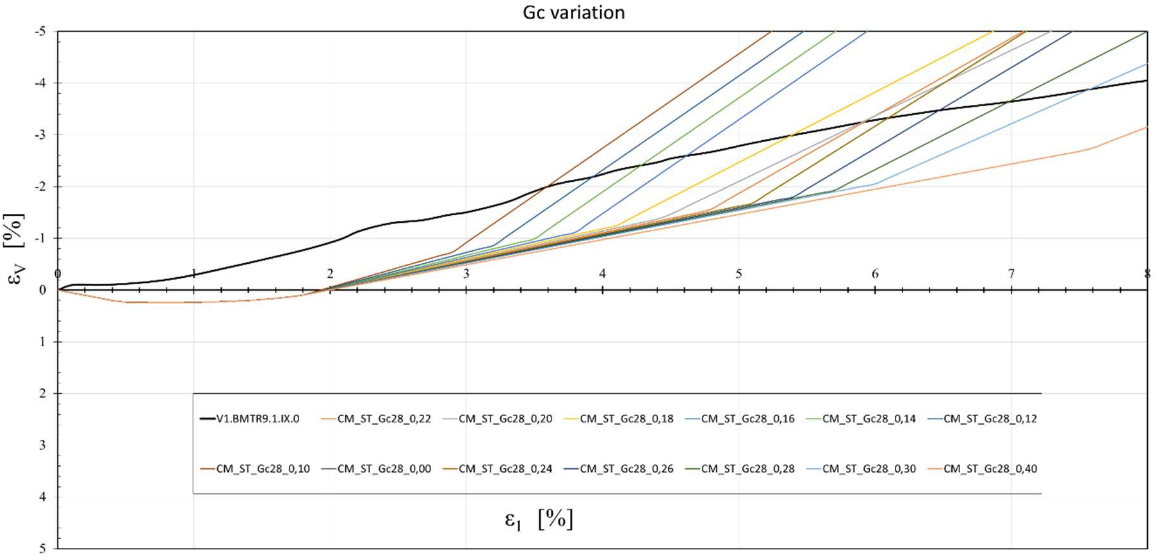
Gc variation
-5
-4
-3
-2
-1
0
1
2
3
4
5
ε_V [%]
0
2
3
4
5
6
7
8
V1.BMTR9.1.IX.0
CM_ST_Gc28_0,22
CM_ST_Gc28_0,20
CM_ST_Gc28_0,18
CM_ST_Gc28_0,16
CM_ST_Gc28_0,14
CM_ST_Gc28_0,12
CM_ST_Gc28_0,10
CM_ST_Gc28_0,00
CM_ST_Gc28_0,24
CM_ST_Gc28_0,26
CM_ST_Gc28_0,28
CM_ST_Gc28_0,30
CM_ST_Gc28_0,40
ε_1 [%]

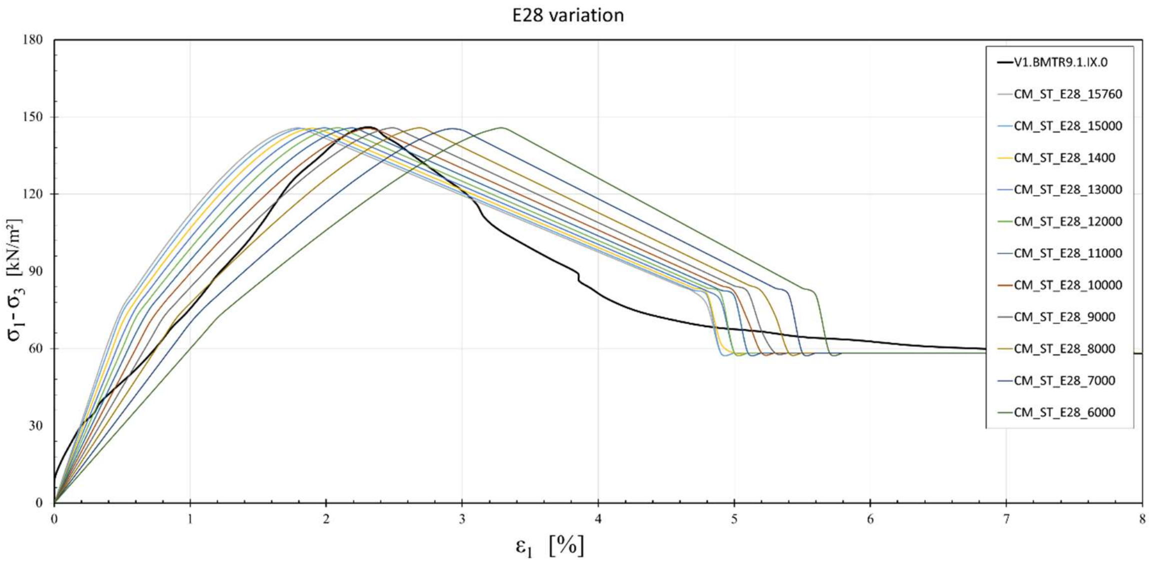
E28 variation
σ1 - σ3 [kN/m²]
ε1 [%]
0
30
60
90
120
150
180
0
1
2
3
4
5
6
7
8
V1.BMTR9.1.IX.0
CM_ST_E28_15760
CM_ST_E28_15000
CM_ST_E28_1400
CM_ST_E28_13000
CM_ST_E28_12000
CM_ST_E28_11000
CM_ST_E28_10000
CM_ST_E28_9000
CM_ST_E28_8000
CM_ST_E28_7000
CM_ST_E28_6000

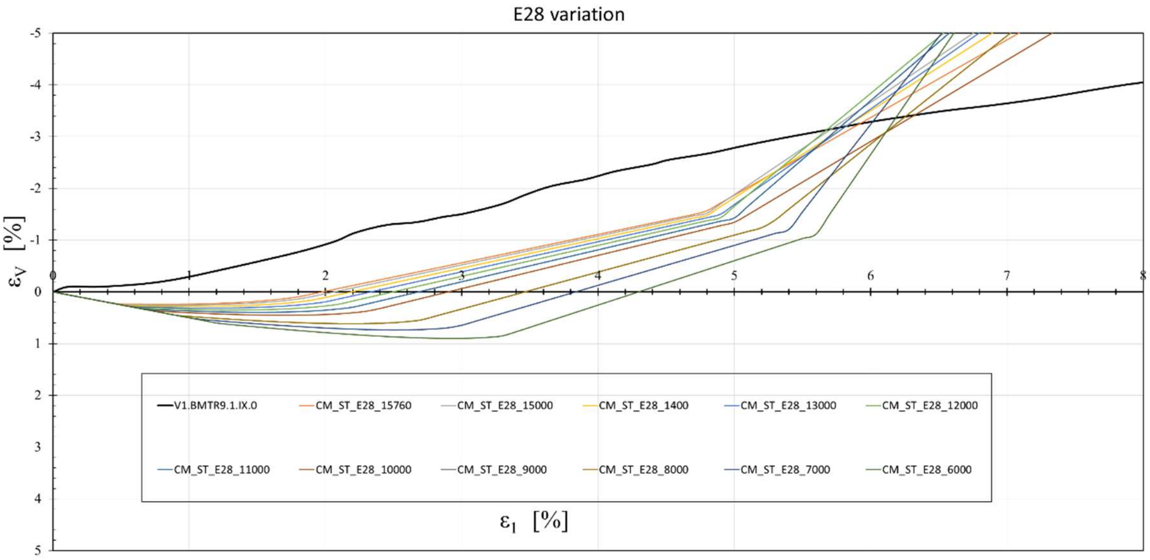
E28 variation
εV [%]
ε1 [%]
-5
-4
-3
-2
-1
0
1
2
3
4
5
0
1
2
3
4
5
6
7
8
V1.BMTR9.1.IX.0
CM_ST_E28_15760
CM_ST_E28_15000
CM_ST_E28_1400
CM_ST_E28_13000
CM_ST_E28_12000
CM_ST_E28_11000
CM_ST_E28_10000
CM_ST_E28_9000
CM_ST_E28_8000
CM_ST_E28_7000
CM_ST_E28_6000

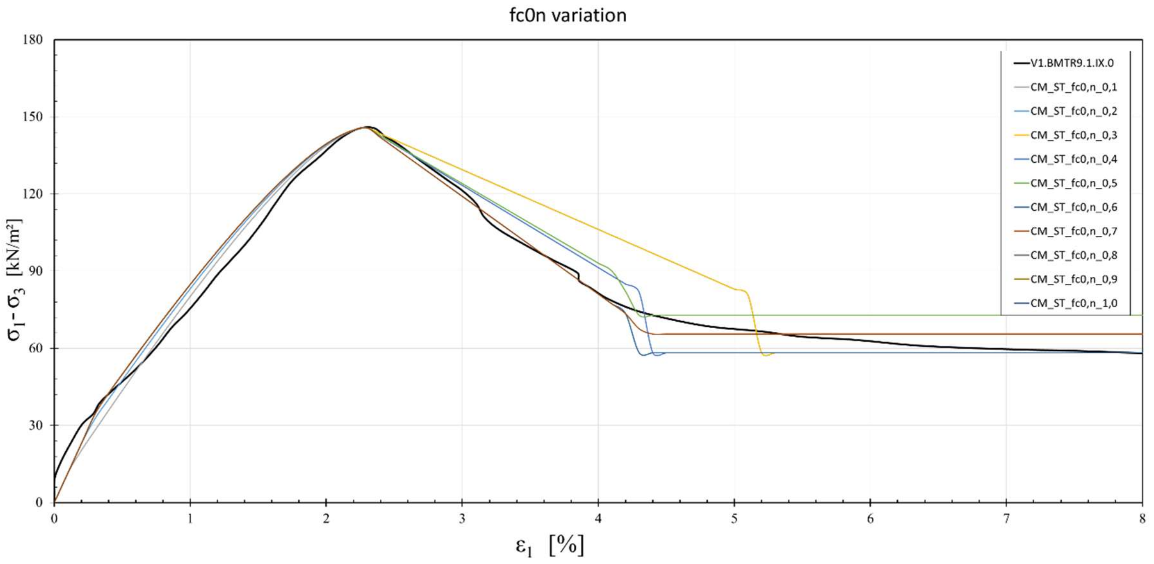
fc0n variation
180
150
120
90
60
30
0
$\sigma_1 - \sigma_3$ [kN/m²]
0
1
2
3
4
5
6
7
8
ε_1 [%]
V1.BMTR9.1.IX.0
CM_ST_fc0,n_0,1
CM_ST_fc0,n_0,2
CM_ST_fc0,n_0,3
CM_ST_fc0,n_0,4
CM_ST_fc0,n_0,5
CM_ST_fc0,n_0,6
CM_ST_fc0,n_0,7
CM_ST_fc0,n_0,8
CM_ST_fc0,n_0,9
CM_ST_fc0,n_1,0

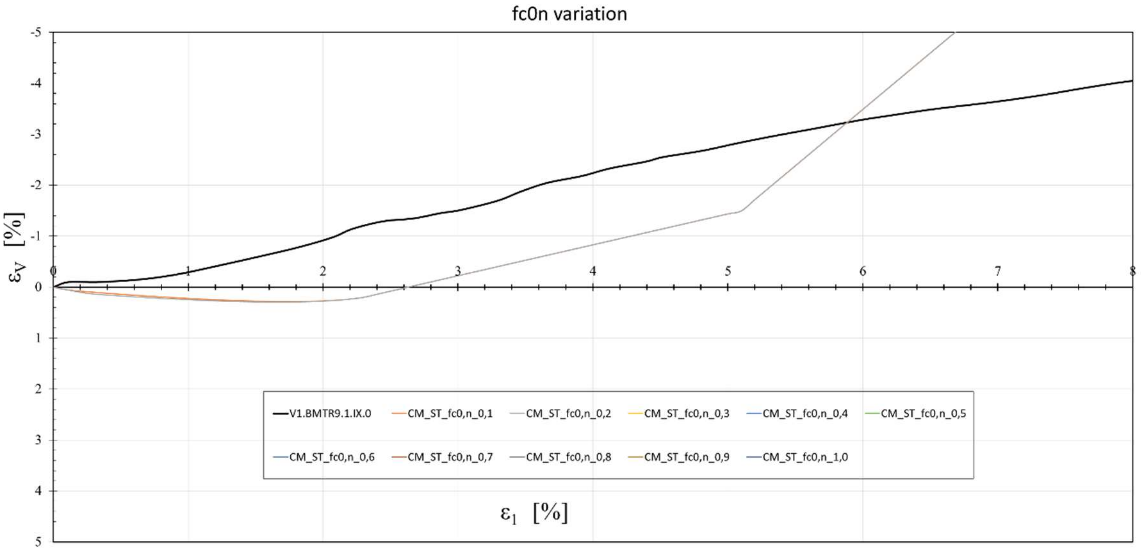
fc0n variation
-5
-4
-3
-2
-1
0
1
2
3
4
5
ε_V [%]
0
1
2
3
4
5
6
7
8
ε_1 [%]
V1.BMTR9.1.IX.0
CM_ST_fc0,n_0,1
CM_ST_fc0,n_0,2
CM_ST_fc0,n_0,3
CM_ST_fc0,n_0,4
CM_ST_fc0,n_0,5
CM_ST_fc0,n_0,6
CM_ST_fc0,n_0,7
CM_ST_fc0,n_0,8
CM_ST_fc0,n_0,9
CM_ST_fc0,n_1,0

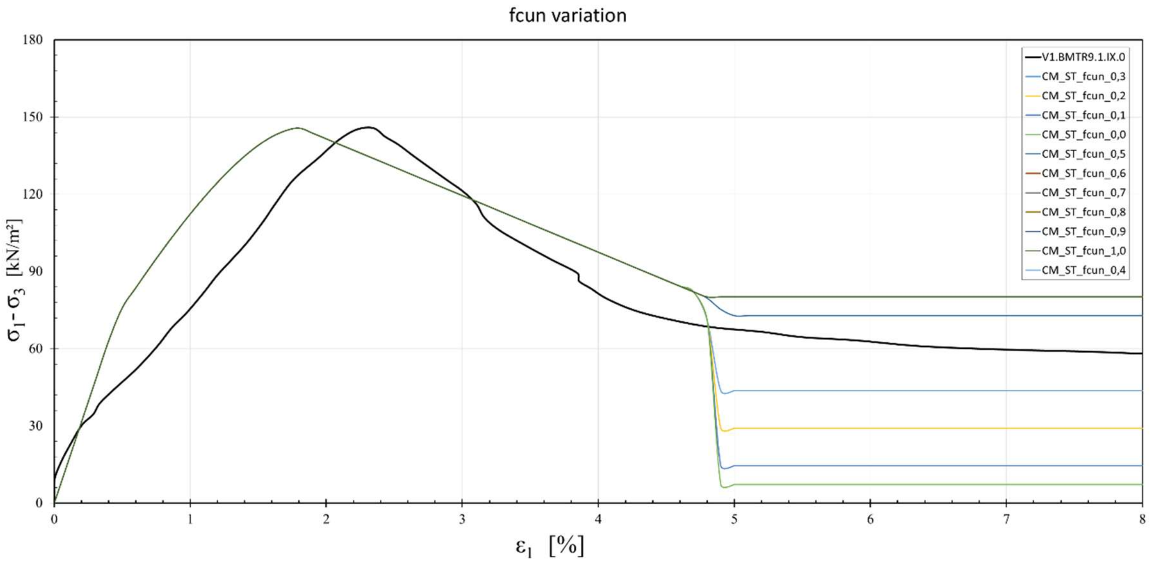
fcun variation
180
150
120
90
60
30
0
0
1
2
3
4
5
6
7
8
σ1 - σ3 [kN/m²]
ε1 [%]
V1.BMTR9.1.IX.0
CM_ST_fcun_0,3
CM_ST_fcun_0,2
CM_ST_fcun_0,1
CM_ST_fcun_0,0
CM_ST_fcun_0,5
CM_ST_fcun_0,6
CM_ST_fcun_0,7
CM_ST_fcun_0,8
CM_ST_fcun_0,9
CM_ST_fcun_1,0
CM_ST_fcun_0,4

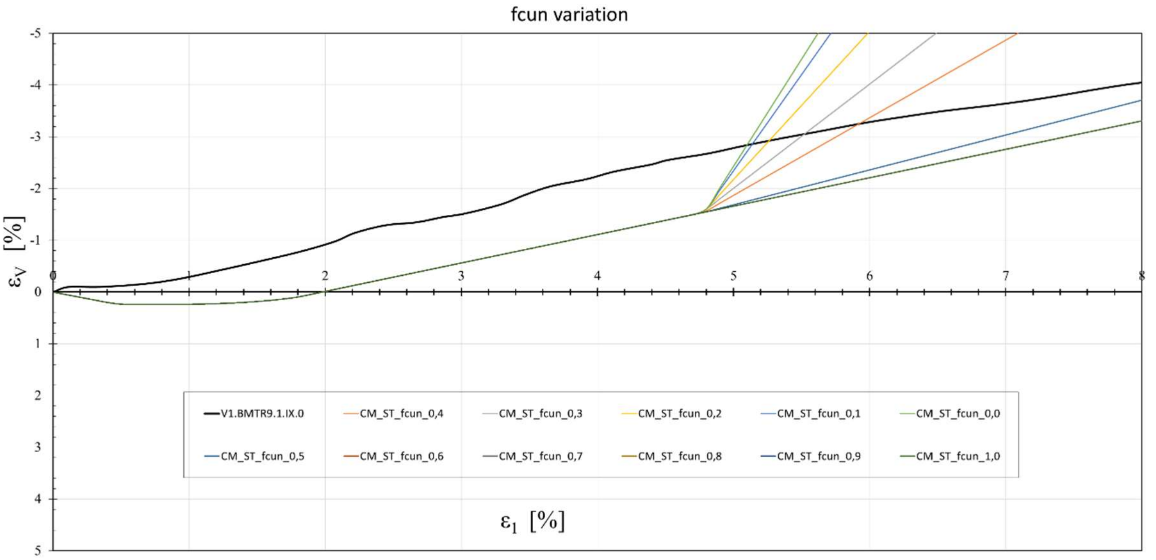
fcun variation
-5
-4
-3
-2
-1
0
1
2
3
4
5
0
2
3
4
5
6
7
8
εV [%]
ε1 [%]
V1.BMTR9.1.IX.0
CM_ST_fcun_0,4
CM_ST_fcun_0,3
CM_ST_fcun_0,2
CM_ST_fcun_0,1
CM_ST_fcun_0,0
CM_ST_fcun_0,5
CM_ST_fcun_0,6
CM_ST_fcun_0,7
CM_ST_fcun_0,8
CM_ST_fcun_0,9
CM_ST_fcun_1,0

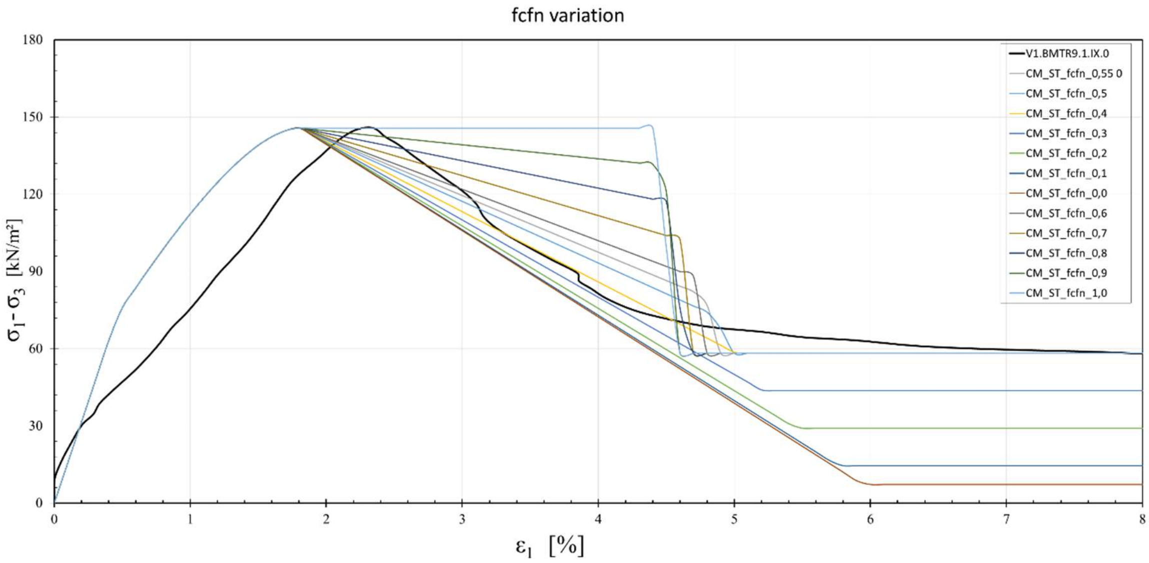
fcfn variation
$\sigma_1 - \sigma_3$ [kN/m²]
180
150
120
90
60
30
0
0
1
2
3
4
5
6
7
8
ε_1 [%]
V1.BMTR9.1.IX.0
CM_ST_fcfn_0,55 0
CM_ST_fcfn_0,5
CM_ST_fcfn_0,4
CM_ST_fcfn_0,3
CM_ST_fcfn_0,2
CM_ST_fcfn_0,1
CM_ST_fcfn_0,0
CM_ST_fcfn_0,6
CM_ST_fcfn_0,7
CM_ST_fcfn_0,8
CM_ST_fcfn_0,9
CM_ST_fcfn_1,0

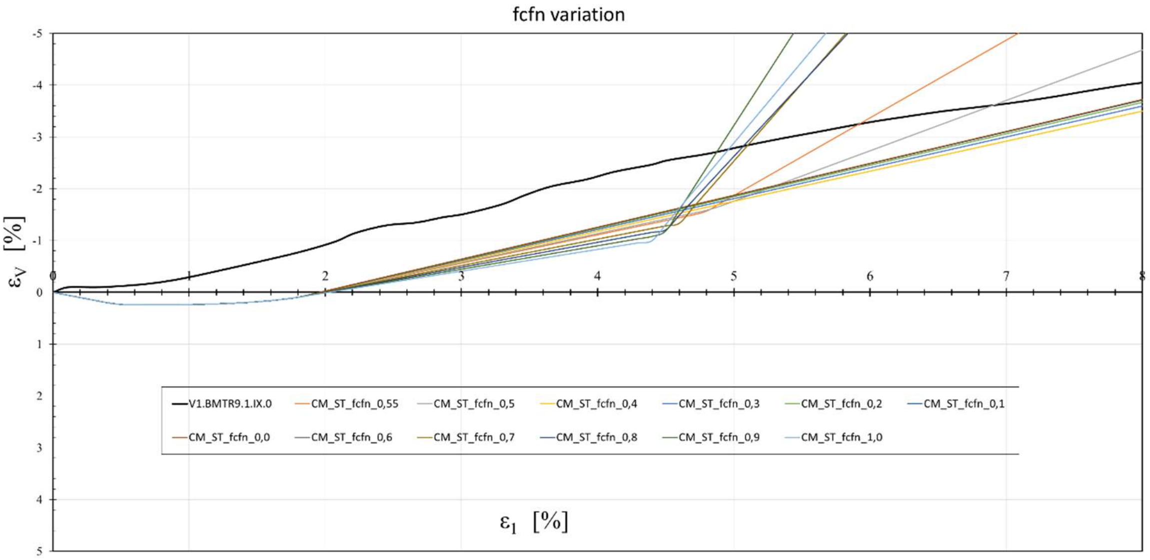
fcfn variation
ε_V [%]
-5
-4
-3
-2
-1
0
1
2
3
4
5
0
2
3
4
5
6
7
8
ε_1 [%]
V1.BMTR9.1.IX.0
CM_ST_fcfn_0,55
CM_ST_fcfn_0,5
CM_ST_fcfn_0,4
CM_ST_fcfn_0,3
CM_ST_fcfn_0,2
CM_ST_fcfn_0,1
CM_ST_fcfn_0,0
CM_ST_fcfn_0,6
CM_ST_fcfn_0,7
CM_ST_fcfn_0,8
CM_ST_fcfn_0,9
CM_ST_fcfn_1,0